APPENDICES TO:

Ramp-scale geomodel for reservoir and stratigraphic analysis of the Hugoton field (Wolfcampian, midcontinent U.S.A.)

By

Martin Kenneth Dubois

B.S. Geophysics Option in Geology, Kansas State University, 1974
M.S. *Honors* Geology, The University of Kansas, 1980

Submitted to the Department of Geology
and the Faculty of the Graduate School of
The University of Kansas in partial
fulfillment of the requirements for the
degree of Doctor of Philosophy
2007

ABSTRACT

Martin K. Dubois, Ph.D.
Department of Geology, April 2007
University of Kansas

The full-field model of the 70-year-old Hugoton field (largest in NA) is a comprehensive lithologic and petrophysical view of a giant reservoir system in a 108-million cell model covering 10,000-mi^2 (26,000-km^2). It is a quantitative basis for evaluating remaining gas, particularly in low-permeability intervals, and will aid field management and enhance ultimate recovery. The model is also a tool for developing depositional models and for understanding controls on sedimentation. Both the knowledge gained and the techniques and workflow employed have implications for understanding and modeling similar reservoir systems worldwide.

Accurate representation of lithofacies in the model is critical because water saturation from wireline logs is inaccurate due to filtrate invasion. Lithofacies-based petrophysical properties are used to estimate water saturation. Neural-network prediction of lithofacies using wireline logs and two geologic variables is effective in predicting lithofacies at wells. Between wells, lithofacies and wireline-log porosity, corrected by lithofacies-dependent algorithms, are reliably represented by stochastic methods. Permeability, water saturation, and gas in place at the cell level are calculated by lithofacies- and porosity-dependent petrophysical transforms. Based on the model, 963 billion m^3 (34 tcf) of the produced gas represents 65-70% of original gas in place. The reservoir is a layered, differentially depleted system, and most remaining gas is in intervals having lower permeability.

The model illustrates shifting sedimentation patterns related to glacioeustacy on a large, stable, gently sloped ramp. The 160-m reservoir comprises thirteen upward-shoaling carbonate cycles vertically stacked in a low-relief setting. Lithofacies bodies are laterally extensive and reservoir storage and flow units, mostly grain-supported marine carbonate, exhibit broad lateral continuity. Carbonate cycles are separated by fine-grained siliciclastic strata (mostly loess) deposited in a savannah-like setting. Climate variability controlled sediment supply and delivery. Relatively dry conditions and low vegetative cover during low sea level allowed fine siliciclastic sediments to be delivered to the ramp by eolian processes where they were stabilized by vegetation in an aggradational landscape. During high sea level wetter conditions and increased vegetation curtailed siliciclastic supply to a flooded, carbonate-dominated ramp. The results illustrate new climate-controlled mechanisms for cyclicity in fine-grained siliciclastic strata.

Table of Contents

List of Tables

Table **Page**

List of Figures

Figure **Page**

APPENDIX A

Core and lithofacies data

APPENDIX A – Core and lithofacies data

Lithofacies determination is critical to most geologic studies and is the foundation for Chapters 3 and 4. Methods for describing core and determining lithofacies, presented elsewhere, are summarized. Examples of lithofacies data and their distribution are presented and the locations of data that are accessible via the web are provided.

Data access

Digital core description and measured petrophysical properties are available as an Appendix (Core Data and Descriptions Database) to Dubois et al. (2006) at http://www.kgs.ku.edu/PRS/publication/2007/OFR07_06/index.html. Whole core, core slab, and thin section photomicrographs are available from the Kansas Geological Survey website, accessible via http://www.kgs.ku.edu/Magellan/CoreLibrary/image.html.

Core data distribution

Twenty-nine of approximately 100 continuous cores were selected for lithofacies analysis on the basis of length (longest selected), geographic position (sampling distribution), and availability of core analysis and wireline log data (Table A-1 and Figure A-1). In most cases, selected cores included either the entire Chase (twelve) or Council Grove (twelve) interval, or covered both intervals (five). Twenty-seven were used as training data for neural networks (Appendix B). In all 7400 ft of core (2255 m) was examined, approximately equally divided between the Chase and Council Grove Groups. Dubois described all Council Grove core and some of the Chase. Nathan Winters, under Dubois close supervision, described most of the Chase core.

Core description methods

Two approaches to the lithofacies determination task were required because of the nature of the problems being studied. In the balance of this appendix, geomodel lithofacies are those used in Chapter 3 and core lithofacies are those used in Chapter 4. Building the Hugoton geomodel (Chapter 3) required splitting the lithofacies spectrum into broad (coarser) lithofacies classes because of the limitations of recognizing lithofacies with wireline logs. The number of geomodel lithofacies classes and the criteria for defining classes involved four criteria: (1) maximum number of lithofacies recognizable by neural networks using petrophysical wireline log curves and other variables; (2) minimum number of lithofacies needed to accurately represent lithologic and petrophysical heterogeneity; (3) maximum distinction of core petrophysical properties among classes; and 4) the relative contribution of a lithofacies class to storage and flow. Eleven geomodel lithofacies classes, eight marine and three continental, were determined to be optimal. The methods for determining geomodel lithofacies were tailored to the primary goal for the study: develop a geologic and petrophysical model for the Hugoton gas field. Because petrophysical properties are a function of lithofacies, permeability is a function of pore throat diameter, and pore throat diameter is a function of primary texture, the description and classification schemes were designed to split the lithofacies spectrum by primary texture.

Siliciclastic intervals of predominately continental origin were the subject of Chapter 4. This studies focus was on determining the depositional controls on lithofacies required more narrow (finer) lithofacies classes. Digital core description data compiled for the geomodel study, in conjunction with additional sedimentary and pedogenic tabulated data, thin sections, and text descriptions of core were employed. The three dominantly continental geomodel lithofacies were split to nine core lithofacies in the study.

Geomodel lithofacies

Slabbed core was examined with the aid of a binocular microscope and data recorded at 0.5 ft (0.15 m) intervals using a quantitative, digital lithofacies description system described in Dubois et al., 2003 (Table A-2). In addition to the digital description, relevant notes and sketches were recorded to supplement the digital description. The sample rate was chosen because digital wireline logs are typically sampled at this rate and the interval is approximately the thickness of the thinnest lithofacies beds in core. Core depths were precisely correlated with wireline logs and depth corrected. Thin sections for selected samples were used to validate grain size estimated in core, determine grain composition and biotic constituents, and to examine finer details of sedimentary structures and pedogenic features for determining depositional facies. Three of the twelve descriptor digits recorded, rock type (digit 1), texture (digit 2), and principal pore (digit 6), are sufficient to discriminate the eleven geomodel lithofacies (Table A-3), although other digits were considered initially in the process of determining class boundaries. A sample of the digital lithofacies description available on line is provided in Tables A-4 and A-5.

Core lithofacies for Council Grove Group siliciclastic strata

Thirteen cores were studied in detail and provide the basic data for Chapter 4 (Figure A-2). Core lithofacies were determined in thirteen cores primarily on the basis of six of the twelve digital descriptor variables recorded in the table described above and seven additional sedimentary and pedogenic features tabulated (Table A-6). Thin sections for selected samples were again used, particularly for determining depositional facies (e.g., delineating nodular carbonate mudstone from pedogenic caliche). Table A-7 provides a comparison of geomodel and core lithofacies.

References

Dubois, M. K., Byrnes, A. P., Bohling, G. C., Seals, S.C., and Doveton, J.H., 2003, Statistically-based lithofacies predictions for 3-D reservoir modeling: examples from the Panoma (Council Grove) Field, Hugoton Embayment, Southwest Kansas (abs): Proceedings AAPG 2003 Annual Convention, Salt Lake City, Utah, v.12, p. A44, *and* Kansas Geological Survey Open File Report #2003-30, 3 panels, http://www.kgs.ku.edu/PRS/publication/2003/ofr2003-30/index.html (accessed March 22, 2007).

Dubois, M. K., A. P. Byrnes, S. Bhattacharya, G. C. Bohling, J. H. Doveton, and R. E. Barba, 2006, Hugoton Asset Management Project (HAMP): Hugoton Geomodel Final Report, Kansas Geological Survey, Open-File Report 2007-6, 682 p., http://www.kgs.ku.edu/PRS/publication/2007/OFR07_06/index.html (accessed March 22, 2007).

WELL NAME	WELL NO	OPERATOR	API	SEC	TWP	RGE	LAT	LON	DATUM	TD	CHASE	COUNCIL GROVE	CORE TOP	CORE BASE
SHANKLE 2-9	2-9	CITIES SERVICE OIL CO	15093212500000	9	23S	37W	38.0634	-101.39	3303	5150	2540	2782	2459	3182
SHRIMPLIN GU	2-HI	AMOCO PRODUCTION CO	15055210450000	7	24S	33W	37.9781	-100.99	2883	3084	2517	2802	2420	3076
BEATY	2-E	AMOCO PRODUCTION CO	15093201340000	20	25S	38W	37.8598	-101.51	3179	2878	2372	2627	2608	2878
MAX COHEN	C-3	AMOCO PRODUCTION COM	15093207810000	27	25S	38W	37.8497	-101.47	3175	6400	2378	2651	2370	2680
CROSS H CATTLE	1-6	AMOCO PRODUCTION CO	15075205430000	6	25S	39W	37.9106	-101.65	3222	3150	2353	2574	2345	3085
ENGLERT	1	AMOCO PRODUCTION COM	15075202010000	27	25S	39W	37.8472	-101.59	3333	3000	2478	2728	2440	2557
NOLAN	2	MOBIL OIL CORPORATIO	15055206160000	24	26S	34W	37.7735	-100.99	2950	3200	2580	2858	2821	3061
ALEXANDER D	2	CITIES SERVICE OIL CO	15067203380000	29	27S	35W	37.6746	-101.17	3100	3150	2605	2886	2881	3122
CRAFT G.U.	3-HI	AMOCO PRODUCTION COM	15067206520000	22	28S	38W	37.6016	-101.47	3108	3119	2345	2624	2312	2908
STUART	3-34R	PIONEER NATURAL RES	15067214150000	34	29S	35W	37.4857	-101.14	2994	3100	2500	2808	2756	3045
CAROL EILERTS	1	AMOCO PRODUCTION COM	15081202780000	8	30S	32W	37.4513	-100.84	2919	5852	2681	2982	2675	2978
LUKE GU	4	AMOCO PRODUCTION CO	15187206610000	8	30S	39W	37.45	-101.61	3226	3347	2328	2615	2600	3024
PRATER GAS UNIT A	2	AMOCO PRODUCTION COM	15175202500000	22	31S	33W	37.3372	-100.89	2877	3400		2911	2928	3167
CHURCHMAN BIBLE	1	MOBIL OIL CORPORATIO	15189209360000	15	31S	35W	37.3568	-101.11	3021	6000	2631	2918	2900	3124
NEWBY	2-28R	PIONEER NATURAL RES	15189222250000	28	31S	37W	37.3172	-101.35	3112	3110	2516	2832	2811	3058
FLOWER	1A	ANADARKO PETROLEUM C	15189218570000	25	31S	38W	37.319	-101.41	3139	2948	2473	2789	2441	3005
MONTGOMERY G.U.	3HI B	AMOCO PRODUCTION COM	15129208440000	5	31S	39W	37.385	-101.58	3210	3134	2401	2686	2407	3036
KIMZEY	A-1	ANADARKO PRODUCTION	15189201830000	8	33S	35W	37.1229	-101.4	3167	3156	2605	2922	2892	3156
CRAWFORD UNIT	2	MOBIL OIL CORPORATIO	15189206910000	8	33S	35W	37.1893	-101.15	2983	3200	2649	2964	2972	3195
NIX NO 1 UNIT	3	NORTHERN NATURAL GAS	15189206570000	25	33S	36W	37.1521	-101.19	3025	3200	2657	2974	2632	2937
YOUNGREN J OWWO	1-H	ANADARKO PETROLEUM C	15189217560000	4	33S	38W	37.2029	-101.46	3174	3200	2478	2783	2470	2960
HONOUR A	2H	ANADARKO PET CORP	15129212450000	25	33S	41W	37.1527	-101.72	3328	2775	2224	2520	2130	2449
DUNNE-HOFFMAN K	3-H	ANADARKO PETROLEUM C	15189217740000	16	35S	38W	37.0069	-101.46	3212	3066	2650	2977	2608	3066
HAAR `C`	5	ANADARKO PET CORP	35139222740000	30	6N	13E	36.9628	-101.69	3432	6920	2561	2895	2500	2813
HOOBLER ESTATE UNIT	2	MOBIL OIL CORP	35139221670000	20	6N	17E	36.9684	-101.25	3052	3066	2722	3049	2685	3066
KEENAN `A`	5	ANADARKO PET CORP	35139221690000	26	4N	13E	36.7788	-101.62	3228	7040	2597	2935	2590	2874
STONEBRAKER /A/	81	CITIES SERVICE OIL CO	35139207330000	14	2N	12E	36.6371	-101.74	3237	3565	2564	2894	2800	3129
BUF	3	PHILLIPS PET ET AL	35139222110000	27	2N	15E	36.6125	-101.43	3106	3000	2694		2640	2892.5
LURE	2	PHILLIPS PET ET AL	35139222700000	24	1N	13E	36.5337	-101.61	3288	3050	2806		2716	2977

Table A-1. Table of wells with core utilized in the Hugoton studies. Wells are sorted from north to south.

Hugoton Digital Rock Classification System

	1	2	3	4	5	6
CODE	Rock Type	Dunham/Folk Classification	Consolidation/Fracturing	Clay Content	Grain Size	Principal Pore Type
9	Evaporite	cobble conglomerate	unconsolidated	Frac-fill 10-50%	vcrs rudite/cobble congl (>64mm)	cavern vmf (>64mm)
8	Dolomite	sucrosic/pebble conglomerate	poorly cemented, high porosity	Frac-fill 5-10%	med-crs rudite/pebble congl (4-64mm)	med-lrg vmf (4-64mm)
7	Dolomite-Limestone	baffle-boundstone/vcrs sandstone	cemented, >10% porosity, highly fractured	Shale >90%	fn rudite/vcrs sand (1-4mm)	sm vmf (1-4mm)
6	Dolomite-Siliciclastic	grainstone/crs sandstone	cemented, >10% porosity, fractured	Shale 75-90%	arenite/crs sand (500-1000um)	crs(500-1000um)
5	Limestone	packstone-grainstone/med sandstone	cemented, >10% porosity, unfractured	Shale 50-75%	arenite/med sand (250-500um)	med(250-500um)
4	Carbonate-Siliciclastic	packstone/fn sandstone	well cemented, 3-10% porosity, highly fractured	Shale 25-50%	arenite/fn sand (125-250um)	fn (125-250um)
3	Siliciclastic-Carbonate	wackestone-packstone/vfn sandstone	well cemented, >3-10% porosity, fractured	Shale 10-25%	arenite/vfn sand (62-125um)	pin-vf (62-125um)
2	Marine Siliciclastic	wackestone/crs siltstone	well cemented, >3-10% porosity, unfractured	Whispy 5-10%	crs lutite/crs silt (31-62um)	pinpoint (31-62um)
1	Continental Siliciclastic	mudstone-wackestone/vf-m siltstone	highly cemented, fractured	Trace 1-5%	fn-med lutite/vf-m silt (4-31um)	microporous (<31um)
0	Shale	mudstone/shale/clay	totally cemented, dense, unfractured	Clean <1%	clay (<4um)	nonporous

	7	8	9	10	11	12
CODE	Subsidiary Pore Type	Cement/Pore-Filling-Mineral	Bedding	Water Depth/Shelf Position	Faunal Assemblage	Color
9	cavern vmf (>64mm)	sulfide r=3.85-5.0	massive/structureless	Bathyal	Normal, one dominant (<3)	black
8	med-lrg vmf (4-64mm)	siderite r=3.89	planar, low angle X-bed	Steepened Slope	Normal, not diverse (2-4)	dark gray
7	sm vmf (1-4mm)	phosphate r=3.13-3.21	lrg X-bed (>4mm), trough	Outer Shelf	Normal, diverse (4+)	gray
6	crs(500-1000um)	anhydrite r=2.35-2.98	sm X-bed (<4mm), ripple	Mid-shelf	Mixed, diverse (5+)	light gray
5	med(250-500um)	dolomite r=2.87	flasier	Upper Shelf (lower)	Mixed, not diverse (<4)	shades of green
4	fn (125-250um)	calcite r=2.71	wavy bedded/cont. layers	Upper Shelf (upper)	Restricted, diverse (5+)	white
3	pin-vf (62-125um)	quartz r=2.65	lenticular/discont. layers	Intertidal	Restricted, not diverse(2-4)	tan
2	pinpoint (31-62um)	clay r=2.0-2.7	convolute/lrg burrows	Supratidal Carbonate	Restricted, one dominant +2-4	brown
1	microporous (<31um)	carbonaceous r=2.0	churned/bioturbated	Supratidal Clastic	Restricted, one dominant +0-1	red-brown
0	nonporous	uncemented r=1.0	vertical k barriers	Continental	Absent	red

Examples:

52-505-534-9444
Limestone, grainstone, cemented/unfractured, clean (<1% clay,) medium arenite (250-500um), medium sized principle pore (250-500um), pinpoint-very fine sized subsidiary pore size (31-62um), calcite cement, massive bedded, upper shelf, restricted-diverse fauna, white color.

12-322-215-9001
Continental siliciclastic, coarse siltstone, well cemented/fractured, wispy clay (5-10% clay), coarse silt sized (31-62um), pipoint primary pores (31-62um), microporous subsidiary pores (<31um), dolomite cement, massive bedded, continental, absent of fauna, red-brown color.

Table A-2. Digital lithofacies description system (modified after Dubois et al, 2003). Twelve-digit classification system used for core descriptions at half-foot (0.15-m) intervals, gathered by visual observation with the aid of binocular microscope. Three digits (shaded blue) were required for distinguishing 11 geomodel lithofacies (Table A-3.)

Geomodel Lithofacies Code	Description Code	Geomodel Lithofacies
0 or 11	1/>2	very-fine-grained sandstone (continental)
1	1/2	coarse-grained siltstone (continental)
2	1/0-1	fine- to medium-grained siltstone (continental)
3	0,2/<3	siltstone or shale (marine)
4	3-8/0-1	mudstone or mudstone-wackestone
5	3-8/2-3	wackestone or wackestone-packstone
6	6-8/8/*/*/*/<3	very-fine to fine-crystalline dolomite
7	3-8/4-5-6	packstone or packstone-grainstone
8	3-8/7	phylloid algal bafflestone
9	7-8/8/*/*/*/>2	fine- to medium-crystalline moldic dolomite
10	2/3-7	very-fine-grained sandstone (marine)

digit1/digit2/digit3…….*indicates skip

Table A-3. Geomodel lithofacies code, digital description code, and geomodel lithofacies. Three digits are sufficient to discriminate the eleven lithofacies. Geomodel lithofacies code for very-fine-grained-sandstone (continental) is 11 “outside” of the geomodel because of computer code constraints. Inside the geomodels it is equal to 0.

	A	B	C	D	E	F	G	H	I	J	K	L	M	N	Q	R
1	Appendix 4.2.1 Core Description & Core Analysis Data															LITHOFACIES CODE
2	API NUMBER	OPERATOR NAME	LEASE NAME	WELL NUMBER	TOWNSHIP	TOWNSHIP DIRECTION	RANGE	RANGE DIRECTION	SECTION	FIELD NAME	STRATIGRAPHIC UNIT	STRATIGRAPHIC NAME	DEPTH TOP	DEPTH BASE	LITHOLOGIC DATA SOURCE	Geomod4
648	15-189-21857	ANADARKO PET CORP	FLOWER	A1	31	S	38	W	25	HUGOTON	COUNCIL GROVE GROUP	A1 SH	2798	2798.5	MKD	1
649	15-189-21857	ANADARKO PET CORP	FLOWER	A1	31	S	38	W	25	HUGOTON	COUNCIL GROVE GROUP	A1 SH	2798.5	2799	MKD	1
650	15-189-21857	ANADARKO PET CORP	FLOWER	A1	31	S	38	W	25	HUGOTON	COUNCIL GROVE GROUP	A1 SH	2799	2799.5	MKD	1
651	15-189-21857	ANADARKO PET CORP	FLOWER	A1	31	S	38	W	25	HUGOTON	COUNCIL GROVE GROUP	A1 SH	2799.5	2800	MKD	1
652	15-189-21857	ANADARKO PET CORP	FLOWER	A1	31	S	38	W	25	HUGOTON	COUNCIL GROVE GROUP	A1 SH	2800	2800.5	MKD	1
653	15-189-21857	ANADARKO PET CORP	FLOWER	A1	31	S	38	W	25	HUGOTON	COUNCIL GROVE GROUP	A1 SH	2800.5	2801	MKD	1
654	15-189-21857	ANADARKO PET CORP	FLOWER	A1	31	S	38	W	25	HUGOTON	COUNCIL GROVE GROUP	A1 SH	2801	2801.5	MKD	2
655	15-189-21857	ANADARKO PET CORP	FLOWER	A1	31	S	38	W	25	HUGOTON	COUNCIL GROVE GROUP	A1 SH	2801.5	2802	MKD	2
656	15-189-21857	ANADARKO PET CORP	FLOWER	A1	31	S	38	W	25	HUGOTON	COUNCIL GROVE GROUP	A1 SH	2802	2802.5	MKD	2
657	15-189-21857	ANADARKO PET CORP	FLOWER	A1	31	S	38	W	25	HUGOTON	COUNCIL GROVE GROUP	A1 SH	2802.5	2803	MKD	2
658	15-189-21857	ANADARKO PET CORP	FLOWER	A1	31	S	38	W	25	HUGOTON	COUNCIL GROVE GROUP	A1 SH	2803	2803.5	MKD	2
659	15-189-21857	ANADARKO PET CORP	FLOWER	A1	31	S	38	W	25	HUGOTON	COUNCIL GROVE GROUP	A1 SH	2803.5	2804	MKD	2
660	15-189-21857	ANADARKO PET CORP	FLOWER	A1	31	S	38	W	25	HUGOTON	COUNCIL GROVE GROUP	A1 SH	2804	2804.5	MKD	2
661	15-189-21857	ANADARKO PET CORP	FLOWER	A1	31	S	38	W	25	HUGOTON	COUNCIL GROVE GROUP	A1 SH	2804.5	2805	MKD	2
662	15-189-21857	ANADARKO PET CORP	FLOWER	A1	31	S	38	W	25	HUGOTON	COUNCIL GROVE GROUP	A1 SH	2805	2805.5	MKD	2
663	15-189-21857	ANADARKO PET CORP	FLOWER	A1	31	S	38	W	25	HUGOTON	COUNCIL GROVE GROUP	A1 SH	2805.5	2806	MKD	2
664	15-189-21857	ANADARKO PET CORP	FLOWER	A1	31	S	38	W	25	HUGOTON	COUNCIL GROVE GROUP	A1 SH	2806	2806.5	MKD	2
665	15-189-21857	ANADARKO PET CORP	FLOWER	A1	31	S	38	W	25	HUGOTON	COUNCIL GROVE GROUP	A1 SH	2806.5	2807	MKD	2
666	15-189-21857	ANADARKO PET CORP	FLOWER	A1	31	S	38	W	25	HUGOTON	COUNCIL GROVE GROUP	A1 SH	2807	2807.5	MKD	2
667	15-189-21857	ANADARKO PET CORP	FLOWER	A1	31	S	38	W	25	HUGOTON	COUNCIL GROVE GROUP	A1 SH	2807.5	2808	MKD	2
668	15-189-21857	ANADARKO PET CORP	FLOWER	A1	31	S	38	W	25	HUGOTON	COUNCIL GROVE GROUP	A1 SH	2808	2808.5	MKD	2
669	15-189-21857	ANADARKO PET CORP	FLOWER	A1	31	S	38	W	25	HUGOTON	COUNCIL GROVE GROUP	A1 SH	2808.5	2809	MKD	2
670	15-189-21857	ANADARKO PET CORP	FLOWER	A1	31	S	38	W	25	HUGOTON	COUNCIL GROVE GROUP	A1 SH	2809	2809.5	MKD	2
671	15-189-21857	ANADARKO PET CORP	FLOWER	A1	31	S	38	W	25	HUGOTON	COUNCIL GROVE GROUP	A1 SH	2809.5	2810	MKD	2
672	15-189-21857	ANADARKO PET CORP	FLOWER	A1	31	S	38	W	25	HUGOTON	COUNCIL GROVE GROUP	A1 SH	2810	2810.5	MKD	2
673	15-189-21857	ANADARKO PET CORP	FLOWER	A1	31	S	38	W	25	HUGOTON	COUNCIL GROVE GROUP	A1 LM	2810.5	2811	MKD	6
674	15-189-21857	ANADARKO PET CORP	FLOWER	A1	31	S	38	W	25	HUGOTON	COUNCIL GROVE GROUP	A1 LM	2811	2811.5	MKD	6
675	15-189-21857	ANADARKO PET CORP	FLOWER	A1	31	S	38	W	25	HUGOTON	COUNCIL GROVE GROUP	A1 LM	2811.5	2812	MKD	6
676	15-189-21857	ANADARKO PET CORP	FLOWER	A1	31	S	38	W	25	HUGOTON	COUNCIL GROVE GROUP	A1 LM	2812	2812.5	MKD	6
677	15-189-21857	ANADARKO PET CORP	FLOWER	A1	31	S	38	W	25	HUGOTON	COUNCIL GROVE GROUP	A1 LM	2812.5	2813	MKD	5
678	15-189-21857	ANADARKO PET CORP	FLOWER	A1	31	S	38	W	25	HUGOTON	COUNCIL GROVE GROUP	A1 LM	2813	2813.5	MKD	5
679	15-189-21857	ANADARKO PET CORP	FLOWER	A1	31	S	38	W	25	HUGOTON	COUNCIL GROVE GROUP	A1 LM	2813.5	2814	MKD	7
680	15-189-21857	ANADARKO PET CORP	FLOWER	A1	31	S	38	W	25	HUGOTON	COUNCIL GROVE GROUP	A1 LM	2814	2814.5	MKD	5
681	15-189-21857	ANADARKO PET CORP	FLOWER	A1	31	S	38	W	25	HUGOTON	COUNCIL GROVE GROUP	A1 LM	2814.5	2815	MKD	4
682	15-189-21857	ANADARKO PET CORP	FLOWER	A1	31	S	38	W	25	HUGOTON	COUNCIL GROVE GROUP	A1 LM	2815	2815.5	MKD	4
683	15-189-21857	ANADARKO PET CORP	FLOWER	A1	31	S	38	W	25	HUGOTON	COUNCIL GROVE GROUP	A1 LM	2815.5	2816	MKD	4
684	15-189-21857	ANADARKO PET CORP	FLOWER	A1	31	S	38	W	25	HUGOTON	COUNCIL GROVE GROUP	A1 LM	2816	2816.5	MKD	4
685	15-189-21857	ANADARKO PET CORP	FLOWER	A1	31	S	38	W	25	HUGOTON	COUNCIL GROVE GROUP	A1 LM	2816.5	2817	MKD	4
686	15-189-21857	ANADARKO PET CORP	FLOWER	A1	31	S	38	W	25	HUGOTON	COUNCIL GROVE GROUP	A1 LM	2817	2817.5	MKD	4
687	15-189-21857	ANADARKO PET CORP	FLOWER	A1	31	S	38	W	25	HUGOTON	COUNCIL GROVE GROUP	A1 LM	2817.5	2818	MKD	4
688	15-189-21857	ANADARKO PET CORP	FLOWER	A1	31	S	38	W	25	HUGOTON	COUNCIL GROVE GROUP	A1 LM	2818	2818.5	MKD	4
689	15-189-21857	ANADARKO PET CORP	FLOWER	A1	31	S	38	W	25	HUGOTON	COUNCIL GROVE GROUP	A1 LM	2818.5	2819	MKD	4
690	15-189-21857	ANADARKO PET CORP	FLOWER	A1	31	S	38	W	25	HUGOTON	COUNCIL GROVE GROUP	A1 LM	2819	2819.5	MKD	4
691	15-189-21857	ANADARKO PET CORP	FLOWER	A1	31	S	38	W	25	HUGOTON	COUNCIL GROVE GROUP	A1 LM	2819.5	2820	MKD	4
692	15-189-21857	ANADARKO PET CORP	FLOWER	A1	31	S	38	W	25	HUGOTON	COUNCIL GROVE GROUP	A1 LM	2820	2820.5	MKD	4
693	15-189-21857	ANADARKO PET CORP	FLOWER	A1	31	S	38	W	25	HUGOTON	COUNCIL GROVE GROUP	A1 LM	2820.5	2821	MKD	5
694	15-189-21857	ANADARKO PET CORP	FLOWER	A1	31	S	38	W	25	HUGOTON	COUNCIL GROVE GROUP	A1 LM	2821	2821.5	MKD	7

Table A-4. Sample of digital core description table available online. Basic well information is displayed in this portion of the table, which is continued in Table A-5.

L	M	N	Q	R	S	T	U	V	W	X	Y	Z	AA	AB	AC	AD	AJ
				LITHOFACIES CODE	ROCK TYPE	LITHOLOGIC CLASS-IFICATION	CONSOLID-ATION/ FRACTURING	CLAY CONTENT	GRAIN SIZE	PRINCIPAL PORE TYPE	SUBSIDIARY PORE TYPE	CEMENT/ PORE FILLING	BEDDING	WATER DEPTH	FAUNAL ASSEMBL AGE	COLOR	DEPTH CORRECTION CORE PLUS TO LOG
STRATIGRAPHIC NAME	DEPTH TOP	DEPTH BASE	LITHOLOGIC DATA SOURCE	Geomod4	1	2	3	4	5	6	7	8	9	10	11	12	
A1 SH	2798	2798.5	MKD	1	1	2		3		1		4	9	0	0	1	0
A1 SH	2798.5	2799	MKD	1	1	2		3		1		4	9	0	0	1	0
A1 SH	2799	2799.5	MKD	1	1	2		3		1		4	9	0	0	1	0
A1 SH	2799.5	2800	MKD	1	1	2		3		1		4	9	0	0	1	0
A1 SH	2800	2800.5	MKD	1	1	2		3		1		4	9	0	0	1	0
A1 SH	2800.5	2801	MKD	1	1	2		3		1		4	9	0	0	1	0
A1 SH	2801	2801.5	MKD	2	1	1		4		1		4	9	0	0	0	0
A1 SH	2801.5	2802	MKD	2	1	1		4		1		4	9	0	0	0	0
A1 SH	2802	2802.5	MKD	2	1	1		4		1		4	9	0	0	0	0
A1 SH	2802.5	2803	MKD	2	1	1		4		1		4	9	0	0	0	0
A1 SH	2803	2803.5	MKD	2	1	1		4		1		4	9	0	0	0	0
A1 SH	2803.5	2804	MKD	2	1	1		4		1		4	9	0	0	6	0
A1 SH	2804	2804.5	MKD	2	1	1		4		1		4	9	0	0	6	0
A1 SH	2804.5	2805	MKD	2	1	1		4		1		4	9	0	0	0	0
A1 SH	2805	2805.5	MKD	2	1	1		4		1		4	9	0	0	0	0
A1 SH	2805.5	2806	MKD	2	1	1		4		1		4	9	0	0	0	0
A1 SH	2806	2806.5	MKD	2	1	1		4		1		4	9	0	0	0	0
A1 SH	2806.5	2807	MKD	2	1	1		4		1		4	9	0	0	0	0
A1 SH	2807	2807.5	MKD	2	1	1		4		1		4	9	0	0	6	0
A1 SH	2807.5	2808	MKD	2	1	1		4		1		4	9	0	0	0	0
A1 SH	2808	2808.5	MKD	2	1	1		4		1		4	9	0	0	0	0
A1 SH	2808.5	2809	MKD	2	1	1		4		1		4	9	0	0	0	0
A1 SH	2809	2809.5	MKD	2	1	1		4		1		2	9	0	0	0	0
A1 SH	2809.5	2810	MKD	2	1	1		4		1		2	9	0	0	0	0
A1 SH	2810	2810.5	MKD	2	1	1		4		0		2	0	0	0	6	0.5
A1 LM	2810.5	2811	MKD	6	8	8		0	1	0	1	3	1	3	1	3	0.5
A1 LM	2811	2811.5	MKD	6	8	8		0	1	0	1	3	1	3	1	3	0.5
A1 LM	2811.5	2812	MKD	6	8	8		0	1	0	1	3	1	3	1	3	0.5
A1 LM	2812	2812.5	MKD	6	8	8		0	1	0	1	3	1	3	1	3	0.5
A1 LM	2812.5	2813	MKD	5	7	2		0	1	0	1	4	3	4	3	6	0.5
A1 LM	2813	2813.5	MKD	5	7	2		0	1	0	1	4	3	4	3	6	0.5
A1 LM	2813.5	2814	MKD	7	7	4		0	4	0	1	4	4	4	4	6	0.5
A1 LM	2814	2814.5	MKD	5	6	2		1	1	1	1	4	3	4	3	5	0.5
A1 LM	2814.5	2815	MKD	4	6	1		1	1	1	1	4	3	4	3	5	0.5
A1 LM	2815	2815.5	MKD	4	3	1		3	1	0	1	5	4	5	4	7	0.5
A1 LM	2815.5	2816	MKD	4	3	1		3	1	0	1	5	4	5	4	7	0.5
A1 LM	2816	2816.5	MKD	4	3	1		3	1	0	1	5	4	5	4	7	0.5
A1 LM	2816.5	2817	MKD	4	3	1		3	1	0	1	5	4	5	4	7	0.5
A1 LM	2817	2817.5	MKD	4	3	1		3	1	0	1	5	4	5	4	7	0.5
A1 LM	2817.5	2818	MKD	4	3	1		3	1	0	1	5	4	5	4	7	0.5
A1 LM	2818	2818.5	MKD	4	3	1		3	1	0	1	5	4	5	4	7	0.5
A1 LM	2818.5	2819	MKD	4	3	1		3	1	0	1	5	4	5	4	7	0.5
A1 LM	2819	2819.5	MKD	4	3	1		3	1	0	1	5	4	5	4	7	0.5
A1 LM	2819.5	2820	MKD	4	3	1		3	1	0	1	5	4	5	4	7	0.5
A1 LM	2820	2820.5	MKD	4	3	1		3	1	0	1	5	4	5	4	7	0.5
A1 LM	2820.5	2821	MKD	5	3	2		3	1	0	1	5	5	5	5	7	0.5
A1 LM	2821	2821.5	MKD	7	4	4		1	5	0	1	5	5	5	5	7	0.5

Table A-5. Digital core description table, continued. Digital description of core at half-foot (0.15 m) intervals is illustrated.

	A	B	C	D	E	F	G	H	I	J	K	L	M	N	O	P	Q	R	S	T	U	V	W	X	Y	Z	AA	AB	AC
6								Sedimentary and pedogenic features in contiental siliciclastic intervals										ROCK TYPE	LITHOLOGIC CLASSIFICATION	LIDATION/FRACTURING	CLAY CONTENT	GRAIN SIZE	PRINCIPAL PORE TYPE	SUBSIDIARY PORE TYPE	CEMENT/PORE FILLING	BEDDING	WATER DEPTH	FAUNAL ASSEMBLAGE	COLOR
7	API	Elog Depth	GROUP	Formation-Member	Well No	Lease_Name	Core Depth	Laminations	Anhydrite	Peds or slickensides	Caliche/cement	Roots	Burrows	Redox	Pedogenic Features	Core Siliciclastic Lithofacies Code	Geomodel Lithofacies	1	2	3	4	5	6	7	8	9	10	11	12
50	1507520543000 0	2596.5	COUNCIL GROVE (	A1SH	1-6	CROSS H CATTLE	2594.5					R	AMB-s	RH	Rz-Amb-Rdx	8	11	1	3		1	3	2		4	1	0	0	1
51	1507520543000 0	2597	COUNCIL GROVE (	A1SH	1-6	CROSS H CATTLE	2595					R	AMB-s	RH	Rz-Amb-Rdx	8	11	1	3		1	3	2		4	1	0	0	1
52	1507520543000 0	2597.5	COUNCIL GROVE (	A1SH	1-6	CROSS H CATTLE	2595.5					R	AMB-s	RH	Rz-Amb-Rdx	8	11	1	3		1	3	2		4	1	0	0	1
53	1507520543000 0	2598	COUNCIL GROVE (	A1SH	1-6	CROSS H CATTLE	2596					R	AMB-s	RH	Rz-Amb-Rdx	8	11	1	3		1	3	1		4	1	0	0	1
54	1507520543000 0	2598.5	COUNCIL GROVE (	A1SH	1-6	CROSS H CATTLE	2596.5					R		RH	Rz-Rdx	8	11	1	3		1	3	1		4	1	0	0	1
55	1507520543000 0	2599	COUNCIL GROVE (	A1SH	1-6	CROSS H CATTLE	2597									8	11	1	3		1	3	2		4	9	0	0	1
56	1507520543000 0	2599.5	COUNCIL GROVE (	A1SH	1-6	CROSS H CATTLE	2597.5									8	11	1	3		1	3	2		4	9	0	0	1
57	1507520543000 0	2600	COUNCIL GROVE (	A1SH	1-6	CROSS H CATTLE	2598									7	1	1	2		2	2	2		4	9	0	0	1
58	1507520543000 0	2600.5	COUNCIL GROVE (	A1SH	1-6	CROSS H CATTLE	2598.5									7	1	1	2		2	2	2		4	9	0	0	1
59	1507520543000 0	2601	COUNCIL GROVE (	A1SH	1-6	CROSS H CATTLE	2599									7	1	1	2		2	2	2		4	9	0	0	1
60	1507520543000 0	2601.5	COUNCIL GROVE (	A1SH	1-6	CROSS H CATTLE	2599.5									7	1	1	2		3	2	1		4	9	0	0	1
61	1507520543000 0	2602	COUNCIL GROVE (	A1SH	1-6	CROSS H CATTLE	2600				AN	R			CalNod-Rz	7	1	1	2		2	2	1		4	9	0	0	1
62	1507520543000 0	2602.5	COUNCIL GROVE (	A1SH	1-6	CROSS H CATTLE	2600.5				AN	R			CalNod-Rz	8	11	1	3		1	3	2		4	1	0	0	1
63	1507520543000 0	2603.5	COUNCIL GROVE (	A1SH	1-6	CROSS H CATTLE	2601				AN	R	AMB-b		CalNod-Rz-Amb	8	11	1	3		1	3	2		4	1	0	0	1
64	1507520543000 0	2604	COUNCIL GROVE (	A1SH	1-6	CROSS H CATTLE	2601.5					R	AMB-b		Rz-Amb	8	11	1	3		1	3	2		4	1	0	0	1
65	1507520543000 0	2604.5	COUNCIL GROVE (	A1SH	1-6	CROSS H CATTLE	2602					R	AMB-s		Rz-Amb	8	11	1	3		1	3	2		4	1	0	0	1
66	1507520543000 0	2605	COUNCIL GROVE (	A1SH	1-6	CROSS H CATTLE	2602.5					R	AMB-s		Rz-Amb	8	11	1	3		1	3	2		4	1	0	0	1
67	1507520543000 0	2605.5	COUNCIL GROVE (	A1SH	1-6	CROSS H CATTLE	2603					R	AMB-s		Rz-Amb	8	11	1	3		1	3	2		4	1	0	0	1
68	1507520543000 0	2606	COUNCIL GROVE (	A1SH	1-6	CROSS H CATTLE	2603.5						AMB-s		Amb	8	11	1	3		1	3	2		4	1	0	0	1
69	1507520543000 0	2606.5	COUNCIL GROVE (	A1SH	1-6	CROSS H CATTLE	2604									7	1	1	2		2	2	1		4	9	0	0	1
70	1507520543000 0	2607	COUNCIL GROVE (	A1SH	1-6	CROSS H CATTLE	2604.5									7	1	1	2		2	2	1		4	4	0	0	1
71	1507520543000 0	2607.5	COUNCIL GROVE (	A1SH	1-6	CROSS H CATTLE	2605									4	2	1	1		4	1	1		4	4	0	0	6
72	1507520543000 0	2608	COUNCIL GROVE (	A1SH	1-6	CROSS H CATTLE	2605.5	F								9	1	4	0		2	1	0		4	2	0	0	4
73	1507520543000 0	2608.5	COUNCIL GROVE (	A1SH	1-6	CROSS H CATTLE	2606									7	1	1	2		2	2	1		4	9	0	0	1
74	1507520543000 0	2609	COUNCIL GROVE (	A1SH	1-6	CROSS H CATTLE	2606.5					R-anhy fill?			Rz	7	1	1	2		3	2	1		4	4	0	0	1
75	1507520543000 0	2609.5	COUNCIL GROVE (	A1SH	1-6	CROSS H CATTLE	2607	P				R-anhy fill?			Rz	7	1	1	2		3	2	1		4	4	0	0	1
76	1507520543000 0	2610.5	COUNCIL GROVE (	A1SH	1-6	CROSS H CATTLE	2607.5	P-mn				R-anhy fill?			Rz	3	1	1	2		4	2	1		4	8	0	0	5
77	1507520543000 0	2611	COUNCIL GROVE (	A1SH	1-6	CROSS H CATTLE	2608									5	1	1	2		4	2	1		4	9	0	0	5
78	1507520543000 0	2611.5	COUNCIL GROVE (	A1SH	1-6	CROSS H CATTLE	2608.5		dnb							2	1	1	2		4	2	1		4	4	0	0	5
79	1507520543000 0	2634	COUNCIL GROVE (	B1SH	1-6	CROSS H CATTLE	2631			ped-like						5	2	1	1		4	1				9	0	0	7
80	1507520543000 0	2634.5	COUNCIL GROVE (	B1SH	1-6	CROSS H CATTLE	2631.5			ped-like						5	2	1	1		4	1				9	0	0	7
81	1507520543000 0	2635	COUNCIL GROVE (	B1SH	1-6	CROSS H CATTLE	2632			ped-like						5	2	1	1		4	1				9	0	0	7
82	1507520543000 0	2635.5	COUNCIL GROVE (	B1SH	1-6	CROSS H CATTLE	2632.5			ped-like						5	2	1	1		4	1				9	0	0	7
83	1507520543000 0	2636	COUNCIL GROVE (	B1SH	1-6	CROSS H CATTLE	2633									7	1	1	2		3	2					0	0	1
84	1507520543000 0	2636.5	COUNCIL GROVE (	B1SH	1-6	CROSS H CATTLE	2633.5									7	1	1	2		3	2					0	0	1
85	1507520543000 0	2637	COUNCIL GROVE (	B1SH	1-6	CROSS H CATTLE	2634									7	1	1	2		3	2					0	0	1
86	1507520543000 0	2637.5	COUNCIL GROVE (	B1SH	1-6	CROSS H CATTLE	2634.5									7	1	1	2		3	2					0	0	1
87	1507520543000 0	2638	COUNCIL GROVE (	B1SH	1-6	CROSS H CATTLE	2635					R			Rz	9	1	4	0		3	2				2	0	0	4
88	1507520543000 0	2638.5	COUNCIL GROVE (	B1SH	1-6	CROSS H CATTLE	2635.5					R			Rz	9	1	4	0		3	2				2	0	0	4
89	1507520543000 0	2639	COUNCIL GROVE (	B1SH	1-6	CROSS H CATTLE	2636					R			Rz	9	1	4	0		2	2				2	0	0	4
90	1507520543000 0	2639.5	COUNCIL GROVE (	B1SH	1-6	CROSS H CATTLE	2636.5					R			Rz	9	1	4	0		2	2				2	0	0	4
91	1507520543000 0	2640	COUNCIL GROVE (	B1SH	1-6	CROSS H CATTLE	2637					R			Rz	7	1	1	2		3	2					0	0	1
92	1507520543000 0	2640.5	COUNCIL GROVE (	B1SH	1-6	CROSS H CATTLE	2637.5					R			Rz	7	1	1	2		3	2					0	0	1
93	1507520543000 0	2641	COUNCIL GROVE (	B1SH	1-6	CROSS H CATTLE	2638									7	1	1	2		3	2					0	0	1
94	1507520543000 0	2641.5	COUNCIL GROVE (	B1SH	1-6	CROSS H CATTLE	2638.5					R-anhy?			Rz	7	1	1	2		3	2					0	0	1
95	1507520543000 0	2642	COUNCIL GROVE (	B1SH	1-6	CROSS H CATTLE	2639					R-anhy?			Rz	7	1	1	2		3	2					0	0	1
96	1507520543000 0	2642.5	COUNCIL GROVE (	B1SH	1-6	CROSS H CATTLE	2639.5					R-anhy?			Rz	6	2	1	1		4	2					0	0	1
97	1507520543000 0	2643	COUNCIL GROVE (	B1SH	1-6	CROSS H CATTLE	2640									6	2	1	1		4	2					0	0	1

Key to sedimentary and pedogenic features

Laminations*
- F -f aint
- P - planar

Anhydrite
- on - organized nodules
- dnb - distinct nodular bedding

Peds or slickensides
- peds
- ped-like
- peds-clods
- slickensides

Caliche/ cement
- SN - scattered nodulesd
- AN - abundant nodules
- Mct - micritic cement
- Calcic

Roots
- R - rhizolith
- R? - possible rhizolith
- R - anhydrite filled rhizolith

Burrows
- AMB-b - bold adhesive meniscate burrow
- AMB-s - subtle adhesive meniscate burrow
- Other - othr burrow type

Redox
- RH - reduction halo
- SH - slight halo
- C - continuous

Pedogenic Features (compiled)
- Amb - adhesive miniscate burrows
- Rdx - redoximorphic mottles
- Rz - rhizoliths
- CalNod-caliche nodules

* distinctive thin laminations (not variety in gray muddy siltstone-laminated)

Table A-6. Example of table used to discriminate core lithofacies in the siliciclastic intervals of the Council Grove Group. Highlighted are information used to delineate core lithofacies. Core and geomodel lithofacies are provided in columns P and Q.

	Core Lithofacies Code	Core Lithofacies	Geomodel Lithofacies Code	Geomodel Lithofacies	Volumetric proportion
Main	6	Fine- to medium-grained siltstone	2	fine- to medium-grained siltstone	0.28
	7	Coarse-grained siltstone	1	coarse-grained siltstone	0.44
	8	Very-fine-grained sandstone	11 (0)	very-fine-grained sandstone	0.12
Lesser	5	Gray muddy siltstone-blocky	mostly 2	mostly fine- to medium-grained siltstone	0.08
	4	Gray muddy siltstone-laminated	mostly 3	mostly fine- to medium-grained siltstone	0.03
	2	Primary evaporite	1 or 2	one of "main" siltstones	0.01
	3	Laminated sandstone and siltstone	mostly 11 (0)	mostly very-fine-grained sandstone	0.01
	9	Nodular carbonate mudstone	1 or 2	one of "main" siltstones	0.02
	10	Fossiliferous, laminated or burrowed	3, 4, 5, 7, or 10	marine lithofacies	0.01

Table A-7. Core lithofacies, corresponding geomodel lithofacies, and volumetric proportions of lithofacies. Proportion data are from 84 siliciclastic intervals in 13 wells that were studied in detail. Eighty-four percent of core-lithofacies are the same lithofacies in the geomodel.

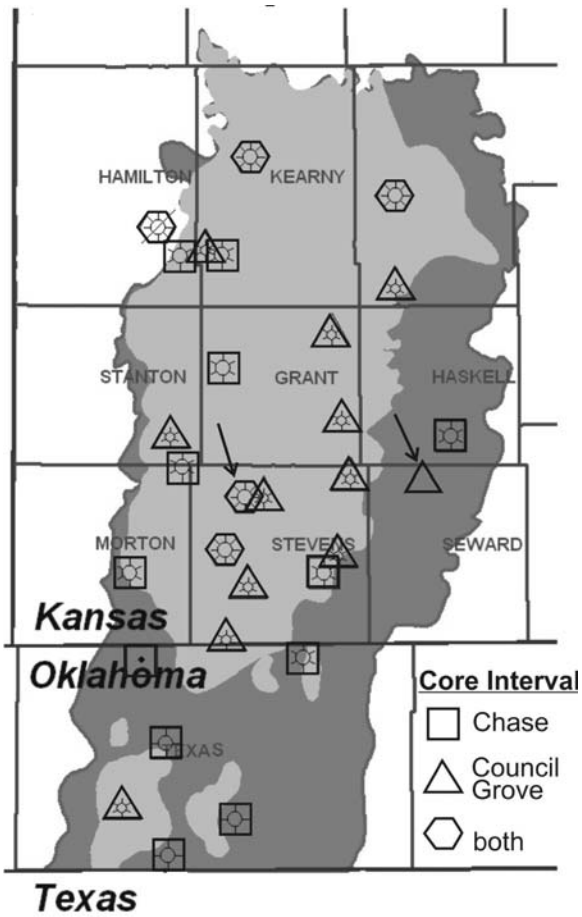

Figure A-1. *(Figure C-1B in Appendix C)* Core training set for Geomod4 includes data from 27 wells, four with both Chase Group and Council Grove Group core, twelve with Chase Group only, and eleven with Council Grove Group only. Two wells with arrows were not part of the training set. Wireline logs for the one in Stevens County were not satisfactory and the well in Seward County was added late.

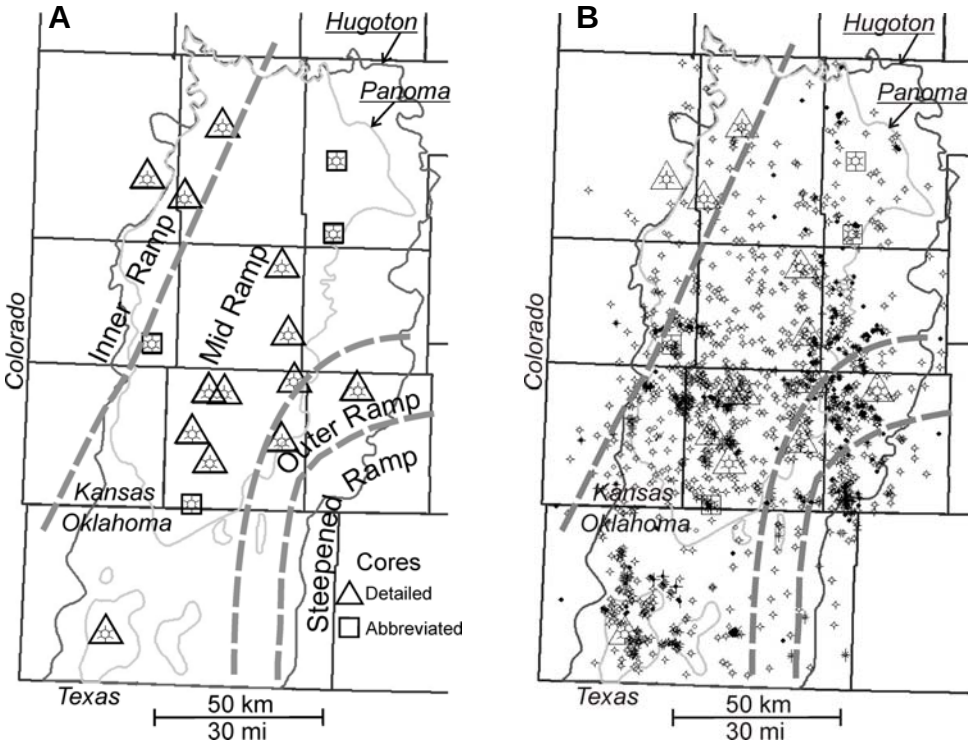

Figure A-2. *(Figure 4-6 in Chapter 4* **(A)** Core from 17 wells were examined, 13 in detail for the Council Grove Group siliciclastic intervals study. Abbreviated descriptions, sufficient for geomodel lithofacies, were obtained in four wells. **(B)** Well and core control for Council Grove Group geomodel. Geomodel lithofacies in 1234 wells (smaller well symbols) were predicted by neural networks, trained on core from 17 wells (larger well symbols).

APPENDIX B

Training, implementation, and effectiveness of neural networks

APPENDIX B – Training, implementation, and effectiveness of neural networks

Designing neural networks for lithofacies classification and using the predicted lithofacies in building large cellular geomodels is an iterative process. Chapter 3 describes the complex workflow for the Hugoton project and discusses the iterative nature of the project. Four iterations of model building have been completed (Table B-1) with the amount of data increasing with every iteration. Neural networks were established as the preferred classification tool in Chapter 2 early in the process using data for geomod1. Chapter 3 is based on geomod3, and Chapter 4 used the Council Grove portion of Geomod4. Geomod3 and geomod4 are very similar and are discussed in Appendix C. The discussion below is for neural network training for geomod4 based on data from core from 27 wells total, 15 with Council Grove core and 16 with Chase Core (Figure B-1).

As discussed in Chapter 2, several approaches for predicting lithofacies from wire-line log variables and geologic constraining variables (GCV). The neural network approach was determined most effective and was implemented in building the Hugoton model. Chapter 2 describes the neural network used and why it was more effective than other methods including parametric (classical multivariate statistical methods) and other non-parametric methods. Chapter 3 discusses how neural networks were applied as part of the workflow for building geomodels. This was a collaborative project and it should be noted that Geoffrey Bohling optimized neural network parameters through cross-validation, provided guidance on their implementation and wrote the code for batch processing lithofacies prediction for large volumes of wells. This appendix provides more details on some aspects of both chapters:

1) A closer look at how neural networks work, particularly in this application.
2) Description of the workflow for applying neural networks in this project.
3) Discussion on the effectiveness (accuracy).

Neural networks

Neural networks are non-parametric computational models that may be used as classification tools that match patterns of multiple variables with a class of objects. They are particularly useful in classification problems that involve a high number of dimensions and non-linear relationships between variables, and are well suited for lithofacies classification problems. Neural networks have been deployed increasingly over the past twenty years in lithofacies classification (e.g., Baldwin et al., 1990; Rogers et al., 1992; Kapur et al.1998; Grotsch and Mercadier, 1999; Saggaf and Nebrija, 2000; Russell et al., 2003). They owe their name to their structure being similar to that of the human brain's system of intricately connected neurons, and neural networks function in a similar manner. Human brains learn to associate patterns of multiple variables with certain objects. This permits an individual to differentiate very slight variations in an object's features, in human faces for an example, and to use the differences to recognize individuals from a larger population. Like the human brain, a neural network needs to be trained. The neural network used is simple single hidden-layer feed-forward network, which is included in Kipling, an Excel™ add-in developed by Bohling and Doveton (2000). This particular application was chosen because of the ease of operation, simplicity, viewable input and output weights, and it required no special software.

Neural networks are comprised of a single input layer, single output layer, and, theoretically, any number of hidden layers. A simple neural network with a single hidden layer was used in this project. The number of nodes in the input layer is equal to the number of variables (input variables) used to define the lithofacies. In this case six or seven. The number of nodes in the output layer is equal to the number of possible lithofacies (ten). Number of nodes in the hidden layers is theoretically limitless; however twenty were determined to be the optimal number in this classification problem.

Hidden layer node inputs are the sum of the products of the input variables and a weight (a constant). In each hidden layer node, the weighted sums are passed

through a sigmoid transfer function that transforms the inputs to output values ranging between zero and one, forming an S-shaped basis function. These outputs, multiplied by hidden layer node weights (constants), are the inputs to the output layer. Like in the hidden layer, the sums of the products are passed through a transfer function, in this case a softmax function, which scales the output to a value between zero and one. Output values are the probability of the example being evaluated belonging to each of the lithofacies classes.

The neural network is trained in a feed-forward, back-propagating process. Training attempts to find the optimal solution for a set of training data (core-defined lithofacies and associated predictor variables) by adjusting the weights in an iterative process. Setting the weights to values between –1 and 1, randomly, initializes the neural network. During each iteration, input variables are fed forward and outputs are derived. Outputs are compared with the lithofacies probabilities for the example, a set of zeros except for a single unit one (representing the known lithofacies). A weight adjustment factor is computed on the basis of the difference. The weight adjustment factor is applied to the weights between the nodes (back-propagation) to complete the first iteration for the given example. The process is performed on all examples in the training set to complete the iteration. The number of iterations is either defined or the neural network may be allowed to train until a specified level of error has been attained. In this application the number of iterations was set at 100. Because the training process starts from a random set of initial weights there are multiple, equally likely "realizations" of the trained neural network based on a given training dataset.

Neural network in this application

The neural network implemented in Kipling2.xla (Bohling and Doveton, 2000) is a simple single hidden-layer feed-forward network, as illustrated in Figure B-2 and described in Chapter 11 of Hastie et al. (2001). In this neural network there are three parameters to set, number of hidden layer nodes, damping parameter and the number of iterations in the training session. Increasing the number of hidden layer

nodes allows the network to more closely reproduce the details of the training dataset, while fewer hidden layer nodes results in more generalized representation. Increasing the damping parameter forces the network weights to be smaller in magnitude, which results in a smoother or more generalized representation of the training data. More iterations allow a closer reproduction of the training data. However, the number of hidden layer nodes and damping parameter are the principle controls on the neural network's ability to generalize and their values chosen carefully. The neural network tool uses a simple single hidden-layer neural network with *k* softmax-transformed outputs representing probabilities of membership in *k* different classes, and a categorical prediction, using a "winner-take-all" rule.

The process

Optimize lithofacies classes, predictor variables, and neural network parameters

Optimize lithofacies classes and predictor variables

Key to the successful application of neural networks is choosing the optimal lithofacies classification split, predictor variables (e.g., wireline log curves), and neural network parameters. Determining the number of lithofacies classes and the criteria for defining classes involved four objectives: (1) maximum number of lithofacies recognizable by neural networks using petrophysical wireline-log curves and other variables; (2) minimum number of lithofacies needed to accurately represent lithologic and petrophysical heterogeneity; (3) maximum distinction of core-petrophysical properties among classes; and 4) the relative contribution of a lithofacies class to storage and flow. An optimal solution using these criteria resulted in 11 lithofacies. Choosing predictor variables was by logic, expert knowledge, and a trial-and-error process, constrained by availability. Log curves commonly available in wells drilled since 1970 were used, including gamma ray (GR), neutron porosity (Nphi), density porosity (Dphi), deep induction log (ILD), and photoelectric effect (PE). Other log curves such as spectral gamma ray and sonic log carry substantial property information that would be useful in the classification problem, but their

availability is limited. Input variables included raw log curves (GR and PE) or derivatives of the raw curves (neutron and density porosity average, neutron porosity and density porosity difference (N-D), and log base-10 of ILD). PE is an effective tool fro determining lithology, but is not available in approximately 30% of the wells in the1600 well data set. However, neutron porosity and density porosity difference (N-D) was determined to be an effective surrogate for PE, particularly for delineating dolomite from limestone and siliciclastics from carbonate. Because Dphi on wire-line logs uses a limestone matrix density (2.71 g/cc), Dphi in denser dolomite is underestimated and Dphi in less quartz-rich siliciclastics is slightly over estimated. Log base-10 of ILD was used rather than raw data to transform skewed raw data distribution to a more normal distribution.

Two important additional predictor variables derived from geologic data incorporate geologic knowledge in the variable mix. Formation or member tops (Figure B-3) segregate the Wolfcampian into alternating nonmarine, marine, or intertidal half-cycles, fundamentally different depositional environments. Herington and Holmesville are typically intertidal and the rest of the “Shale” formation and members are non-marine. A nonmarine-marine (NM-M) depositional environment indicator variable was assigned to intervals on the basis of the depth of the top and base of stratigraphic formations or members (1 - nonmarine, 2 - marine, or 3 - intertidal). Relative position (RPos) is the position of a particular sample with respect to the base of its respective nonmarine or marine (formation/member) interval. These two geologic constraining variables (GCV) are important because certain facies are restricted to broadly define depositional environments (nonmarine, marine, intertidal), and facies in the Wolfcampian often have predictable vertical stacking patterns (Dubois et al., 2006).

Two geologic constraining variables (GCV) were included to add geologic information to the set of log values: a code representing the depositional environment (1 - nonmarine, 2 - marine, or 3 - intertidal) associated with each of the 25 members (half-cycles) in the model, and a curve representing the relative vertical position

within each half-cycle, ranging from 0 at the base to 1 at the top. The depositional environment indicator variable, MnM, helps to distinguish between lithofacies with similar petrophysical properties but developed in different broad depositional environments. Including the relative position curve, RelPos, allowed the network to encode information regarding the fairly regular succession of lithofacies succession commonly exhibited within each interval, and thus transfer some of that character to the sequence of predicted lithofacies in each well. The two curves were computed from a database of formation tops using Visual Basic code within an Excel spreadsheet. They were then combined with the wire-line log curves to complete the feature vector used as input to the neural network.

Optimize neural network parameters

The two neural network parameters to optimize, network size (number of hidden layer nodes) and damping parameter, were done so by Bohling through cross-validation methods (Bohling, 2006). Various combinations of the two parameters were tested by holding out different wells of the full training dataset from the training process, predicting on the withheld data and comparing predicted and true lithofacies, and repeating the process many times over. Prediction behavior for different parameter combinations was then analyzed to determine the optimal parameter values, in combination. This process was performed on six neural networks, two each, for the cases with PE and without PE (NoPE), for the Upper Chase (Herington through Gage), lower Chase (Towanda to top of Wreford), and Wreford and Council Grove (combined). Training was split stratigraphically to lump cyclothems with similar characteristics. Although the Wreford is part of the Chase Group, it is more similar to Council Grove cyclothems and was included with the Council Grove.

Crossvalidation results were compared using two metrics, an objective function and misallocation costs. The objective function is a measure of accuracy in the prediction results that is used in the neural network in Kipling2.xls. Misallocation costs are “costs” assigned to the error. Cost is a function of similarity or dissimilarity

between actual and assigned facies. The more dissimilar, the higher the cost (Table B-2). An example of crossvalidation for one example (Wreford and Council Grove PE) is given in Figure B-4. In this case the optimal parameters for network size and damping parameter is 20 nodes and 1 for the objective function metric and 10 and 1 for the cost metric. In this case 20 nodes and damping of 1 were chosen because the 20-node option was significantly better than alternatives when considering the objective function metric and minimally less effective than the 10-node option considering the cost metric. The same parameter values were determined most optimal for all but one of the six neural network cases. The one exception is for the Wreford-Council Grove NoPE case where a damping parameter of 10 was used.

Implementation in Kipling2.xla

Training neural networks and using the trained neural networks to assign lithofacies at half-foot (0.15 m) intervals was accomplished through the following workflow:

1. Organize training data in a tabular form with lithofacies and predictor variables (six or seven) in columns, one example per row (Table B-3).
2. Assemble six sets of files for wells without lithofacies, one set for each of the six neural network cases (defined in 3). Files contain predictor variables (six or seven) in a Log Ascii Standard (LAS) format, one file per well.
3. Train six neural networks, two each (PE and NoPE) for three stratigraphic intervals, upper Chase (Herington through Gage), lower Chase (Towanda to top of Wreford), and Wreford and Council Grove (combined).
4. Train five neural networks for each case using optimal node and damping parameters and 100 iterations. Choose neural network with the lowest objective function.
5. Use the batch process function to predict lithofacies for wells without lithofacies for each of the six cases.

6. Assemble the predicted lithofacies for the three stratigraphic intervals in another application.

Training neural networks in Kipling2.xla is quite simple: 1) Select the training predictor variables (Figure B-5), and 2) Set neural network parameters (Figure B-6) and click “OK”. During training, a measure of the mismatch (objective function) between the actual and predicted lithofacies is recorded after each iteration. Plotting objective function versus iteration provides a view of the training session (Figure B-7). In all cases, the plots approached asymptotic by 40 iterations, and models improved only slightly over the next 100 iterations. Final weights for inputs to, and outputs from the hidden layer are also recorded (Tables B-4 and B-5). The weights are essentially the trained neural network.

Batch process prediction of lithofacies is equally as simple. The neural network chosen is selected (Figure B-8) and the network is “pointed” to a file folder containing the LAS files for processing. Match predictor variables in LAS files to be processed with those in the trained neural network and click “OK” (Figure B-9). The wells are processed and results are exported in an LAS file format, one per well. An example of the output is given in Table B-6. Header lines provide summary information. The first three columns in the table are fields from predictor variable data file and the next eleven are probabilities that the example is one of the eleven lithofacies. Probabilities sum to one and the facies determined to be most probable is the discrete predicted facies that is predicted (winner take all). The “winner” in each example is shaded. The second most probable lithofacies is usually a similar lithofacies. When an error is made, the correct lithofacies is usually the next most probable lithofacies. Probabilities are data that could be used lithofacies prediction and model building and worthy of further study.

Lithofacies prediction accuracy

Accurate representation of eleven lithofacies in the model is important because lithofacies-based petrophysical properties were used to estimate water saturations. However, accuracy of lithofacies assignment in wells without core cannot be determined directly. The 1574 wells without core and the 26 with core (1600 "node" wells) are the basis for lithofacies in the geomodel. Node wells are upscaled from the half-foot (0.15m) to layer scale (2-foot, 0.6 m) and the volume between the wells is populated with lithofacies using stochastic methods. Both quantitative and subjective evaluations of lithofacies prediction accuracy at the node well scale were discussed in Chapters 2 and 3, but addition al detail is given here.

Success metrics

A high degree of absolutely correct classification should not be anticipated because: 1) lithofacies are based on subjective observations, 2) measured properties (log predictor variables) of lithofacies overlap in feature space, and 3) measuring devices tend to average over a two-foot (0.6 m) interval while lithofacies are defined at the half-foot scale (0.15 m). Having a facies classification that is close to the actual (within one facies in the continuum) may be deemed satisfactory because the associated flow capacity as a function of porosity and other physical characteristics of adjacent facies are similar to the actual facies (Dubois et al., 2006). In addition to being correct or nearly correct, it is important that the number of a particular facies predicted by any classifier be relatively close to that in the overall population in order that the ultimate model accurately represents the volumetric distribution of facies. Digital lithofacies codes were required for computer applications and were assigned in a manner that approximates their position in the lithofacies spectrum, but not perfectly. Because the main gas pay facies (facies code 6-10, very-fine crystalline dolomite, packstone-grainstone, phylloid algal bafflestone, fine to medium crystalline dolomite and fine-grained sandstone) are the most important in terms of gas storage

and flow capacity, their accurate representation is critical. To judge whether the objectives were met and to compare classifiers five metrics were used:

1. Close (within one lithofacies) – all lithofacies
2. Correct – all lithofacies
3. Close (within one lithofacies) - lithofacies code 6 through 10
4. Correct - lithofacies code 6 through 10
5. Representation - ratio of lithofacies code 6 through 10 predicted vs. actual.

What is considered "close" in terms of lithofacies?

Lithofacies in the Wolfcampian represent continuum of sedimentary rock types that could be lumped and split in many ways. Finer splitting would result in more refined depositional facies interpretation, provided the finer lithofacies could be recognized on wireline logs. For example, fine-grained peloidal packstone would have been deposited in a different environment than a coarse-grained-bioclast grainstone. However the two lithofacies are indistinguishable by wire-line log signature and the two sub-lithofacies are lumped with the packstone-grainstone lithofacies. A delicate balance exists between accuracy and detail required for maximum utility. An eleven lithofacies split was deemed optimal.

As stated above, digital lithofacies codes approximate their position in the lithofacies spectrum, but not perfectly. Adjacent lithofacies are generally similar, but not in every case. Lithofacies are considered close if the lithofacies predicted is considered a "neighbor", within one lithofacies. Lithofacies that are considered "close" to another are listed below in order of lithofacies code assigned:

1. Coarse-grained siltstone (continental) – 11, very-fine-grained sandstone (continental); and 2, fine-medium grained siltstone (continental)
2. Fine-medium grained siltstone (continental) – coarse-grained siltstone (continental)
3. Siltstone (marine) – 1, coarse-grained siltstone (continental); 4, carbonate mudstone; and 10, very-fine-grained sandstone (marine)

4. Carbonate mudstone – 3, siltstone (marine); and 5, wackestone
5. Wackestone – 4, carbonate mudstone; and 7, packstone-grainstone
6. Very fine to fine crystalline dolomite – 7, packstone-grainstone; and 9, medium crystalline moldic dolomite
7. Packstone-grainstone – 5, wackestone; 7, packstone-grainstone; 8, phylloid algal bafflestone; and 9 medium-crystalline moldic dolomite
8. Phylloid algal bafflestone – 6, very fine to fine crystalline dolomite; and 7 packstone-grainstone
9. Medium crystalline moldic dolomite – 6, very fine to fine crystalline dolomite; and 7 packstone-grainstone
10. Very-fine-grained sandstone (marine) – 3, siltstone (marine); and 11, very-fine-grained sandstone (continental)
11. Very-fine-grained sandstone (continental) – 10, very-fine-grained sandstone (marine); and 1, coarse-grained siltstone (continental)

Adjacent lithofacies codes are generally close neighbors in terms of petrophysical properties, as well as texture and grain type, except for lithofacies 11 (continental very-fine-grained sandstone). Lithofacies 11 belongs at the other end of the spectrum, and in the geomodel it is given the code 0. Permeability for a given porosity is generally greatest with higher numbers starting with code 10 and descending to lithofacies code 2 (fine-to medium-grained siltstone). Lithofacies code 2 has the lowest permeability for a given porosity. At this point in the spectrum, the relationship reverses with code = 1 having greater permeability for a given porosity, and code 11 even greater permeability.

Quantitative measures for lithofacies prediction accuracy

The closest approximation of a true quantitative test of lithofacies prediction accuracy at the node wells is the comparison of actual versus predicted lithofacies in wells with core by using a Jackknife approach: data from one well is withheld from

training, lithofacies is predicted for withheld data and compared with its known lithofacies, and the process is repeated through the entire data set. Figure B-1 illustrates the distribution of core data for the Chase and Council Grove. A Jackknife test was completed for the three stratigraphic intervals and summary statistics for Chase and Council Grove results are given in Table B-7. Also in Table B-7 are summary statistics for the test where neural networks are trained on all training data and predictions made on the same training data (train-test-all, or TTA). In the Jackknife experiment, for each iteration where one well was withheld, three neural networks were trained for each of the three stratigraphic intervals for each case (PE and NoPE), nine networks in all. The three having the lowest objective function were chosen and used to predict lithofacies in the withheld well. The process was repeated throughout the data set and results of all wells summed for evaluation. For the TTA, actual geomod4 neural networks were used. The neural networks selected were the ones having lowest objective function values chosen from a set of five neural network models.

The Jackknife approach yields the worst possible results because the well being tested is the furthest possible from the training data. Geographic position was a primary consideration for core selection, and spacing was purposely fairly wide for efficiency. Because lithofacies vary across the ramp, removing one well from the training can significantly reduce the number of examples of certain lithofacies for training and negatively impact lithofacies prediction for the withheld well. The train-test-all (TTA) method is likely to yield the best possible results, which are likely too optimistic. Neither is a direct test of lithofacies prediction in the model, and lithofacies accuracy in the model probably lies somewhere between the two types of tests.

Summary statistics

Table 8 provides summary statistics for the Jackknife and TTA tests for the Chase, Council Grove, and Wolfcampian (combined intervals). Chase sample count is

6790 and Council Grove is 6504 half-foot (0.15 m) intervals. The Jackknife approach has consistently lower success metric values than does TTA. If actual model node well values are somewhere between the two, lithofacies prediction accuracy for the Wolfcampian is likely 50-66% correct and the predicted lithofacies is within one lithofacies 83-90% of the time. Accuracy is slightly better for the main gas "pay" lithofacies, lithofacies codes 6 through 10 (in order: very fine to fine crystalline dolomite, packstone-grainstone, phylloid algal bafflestone, medium crystalline moldic dolomite, and marine very-fine-grained sandstone). The pay zone lithofacies are likely to be correctly predicted 57-74% of the time and are predicted within one lithofacies 80-90% of the time.

Pivot charts provide more detailed statistics by lithofacies for Jackknife tests (Table B-8) and the TTA approach (Table B-9). Actual and predicted lithofacies occurrences are shown with the diagonal indicating the number of correctly predicted lithofacies in the upper of the two pivot charts in each table. Incorrectly predicted lithofacies counts are shown in the same row in the predicted lithofacies column. The representation metric (predicted lithofacies count/actual lithofacies count) is given by lithofacies is given at the bottom of the upper pivot chart in each table. The lower pivot chart in each table is the same data expressed as a percent of the row (percent of actual lithofacies). Proportion of each lithofacies in the training set is shown on the left of each table. It is important to consider the volumetric proportions when evaluating the data, particularly when only considering data expressed in terms of percent. The following general observations are made:

1. In both Jackknife and TTA, the four lithofacies that are most successfully predicted are continental coarse-grained siltstone continental (1), the most prevalent lithofacies, and the three most dominant pay lithofacies, packstone-grainstone (7), medium crystalline moldic dolomite (9), and marine very-fine-grained sandstone (10).

2. Carbonate mudstone is poorly predicted and not adequately represented when evaluated using either approach. However, it comprises a relatively small volume in the Wolfcampian (6.2%).
3. Lithofacies 6, 8, and 11 (very fine to fine crystalline dolomite, phylloid algal bafflestone, and continental very-fine-grained sandstone) are poorly predicted by the Jackknife approach. However, the correct success metric for the three lithofacies were approximately double and representation metric much improved in the TTA case.
4. Continental coarse-grained siltstone continental (1) is over represented by 18% in both tests, mostly at the expense of continental fine-medium grained siltstone (2).
5. Continental very-fine-grained sandstone (11) is under represented in both test cases mostly due to this lithofacies being predicted as Continental coarse-grained siltstone continental (1).

Discussion of summary statistics

Lithofacies accuracy in the model node wells is likely to lie somewhere between the data presented for the two tests. The question is, which is more likely, particularly in cases where there is significant departure between the two tests (lithofacies 6, 8, 9, 10, and 11). The answer to the question is not quantitatively resolvable, but clues to the disparities lie in the distribution of core with respect to the distribution of these particular lithofacies on the ramp. In all cases, but in particular lithofacies 8, 9, 10, and 11, the lithofacies are confined to a particular position on the ramp and are represented in fewer wells than are other more widely distributed lithofacies. In the Jackknife test, where one well is withheld for testing, the representation of that particular lithofacies in the training set is significantly reduced. Phylloid algal bafflestone (8) comprises less than 1% of the rock volume and is restricted to the Council Grove, and most examples are in three wells in Stevens county (Figure B-1). Medium crystalline moldic dolomite (9), the most prolific

Chase pay zone in terms of storage and flow capacity, is more widespread, covering Stevens and eastern Texas County. However, it is well represented in core from only six wells. Marine very-fine-grained sandstone (10) dominates in the western third of the study area in the Chase and continental very-fine-grained sandstone (11) is most prevalent in only the northwest one-quarter of the study area in the Council Grove. In both cases, the removal of training data of the test well in the Jackknife approach appears to significantly impact the accuracy for prediction of lithofacies on the test well. For these important lithofacies, the accuracy in the node wells could be closer to that represented by the TTA test, although this cannot be proven.

Porosity and permeability in the node wells

Accurate representation of porosity and permeability, controls the utility of the Hugoton geomodel for reservoir management. Because both porosity and permeability are lithofacies dependent, it is important to understand the potential error that is introduced by error in lithofacies prediction. For a given measured log porosity, corrected log porosity varies with lithofacies (Table B-10). Porosity correction algorithms, developed by John Doveton (Chapter 3 and Dubois et al., 2006), were based on empirical data. Impact of lithofacies error is illustrated in Table B-11. The greatest potential error is in the cases where dolomite (lithofacies 6 and 9) or marine very fine-grained sandstone (lithofacies10) is involved. When other lithofacies are predicted as these lithofacies, porosity is generally higher than actual and porosity is lowered when the dolomite lithofacies (lithofacies 6 and 9) or marine very fine-grained sandstone (lithofacies 10) are predicted incorrectly. The potential for error in pore-volume is –15% to +32% for rocks having 10% porosity, a significant range in terms of reservoir volume.

As with porosity, permeability varies with lithofacies for given corrected porosity. Alan Byrnes developed the empirical relationships that define *insitu* Klinkenberg permeability as a function of lithofacies and porosity for geomod4:

```
perm =IF(Facies=1,Pow(10,(8.00*Log(phi_pct)-9.96)),perm)
perm =IF(Facies=2,Pow(10,(8.00*Log(phi_pct)-10.05)),perm)
perm =IF(Facies=3,Pow(10,(7.74*Log(phi_pct)-9.41)),perm)
perm =IF(Facies=4,Pow(10,(9.20*Log(phi_pct)-10.80)),perm)
perm =IF(Facies=5,Pow(10,(7.61*Log(phi_pct)-8.94)),perm)
perm =IF(Facies=6,Pow(10,(9.70*Log(phi_pct)-11.80)),perm)
perm =IF(Facies=7,Pow(10,(7.09*Log(phi_pct)-7.81)),perm)
perm =IF(Facies=8,Pow(10,(8.65*Log(phi_pct)-8.29)),perm)
perm =IF(Facies=9,Pow(10,(9.70*Log(phi_pct)-10.80)),perm)
perm =IF(Facies=10,Pow(10,(9.75*Log(phi_pct)-11.62)),perm)
perm =IF(Facies=11,Pow(10,(6.65*Log(phi_pct)-7.88)),perm)
```

Permeability ranges more than two orders of magnitude (0.009 – 2.291) across the lithofacies spectrum for a given porosity of 10% (Table B-12).

Estimation of error

Error in pore volume

As with lithofacies, it is not possible to determine directly the error in pore volume (product of porosity and height) in the model, nor even at the node wells. However, a range of possible error introduced by inaccurate lithofacies can be estimated by comparing pore volumes calculated for core lithofacies using corrected log porosity values with pore volumes calculated for lithofacies using the Jackknife and TTA approaches (Table B-13). Error can be analyzed from two perspectives: 1) actual pore volume by predicted lithofacies (sum by lithofacies in the table), and 2) pore volume estimated for the interval (sum by intervals in the table). The first metric is a comparison of lithofacies pore volume, however the second is more critical for reservoir modeling because it identifies potential volumetric error in the model. When summed by lithofacies, potential pore volume error is proportional to lithofacies prediction error (e.g., carbonate mudstone pore volume is significantly under

represented in the model). When summed by interval, pore volume error is the error introduced by error in lithofacies assignment (Table B-11). Pore volume error due to error in lithofacies is always in the negative direction for dolomite lithofacies and positive for marine siltstone and carbonated mudstone. On the basis of this analysis, pore volume in the model is likely to be overestimated by 5.9% to 6.1%, due to error in lithofacies prediction.

Error in permeability

Flow capacity (product of permeability and height, Kh) and is an important component of a reservoir model because it represents the capacity of the reservoir to produce hydrocarbon. It was analyzed in the same manner as pore volume (above) and data are presented in Table B-14. One difference is that permeability is a power law function of porosity (above). Thus small error in porosity results in more substantial absolute error in permeability, as measured by the % difference of actual versus predicted, than it does for pore volume. Log 10 of the error would be a more appropriate, however, the results are close enough to actual that it was not necessary to go to that length to demonstrate that Kh is probably represented accurately in the model. On the basis of the analysis presented, Kh in the model is likely to be +8.2% to –8.5% of actual.

Conclusions

A single hidden layer neural network was successfully deployed for lithofacies prediction in nearly 1600 “node” wells in the Hugoton geomodel. Accurate lithofacies representation in the model is important because petrophysical properties (porosity, permeability and water saturation) are lithofacies dependent. A high degree of absolute accuracy was not expected and being close, assigning a similar lithofacies, is nearly as good because similar lithofacies have similar properties. Lithofacies prediction accuracy for node wells in the geomodel are likely 50-66% correct and within one lithofacies 83-90% of the time. Accuracy is slightly

better for the main gas "pay" lithofacies, very fine to fine crystalline dolomite, packstone-grainstone, phylloid algal bafflestone, medium crystalline moldic dolomite, and marine very-fine-grained sandstone. The pay zone lithofacies are likely to be correctly predicted 57-74% of the time and are predicted within one lithofacies 80-90% of the time. For reservoir performance prediction, accurate representation of properties in the model is more important than lithofacies. Pore volume is likely over predicted by 6% at the node wells and permeability may be off 8% (plus or minus). The latter is insignificant because permeability is a power law function of porosity. Although considered tolerable, knowing the expected pore volume error is helpful for reservoir analysis and management decisions based on the Hugoton geologic and property model.

References

Baldwin, J.L., Bateman, R.M. and Wheatley, C.L., 1990. Application of a neural network to the problem of mineral identification from well logs. The Log Analyst, 3, 279-293.

Bohling, G.C. and Doveton, J.H., 2000. Kipling.xla: An Excel add-in for nonparametric regression and classification. Kansas Geological Survey, http://www.kgs.ku.edu/software/Kipling/Kipling1.html (accessed March 4, 2007).

Bohling, G. C., 2006, Technology to manage large digital data sets: *chapter in*, M. K. Dubois, A. P. Byrnes, S. Bhattacharya, G. C. Bohling, J. H. Doveton, and R. E. Barba, Hugoton Asset Management Project (HAMP): Hugoton Geomodel Final Report, Kansas Geological Survey, Open-File Report 2007-6, chapter 5, 13 p. http://www.kgs.ku.edu/PRS/publication/2007/OFR07_06/index.html (Accessed March 22, 2007.)

Dubois, M. K., A. P. Byrnes, G. C. Bohling, and J. H. Doveton, 2006, Multiscale geologic and petrophysical modeling of the giant Hugoton gas field (Permian), Kansas and Oklahoma: *in* P. M. Harris and L. J. Weber, eds., Giant reservoirs of the world: From rocks to reservoir characterization and modeling: American Association of Petroleum Geologists Memoir 88, p. 307-353.

Dubois, M. K., G. C. Bohling, and S. Chakrabarti, *in press*, Comparison of four approaches to a rock facies classification problem: Computers & Geosciences.

Grotsch, J. and Mercadier, C., 1999. Integrated 3-D reservoir modeling based on 3-D seismic: the Tertiary Malampaya and Camago buildups, offshore Palawan, Philippines. American Association of Petroleum Geologists Bulletin, 83 (11), 1703-1728.

Hastie, T., Tibshirani, R. and Friedman, J., 2001. The Elements of Statistical Learning: Data Mining, Inference, and Prediction. Springer, New York, NY, 533 pp.

Rogers, S.J., Fang, J.H., Karr, C.L. and Stanley, D.A., 1992. Determination of lithology from well logs using neural networks. American Association of Petroleum Geologists Bulletin, 76, 731-739.

Russell, S.D., Abkar, M., Vissapragada, B. and Walkden, G.M., 2002. Rock types and permeability prediction from dipmeter and image logs: Shuaiba reservoir (Aptian), Abu Dhabi. American Association of Petroleum Geologists Bulletin, 86 (10), 1709-1732.

Saggaf, M.M. and Nebrija, E.L., 2000. Estimation of lithologies and depositional facies from wire-line logs. American Association of Petroleum Geologists Bulletin, 84, 1633-1646.

	Geomod1	Geomod2	Geomod3	Geomod4
Council Grove core	8	9	9	15*
Chase core	0	2	8	16**
Combined core wells	8	9	14	27***
Wells without core	515	1250	1350	1574
Number of lithofacies	8	10	11	11
Model interval	Council Grove	Council Grove and Chase	Council Grove and Chase	Council Grove and Chase
Model area	Kansas	Kansas	Kansas and Oklahoma	Kansas and Oklahoma
Chapter	2	NA	3	4

* 17 wells in study, 15 in Council Grove neural network training set
** 17 wells in study, 16 in Chase neural network training set
*** 29 wells in study, 27 wells in neural network training set

Table B-1. Data volumes, model intervals, geographic coverage, and chapters where discussed for four Hugoton geomodel iterations.

Actual	Assigned Facies										
Facies	F1	F2	F3	F4	F5	F6	F7	F8	F9	F10	F11
F1	0	1	1.5	3	4	4	4	4	4	1.5	1
F2	1	0	2	4	4	4	4	4	4	3	2
F3	1.5	2	0	1	2	3	4	4	4	1	1.5
F4	3	4	1	0	1	2	3	3	4	2	3
F5	4	4	2	1	0	2	1	2	3	4	4
F6	4	4	3	2	2	0	1	1	1	4	4
F7	4	4	4	3	1	1	0	1	1	4	4
F8	4	4	4	3	2	1	1	0	2	4	4
F9	4	4	4	4	3	1	1	2	0	4	4
F10	1.5	3	1	2	4	4	4	4	4	0	1
F11	1	2	1.5	3	4	4	4	4	4	1	0

Table B-2. Misallocation cost matrix. Cost is a function of dissimilarity between actual and assigned facies. The more dissimilar, the higher the cost.

Formation-Member	Well_Name	Depth	Litho-facies	GR	ILD_LOG_10	N-DPHI%	PHIND%	PE	NM_M	RELPOS
A1 SH	NEWBY	2840.5	2	72.53	0.555	6.3	13.45	3.2	1	0.326
A1 SH	NEWBY	2841	2	67.99	0.542	6.1	14.35	3.1	1	0.302
A1 SH	NEWBY	2841.5	1	60.31	0.525	5.0	14.1	3.2	1	0.279
A1 SH	NEWBY	2842	1	55.52	0.504	6.3	11.55	3.2	1	0.256
A1 SH	NEWBY	2842.5	1	56.07	0.486	5.0	11	3.2	1	0.233
A1 SH	NEWBY	2843	1	62.67	0.473	-2.6	15.8	3.2	1	0.209
A1 SH	NEWBY	2843.5	1	66.9	0.471	-2.2	21.4	3.2	1	0.186
A1 SH	NEWBY	2844	1	68.54	0.477	3.1	24.25	3.2	1	0.163
A1 SH	NEWBY	2844.5	1	68.7	0.483	3.3	22.85	3.2	1	0.14
A1 SH	NEWBY	2845	4	63.2	0.489	9.5	17.25	3.4	2	0.116
A1 SH	NEWBY	2845.5	4	60.33	0.493	11.6	15.6	3.7	2	0.093
A1 SH	NEWBY	2846	4	58.16	0.491	12.7	14.35	3.8	2	0.07
A1 SH	NEWBY	2846.5	4	52.61	0.481	9.9	11.45	3.9	2	0.047
A1 SH	NEWBY	2847	2	45.72	0.464	5.2	8.8	3.9	1	0.023
A1 LM	NEWBY	2847.5	5	35.92	0.441	4.5	7.95	4.0	2	1
A1 LM	NEWBY	2848	5	26.62	0.422	3.6	10.7	4.3	2	0.988
A1 LM	NEWBY	2848.5	6	24.14	0.398	5.9	12.55	4.0	2	0.976
A1 LM	NEWBY	2849	6	24.36	0.375	6.5	12.95	3.9	2	0.963
A1 LM	NEWBY	2849.5	6	23.28	0.35	6.5	11.85	4.1	2	0.951
A1 LM	NEWBY	2850	6	25.7	0.334	7.7	10.95	4.1	2	0.939
A1 LM	NEWBY	2850.5	6	28.2	0.336	8.2	11.2	3.7	2	0.927
A1 LM	NEWBY	2851	6	28.35	0.352	8.8	12.1	3.7	2	0.915
A1 LM	NEWBY	2851.5	6	31.71	0.377	9.0	12.8	3.6	2	0.902
A1 LM	NEWBY	2852	6	35.52	0.405	9.1	12.75	3.3	2	0.89

Table B-3. Sample of input data for a neural network training session. Half-foot (0.15 m) intervals include lithofacies defined in core, five wire-line log curves or their derivatives and two geologic constraining variables (last two columns).

Input-to-hidden layer weights

Node	Constant	GR	ILD_LOG_10	N-DPHI%	PHIND%	PE	NM_M	RELPOS
1	-0.329596643	-0.267277	-1.594384037	1.871736	-2.002115	0.831568	-0.676657	1.115806
2	0.65441899	-0.275647	1.636556674	-0.07264	-0.341501	1.17123	0.237242	0.937584
3	-1.564913201	1.222985	-0.483246109	-0.397916	2.79964	0.941885	-0.860552	-0.796483
4	-0.990040104	-0.207388	0.078752552	-0.863665	-1.310306	1.24311	1.462427	0.801518
5	0.645631145	1.788637	1.851967278	0.230077	-0.155956	-0.471591	-1.111277	0.036138
6	0.05380495	0.074359	-0.084250287	-0.094692	0.050045	0.652467	2.728652	2.062532
7	-0.584758625	0.236252	-1.624040389	-1.968773	-2.217787	1.296287	-1.03191	-0.103279
8	-2.448999396	-3.301992	1.035865125	0.50594	1.225348	-0.578483	-0.357206	-0.031313
9	-0.366314296	1.33795	-0.937768001	0.228006	0.385172	2.963993	0.635678	1.279707
10	0.084732115	-0.209047	-0.322168116	-0.251814	-0.890316	-0.714204	-1.483677	1.341003
11	1.247201616	1.099817	0.852517688	0.838744	-1.047927	-0.97679	0.327684	-2.286051
12	0.199832667	0.046429	-0.31227879	-2.289553	0.94651	0.583575	-0.608837	-0.488652
13	0.666178848	0.285035	1.281585461	-0.512088	2.477905	2.114456	-0.849342	0.611696
14	-0.896025412	-1.109323	1.612677229	-0.504198	1.280544	1.047209	1.313703	-0.299143
15	-0.739317735	0.083081	-0.640543547	0.537394	0.478659	0.32588	2.834217	1.553041
16	0.124993395	-0.17345	-0.90628134	-1.525854	-1.923525	-1.651846	0.004141	-1.30996
17	-0.870687665	1.409209	0.766977231	-0.554423	-0.7975	0.328386	1.450828	1.527244
18	0.268474677	0.677007	-1.46675301	1.141078	0.141312	-0.856803	-1.482338	3.282297
19	0.236114805	-0.022666	0.030208025	0.728398	-0.764624	1.407119	1.461846	-0.961055
20	-0.661501466	-2.457459	-0.269488453	1.326038	-0.712979	1.266612	-0.333818	0.414005

Table B-4. Final weights as determined by training session that are applied at the input to the twenty hidden layer nodes, and twenty final biasing constants, one for each input node.

Hidden layer-to-output weights

Node	F11gm401	F11gm402	F11gm403	F11gm404	F11gm405	F11gm406	F11gm407	F11gm408	F11gm409	F11gm410	F11gm411
Constant	-0.088116515	0.743405485	0.780914289	0.335209144	-1.565020053	-0.490051549	0.160364165	-0.2455398	-0.778734061	1.017331453	0.114495484
1	0.749064855	1.580235287	-1.098129769	0.229516803	0.382373082	0.50544227	1.134914087	-1.93736531	-0.363388732	-1.31130987	0.062829723
2	-0.537850125	-0.537064216	1.796691146	0.38187121	-0.844114079	-0.430923077	0.615570447	0.001601777	-0.347464184	-0.91964306	0.827350174
3	-0.802595579	1.28558058	-1.556211132	1.023359203	-0.823858691	0.940882666	-0.461067959	2.032098361	-0.36505976	-1.200275949	-0.026941121
4	-1.441315822	0.239443958	-1.424801729	0.658499106	1.066130099	0.406035374	1.578790407	0.447329	-0.242174007	-0.520785918	-0.719356056
5	1.941821194	1.589412042	-0.319279894	-0.773398933	1.604082008	-1.338790625	-0.621103723	-1.175639975	-0.388746869	0.011319359	-0.627765125
6	-1.489035438	-1.138885201	1.037261016	0.261343873	1.751596646	0.400954159	-0.595377297	0.816156504	-0.366987571	1.177245788	-1.917496088
7	1.676213989	-1.177793192	-0.360913211	-1.060432035	0.395839333	-0.329190651	1.120072497	-0.126707085	-0.438733059	-1.219051915	1.539250137
8	-0.527798749	-0.751088547	-2.497819468	-1.570327334	0.755626403	2.17754243	2.6862695	0.198454682	-0.337898663	-0.314722853	0.270401562
9	-0.149436909	0.131693665	-1.057530491	-0.899229581	1.226569637	2.997003633	-0.609532242	1.419067985	-0.360272089	-1.3530845	-1.342785414
10	0.277607674	1.468519313	-0.09954993	0.81924591	-0.863773873	-1.013165777	-1.411619695	-1.692082808	-0.441250943	0.761262903	2.116012114
11	1.765053289	-1.035018197	2.770231323	0.8319374	0.521306347	0.240019547	-0.745370652	-2.000501918	-0.509672431	-1.095955397	-0.771895276
12	0.558588853	-0.274295842	-0.400030982	-1.123417895	-0.195267516	-1.05407274	0.813847913	1.372132786	-0.41294072	0.409163078	0.158328077
13	1.068218746	2.726978354	0.996597048	0.314276465	-1.223723776	-1.705933911	0.845433827	0.435611573	-0.412025728	-0.926599039	-2.209261535
14	0.876622558	0.076944731	-1.368805125	0.272414336	2.12309241	-0.621513353	0.016147553	0.36169665	-0.368418474	-0.574080083	-0.774804985
15	-1.297638979	-1.767028719	2.046958304	1.071247608	-0.07279951	0.492042276	-0.096149957	0.534451754	-0.38038793	1.291890968	-1.737132019
16	-1.401824184	-0.297681353	-1.0418956	-0.044178747	1.127919428	0.862191856	-0.628986868	-1.594333607	-0.392448774	2.051702581	1.400164441
17	-0.560345075	-0.965800474	-0.687723176	2.115044142	0.771449886	-0.525995339	1.333069484	-0.0600166	-0.283054906	-0.18131204	-0.980167939
18	2.217667038	0.122464215	-0.447184866	-2.200681921	-0.457660387	1.069458209	0.074572568	-2.954137867	-0.332231163	0.405774199	2.500149628
19	-1.711254804	-0.45253877	1.092023308	0.016717677	-0.54858085	0.928308571	1.753837545	1.477443107	-0.460281814	-0.497875721	-1.662603155
20	0.163680038	-0.148265906	-1.140538423	1.39990785	1.047660176	-0.252389468	-1.230499588	1.352019166	-0.275568727	-0.704794712	-0.082875645

Table B-5. Final weights as determined by training session that are applied to the output from each of twenty hidden layer nodes prior to input into the eleven facies output nodes.

Prediction results using data sheet Wrf-Cgrv_PE and neural net sheet NNet26_WrCg-PE

User comment on neural net sheet:	WrfCG PE 20/1/100						
Number of predictor variables:	7						
Predictor variables in NNet26_WrCg-PE:	GR	ILD_ LOG_10	N-DPHI%	PHIND%	PE	NM_M	RELPOS
Predictor variables in Wrf-Cgrv_PE:	GR	ILD_ LOG_11	N-DPHI%	PHIND%	PE	NM_M	RELPOS
Categorical response variable:	F11gm4						
Number of categories:	11						
Continuous response variable:	[NONE]						
Number of variables copied:	3						
Variables copied from Wrf-Cgrv_PE:	F11gm4	ElogDeptl	Lease_Name				

Core F11gm4	Elog Depth	Lease_Name	Probabilities F1	F2	F3	F4	F5	F6	F7	F8	F9	F10	F11	Predicted F11gm4 kpred	Max. Prob-ability pmax
2	2806.5	SHRIMPLIN	0.36	0.62	0.01	0.00	0.00	0.00	0.00	0.00	0.00	0.00	0.00	2	0.62
2	2807	SHRIMPLIN	0.32	0.66	0.01	0.00	0.00	0.00	0.00	0.00	0.00	0.00	0.00	2	0.66
2	2807.5	SHRIMPLIN	0.36	0.62	0.01	0.00	0.00	0.00	0.00	0.00	0.00	0.00	0.00	2	0.62
2	2808	SHRIMPLIN	0.44	0.54	0.01	0.00	0.00	0.00	0.00	0.00	0.00	0.00	0.00	2	0.54
2	2808.5	SHRIMPLIN	0.64	0.34	0.00	0.00	0.00	0.00	0.00	0.00	0.00	0.00	0.01	1	0.64
2	2809	SHRIMPLIN	0.44	0.55	0.01	0.00	0.00	0.00	0.00	0.00	0.00	0.00	0.00	2	0.55
1	2809.5	SHRIMPLIN	0.40	0.58	0.01	0.00	0.00	0.00	0.00	0.00	0.00	0.00	0.00	2	0.58
1	2810.5	SHRIMPLIN	0.56	0.42	0.01	0.00	0.00	0.00	0.00	0.00	0.00	0.00	0.01	1	0.56
1	2811	SHRIMPLIN	0.69	0.26	0.00	0.00	0.00	0.00	0.00	0.00	0.00	0.00	0.04	1	0.69
1	2811.5	SHRIMPLIN	0.71	0.18	0.00	0.00	0.00	0.00	0.00	0.00	0.00	0.00	0.10	1	0.71
1	2812	SHRIMPLIN	0.66	0.14	0.00	0.00	0.00	0.00	0.00	0.00	0.00	0.00	0.19	1	0.66
1	2812.5	SHRIMPLIN	0.54	0.07	0.00	0.00	0.00	0.00	0.00	0.00	0.00	0.00	0.37	1	0.54
1	2813	SHRIMPLIN	0.50	0.06	0.00	0.00	0.00	0.00	0.00	0.00	0.00	0.00	0.43	1	0.50
1	2813.5	SHRIMPLIN	0.48	0.05	0.00	0.00	0.00	0.00	0.00	0.00	0.00	0.00	0.47	1	0.48
11	2734	CROSS H CATTLI	0.15	0.11	0.00	0.00	0.00	0.01	0.00	0.00	0.00	0.00	0.72	11	0.72
11	2734.5	CROSS H CATTLI	0.15	0.08	0.00	0.00	0.00	0.00	0.00	0.00	0.00	0.00	0.76	11	0.76
11	2735	CROSS H CATTLI	0.16	0.07	0.00	0.00	0.00	0.00	0.00	0.00	0.00	0.00	0.76	11	0.76
11	2735.5	CROSS H CATTLI	0.29	0.12	0.00	0.00	0.00	0.00	0.00	0.00	0.00	0.00	0.58	11	0.58
11	2736	CROSS H CATTLI	0.46	0.16	0.00	0.00	0.00	0.00	0.00	0.00	0.00	0.00	0.37	1	0.46
1	2736.5	CROSS H CATTLI	0.61	0.18	0.00	0.00	0.00	0.00	0.00	0.00	0.00	0.00	0.20	1	0.61
1	2737	CROSS H CATTLI	0.65	0.19	0.00	0.00	0.00	0.00	0.00	0.00	0.00	0.00	0.15	1	0.65
11	2737.5	CROSS H CATTLI	0.62	0.18	0.00	0.00	0.00	0.00	0.00	0.00	0.00	0.00	0.18	1	0.62
11	2738	CROSS H CATTLI	0.52	0.11	0.00	0.00	0.00	0.00	0.00	0.00	0.00	0.00	0.36	1	0.52
11	2738.5	CROSS H CATTLI	0.32	0.05	0.00	0.00	0.00	0.00	0.00	0.00	0.00	0.00	0.63	11	0.63
11	2739	CROSS H CATTLI	0.21	0.02	0.00	0.00	0.00	0.00	0.00	0.00	0.00	0.00	0.76	11	0.76
11	2739.5	CROSS H CATTLI	0.20	0.02	0.00	0.00	0.00	0.00	0.00	0.00	0.00	0.00	0.77	11	0.77
11	2740	CROSS H CATTLI	0.18	0.02	0.00	0.00	0.00	0.00	0.00	0.00	0.00	0.00	0.79	11	0.79
11	2740.5	CROSS H CATTLI	0.15	0.02	0.00	0.00	0.00	0.00	0.00	0.00	0.00	0.00	0.82	11	0.82
11	2741	CROSS H CATTLI	0.14	0.01	0.00	0.00	0.00	0.00	0.00	0.00	0.00	0.00	0.84	11	0.84
7	2913.5	NEWBY	0.00	0.00	0.00	0.04	0.13	0.01	0.81	0.01	0.00	0.00	0.00	7	0.81
7	2914	NEWBY	0.00	0.00	0.00	0.06	0.17	0.01	0.75	0.01	0.00	0.00	0.00	7	0.75
7	2914.5	NEWBY	0.00	0.00	0.00	0.07	0.27	0.02	0.63	0.01	0.00	0.00	0.00	7	0.63
7	2915	NEWBY	0.00	0.00	0.00	0.09	0.31	0.04	0.55	0.01	0.00	0.00	0.00	7	0.55
6	2915.5	NEWBY	0.00	0.00	0.01	0.13	0.33	0.11	0.41	0.00	0.00	0.01	0.00	7	0.41
6	2916	NEWBY	0.00	0.00	0.02	0.16	0.31	0.25	0.24	0.00	0.00	0.02	0.00	5	0.31
6	2916.5	NEWBY	0.00	0.00	0.03	0.16	0.33	0.27	0.18	0.00	0.00	0.02	0.00	5	0.33
6	2917	NEWBY	0.00	0.00	0.04	0.14	0.34	0.31	0.15	0.00	0.00	0.01	0.00	5	0.34
6	2917.5	NEWBY	0.00	0.00	0.04	0.15	0.38	0.27	0.14	0.00	0.00	0.01	0.00	5	0.38
6	2918	NEWBY	0.00	0.00	0.04	0.20	0.47	0.11	0.17	0.01	0.00	0.01	0.00	5	0.47
4	2957.5	NEWBY	0.01	0.02	0.03	0.27	0.30	0.19	0.17	0.00	0.00	0.01	0.00	5	0.30
7	2958	NEWBY	0.00	0.01	0.01	0.14	0.27	0.13	0.41	0.00	0.00	0.00	0.00	7	0.41
7	2958.5	NEWBY	0.00	0.00	0.01	0.11	0.31	0.05	0.52	0.01	0.00	0.00	0.00	7	0.52

Table B-6. Selected result output of lithofacies prediction session. Header provides general information regarding the neural network model. Table includes operator selected fields from the input files (first three columns) and calculated probabilities for each of the eleven lithofacies. The predicted discrete lithofacies is the one having the highest probability.

Jackknife	Chase	Council Grove	Wolfcamp (combined)
within 1F	79%	88%	83%
% correct	49%	51%	50%
F6-10 w/in 1F	79%	82%	80%
F6-10 %correct	59%	51%	57%
F6-10 pred/actual	114%	96%	108%

Train-test-all	Chase	Council Grove	Wolfcamp (combined)
within 1F	89%	91%	90%
% correct	71%	61%	66%
F6-10 w/in 1F	90%	88%	90%
F6-10 %correct	80%	61%	74%
F6-10 pred/actual	108%	95%	104%

Table B-7. Summary statistics of neural network prediction accuracy for two cases: Jackknife and Train-Test-All Metrics for each case are accuracy within one lithofacies (within 1F), percent correct, lithofacies code 6 through 10 correct within one lithofacies (F6-10 w/in 1F), lithofacies code 6 through 10 percent correct (F6-10 % correct), and the ratio of lithofacies code 6 through 10 predicted and actual (F6-10 pred/actual).

Wolfcamp (combined) Jacknife		Cont Crs Silt	Cont Fn Silt	Mar Silt	Mdst	Wkst	Fxln Dol	Pkst-Grnst	PA-Baff	Mold-Dol	Mar SS	Cont SS		
	Count of PredFacies	Pred Facies												
Proportion	F11gm4	1	2	3	4	5	6	7	8	9	10	11	Grand Tota	within 1F
21.2%	1	**1969**	569	37	2	7		14		2	111	105	2816	**94%**
11.3%	2	743	**706**	11		5		19		1	12	9	1506	**96%**
7.6%	3	135	12	**358**	24	201	7	53		22	186	10	1008	**70%**
6.2%	4	23	17	99	**31**	383	17	180	4	43	28	1	826	**62%**
13.1%	5	22	21	157	86	**688**	19	609	18	67	57	2	1746	**79%**
3.5%	6	3	5	33	5	61	**108**	139	2	47	58	1	462	**64%**
17.9%	7	13	13	74	38	445	34	**1520**	24	167	57		2385	**90%**
0.8%	8			2		35	3	53	**18**				111	**67%**
7.4%	9	3		34	12	63	19	172		**613**	60	6	982	**80%**
7.0%	10	128	13	59	3	47	8	67		87	**505**	18	935	**62%**
3.9%	11	295	11	23	1			3		3	40	**141**	517	**92%**
	Grand Total	3334	1367	887	202	1935	215	2829	66	1052	1114	293	13294	
	Pred/Actual	**118%**	**91%**	**88%**	**24%**	**111%**	**47%**	**119%**	**59%**	**107%**	**119%**	**57%**	within 1F	**83%**
													% correct	**50%**
													F6-10 w/in 1F	**80%**
													F6-10 %correct	**57%**
													F6-10 pred/actual	**108%**

Wolfcamp (combined) Jacknife		Cont Crs Silt	Cont Fn Silt	Mar Silt	Mdst	Wkst	Fxln Dol	Pkst-Grnst	PA-Baff	Mold-Dol	Mar SS	Cont SS
	Count of PredFacies	Pred Facies										
Proportion	F11gm4	1	2	3	4	5	6	7	8	9	10	11
21.2%	1	**70%**	20%	1%	0%	0%	0%	0%	0%	0%	4%	4%
11.3%	2	49%	**47%**	1%	0%	0%	0%	1%	0%	0%	1%	1%
7.6%	3	13%	1%	**36%**	2%	20%	1%	5%	0%	2%	18%	1%
6.2%	4	3%	2%	12%	**4%**	46%	2%	22%	0%	5%	3%	0%
13.1%	5	1%	1%	9%	5%	**39%**	1%	35%	1%	4%	3%	0%
3.5%	6	1%	1%	7%	1%	13%	**23%**	30%	0%	10%	13%	0%
17.9%	7	1%	1%	3%	2%	19%	1%	**64%**	1%	7%	2%	0%
0.8%	8	0%	0%	2%	0%	32%	3%	48%	**16%**	0%	0%	0%
7.4%	9	0%	0%	3%	1%	6%	2%	18%	0%	**62%**	6%	1%
7.0%	10	14%	1%	6%	0%	5%	1%	7%	0%	9%	**54%**	2%
3.9%	11	57%	2%	4%	0%	0%	0%	1%	0%	1%	8%	**27%**
	Grand Total	25%	10%	7%	2%	15%	2%	21%	0%	8%	8%	2%

Table B-8. Pivot tables illustrating lithofacies prediction results for the entire Wolfcamp using a Jackknife approach. The diagonal (highlighted) are lithofacies predicted correctly. F11 (continental very-fine-grained sandstone) is equal to F0 in geomodels and in Figure B-3.

Wolfcamp (combined)		Cont Crs	Cont				Fxln	Pkst-		Mold-		Cont		
Train-test-all		Silt	Fn Silt	Mar Silt	Mdst	Wkst	Dol	Grnst	PA-Baff	Dol	Mar SS	SS		
	Count of PredFacies	Pred Facies												
Proportion	F11gm4	1	2	3	4	5	6	7	8	9	10	11	Grand Total	within 1F
21.2%	1	**2313**	340	18	2	4		3			41	95	2816	**98%**
11.3%	2	614	**852**	10		6		8			8	8	1506	**97%**
7.6%	3	111	19	**535**	17	136	7	42		15	113	13	1008	**77%**
6.2%	4	20	13	111	**107**	355	15	157		28	17	3	826	**69%**
13.1%	5	20	6	129	23	**1054**	24	397	15	39	35	4	1746	**84%**
3.5%	6	4	1	30	5	63	**201**	75	2	56	25		462	**72%**
17.9%	7	10	9	59	19	365	15	**1784**	15	96	12	1	2385	**95%**
0.8%	8			4		12	2	41	**52**				111	**86%**
7.4%	9	1	2	12	16	17		64		**844**	26		982	**92%**
7.0%	10	53	9	36	2	25	6	54		13	**717**	20	935	**83%**
3.9%	11	173	12	5				1			16	**310**	517	**97%**
	Grand Total	3319	1263	949	191	2037	270	2626	84	1091	1010	454	13294	
	Pred/Actual	**118%**	**84%**	**94%**	**23%**	**117%**	**58%**	**110%**	**76%**	**111%**	**108%**	**88%**	within 1F	**90%**
													% correct	**66%**
													F6-10 w/in 1F	**90%**
													F6-10 %correct	**74%**
													F6-10 pred/actual	**104%**

Wolfcamp (combined)		Cont	Cont				Fxln	Pkst-		Mold-		Cont
Train-test-all		Crs Silt	Fn Silt	Mar Silt	Mdst	Wkst	Dol	Grnst	PA-Baff	Dol	Mar SS	SS
	Count of PredFacies	Pred Facies										
Proportion	F11gm4	1	2	3	4	5	6	7	8	9	10	11
21.2%	1	**82%**	12%	1%	0%	0%	0%	0%	0%	0%	1%	3%
11.3%	2	41%	**57%**	1%	0%	0%	0%	1%	0%	0%	1%	1%
7.6%	3	11%	2%	**53%**	2%	13%	1%	4%	0%	1%	11%	1%
6.2%	4	2%	2%	13%	**13%**	43%	2%	19%	0%	3%	2%	0%
13.1%	5	1%	0%	7%	1%	**60%**	1%	23%	1%	2%	2%	0%
3.5%	6	1%	0%	6%	1%	14%	**44%**	16%	0%	12%	5%	0%
17.9%	7	0%	0%	2%	1%	15%	1%	**75%**	1%	4%	1%	0%
0.8%	8	0%	0%	4%	0%	11%	2%	37%	**47%**	0%	0%	0%
7.4%	9	0%	0%	1%	2%	2%	0%	7%	0%	**86%**	3%	0%
7.0%	10	6%	1%	4%	0%	3%	1%	6%	0%	1%	**77%**	2%
3.9%	11	33%	2%	1%	0%	0%	0%	0%	0%	0%	3%	**60%**
	Grand Total	25%	10%	7%	1%	15%	2%	20%	1%	8%	8%	3%

Table B-9. Pivot tables illustrating lithofacies prediction results for the entire Wolfcamp using the Train-Test-All method. The diagonal (highlighted) are lithofacies predicted correctly.

Corrected Porosity = A + B*Dphi$_{log}$ + C*Nphi$_{log}$

	Lithofacies	Code	Intercept A	Coefficient Dphi B	Coefficient Nphi C
Continental	Very fine-grained sandstone	11*	0.013516	0.8414	0.0000
	Coarse-grained siltstone	1	0.017803	0.8434	0.0000
	Fine to medium-grained siltstone	2	0.017803	0.8434	0.0000
Marine	Marine siltstone	3	0.018539	0.6619	0.0000
	Carbonate mudstone	4	0.018539	0.6619	0.0000
	Wackestone	5	0.000000	0.6151	0.3900
	Very fine- to fine-crystalline dolomite	6	0.047523	0.5842	0.2639
	Packstone-grainstone	7	0.000000	0.6151	0.3900
	Phylloid algal bafflestone	8	0.000000	0.6151	0.3900
	Medium-crystalline moldic dolomite	9	0.047523	0.5842	0.2639
	Very fine-grained sandstone	10	0.063699	0.5610	0.0000

* Lithofacies code is 0 for very fine-grained sandstone (continental) in the geomodel

Table B-10. Porosity correction algorithms developed by John Doveton (Chapter 3 and Dubois et al., 2006). They are based on empirical relationships between wire-line log variables and measured core porosity by lithofacies.

		Log Nphi	5%	10%	15%
		Log Dphi	5%	10%	15%
			Corrected Porosity		
	Lithofacies	**Code**	**Phi=5%**	**Phi=10%**	**Phi=15%**
Continental	Very fine-grained sandstone	11*	5.6%	9.8%	14.0%
	Coarse-grained siltstone	1	6.0%	10.2%	14.4%
	Fine to medium-grained siltstone	2	6.0%	10.2%	14.4%
Marine	Marine siltstone	3	5.2%	8.5%	11.8%
	Carbonate mudstone	4	5.2%	8.5%	11.8%
	Wackestone	5	5.0%	10.1%	15.1%
	Very fine- to fine-crystalline dolomite	6	9.0%	13.2%	17.5%
	Packstone-grainstone	7	5.0%	10.1%	15.1%
	Phylloid algal bafflestone	8	5.0%	10.1%	15.1%
	Medium-crystalline moldic dolomite	9	9.0%	13.2%	17.5%
	Very fine-grained sandstone	10	9.2%	12.0%	14.8%

* Lithofacies code is 0 for very fine-grained sandstone (continental) in the geomodel

Table B-11. Corrected porosity values by lithofacies for typical porosity range in the Wolfcamp calculated by empirical equation in Table B-10.

	Lithofacies	Code	*Insitu* K (md) from transform Phi=5%	Phi=10%	Phi=15%
Continental	Very fine-grained sandstone	11*	0.000586	0.059	0.87
	Coarse-grained siltstone	1	0.000043	0.011	0.28
	Fine to medium-grained siltstone	2	0.000035	0.009	0.23
Marine	Marine siltstone	3	0.000100	0.021	0.49
	Carbonate mudstone	4	0.000043	0.025	1.05
	Wackestone	5	0.000239	0.047	1.02
	Very fine- to fine-crystalline dolomite	6	0.000010	0.008	0.41
	Packstone-grainstone	7	0.001399	0.191	3.38
	Phylloid algal bafflestone	8	0.005703	2.291	76.42
	Medium-crystalline moldic dolomite	9	0.000096	0.079	4.06
	Very fine-grained sandstone	10	0.000016	0.013	0.70

* Lithofacies code is 0 for very fine-grained sandstone (continental) in the geomodel

Table B-12. Insitu permeability (K) in millidarcies (md) by lithofacies for typical porosity range in the Wolfcampian.

		Porosity (PhiH, phi-ft)			*Sum by lithofacies*			*Sum by intervals*	
Count	Proportion		Lithofacies	Code	Actual*	TTA	Jackknife	TTA	Jackknife
517	0.039	Continental	Very fine-grained sandstone	11**	**31.0**	28.6	17.8	31.5	31.9
2816	0.212		Coarse-grained siltstone	1	**120.9**	144.7	149.3	121.0	122.0
1506	0.113		Fine to medium-grained siltstone	2	**60.5**	50.8	56.0	60.6	60.4
1008	0.076	Marine	Marine siltstone	3	**36.5**	31.3	30.4	42.2	45.6
826	0.062		Carbonate mudstone	4	**22.2**	3.8	4.0	28.3	30.1
1746	0.131		Wackestone	5	**70.5**	75.0	71.3	68.5	67.6
462	0.035		Very fine- to fine-crystalline dolomite	6	**33.2**	21.1	16.4	29.5	27.6
2385	0.179		Packstone-grainstone	7	**111.5**	124.8	134.4	111.8	112.2
111	0.008		Phylloid algal bafflestone	8	**7.0**	6.5	4.6	6.9	7.0
982	0.074		Medium-crystalline moldic dolomite	9	**59.2**	64.8	64.5	56.6	53.2
935	0.070		Very fine-grained sandstone	10	**69.1**	73.7	77.7	68.3	68.7
13294				**All**	**590.5**	625.2	626.4	625.2	626.4
					Net effect	**5.9%**	**6.1%**	**5.9%**	**6.1%**

* Corrected porosity and permeability from empirically-derived transforms based on core-defined lithofacies.
** Lithofacies code is 0 for very fine-grained sandstone (continental) in the geomodel

Table B-13. Comparison of pore volume by lithofacies calculated for the training set with that using predicted lithofacies for Train-Test-All (TTA) and Jackknife training methods. Two perspectives are presented: 1) actual pore volume by predicted lithofacies (sum by lithofacies), and 2) pore volume estimated for the interval (sum by intervals).

				Permeability (Kh, md-ft)		*Sum by lithofacies*			*Sum by intervals*	
Count	**Proportion**		**Lithofacies**	**Code**	**Actual***	**TTA**	**Jackknife**		**TTA**	**Jackknife**
517	0.039	Continental	Very fine-grained sandstone	11*	**140.7**	150.0	93.0		134.4	182.8
2816	0.212		Coarse-grained siltstone	1	**42.4**	56.8	84.6		90.7	124.4
1506	0.113		Fine to medium-grained siltstone	2	**8.6**	12.1	28.5		14.8	14.4
1008	0.076	Marine	Marine siltstone	3	**10.1**	5.1	5.2		102.4	190.3
826	0.062		Carbonate mudstone	4	**1.9**	0.6	1.0		127.9	153.8
1746	0.131		Wackestone	5	**242.4**	110.5	91.7		1071.8	1340.4
462	0.035		Very fine- to fine-crystalline dolomite	6	**990.1**	847.2	605.2		2013.8	900.9
2385	0.179		Packstone-grainstone	7	**1429.9**	1499.5	1639.9		1784.4	2706.4
111	0.008		Phylloid algal bafflestone	8	**6443.4**	7653.1	4220.8		6286.8	2572.4
982	0.074		Medium-crystalline moldic dolomite	9	**6998.3**	7300.7	7906.6		5920.2	3390.8
935	0.070		Very fine-grained sandstone	10	**1689.7**	1831.8	1799.6		1920.3	4899.6
13294				**All**	**17997.5**	19467.3	16476.2		19467.4	16476.2

* Corrected porosity and permeability from empirically-derived transforms based on core-defined lithofacies.
** Lithofacies code is 0 for very fine-grained sandstone (continental) in the geomodel

Table B-14. Comparison of flow capacity, expressed as permeability*height (Kh), by lithofacies calculated for the training set with that using predicted lithofacies for Train-Test-All (TTA) and Jackknife training methods. Two perspectives are presented: 1) actual Kh by predicted lithofacies (sum by lithofacies), and 2) Kh estimated for the interval (sum by intervals).

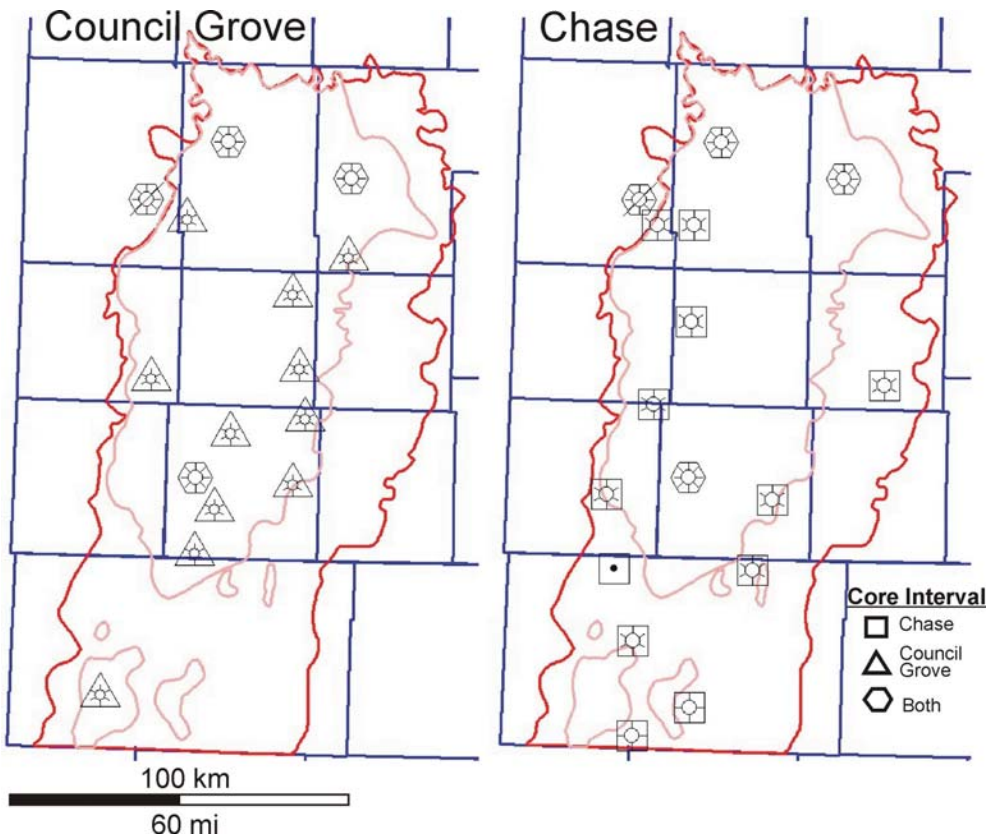

Figure B-1. Distribution of Council Grove and Chase core lithofacies for neural network training. Twenty-seven wells in all, ten with both Chase and Council Grove core.

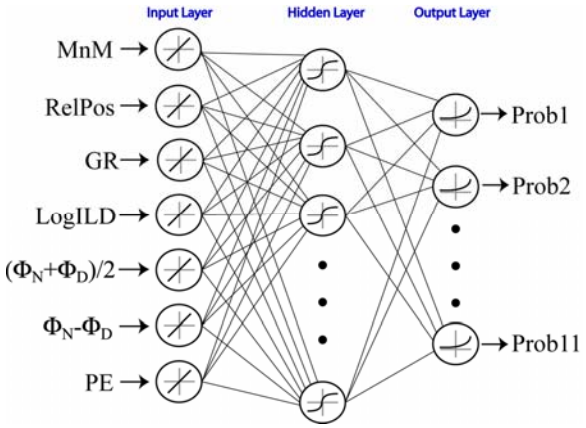

Figure B-2. Structure of neural network employed for predicting lithofacies. Seven predictor variables are the input. Output values are probabilities of membership in different lithofacies (after Bohling, 2006).

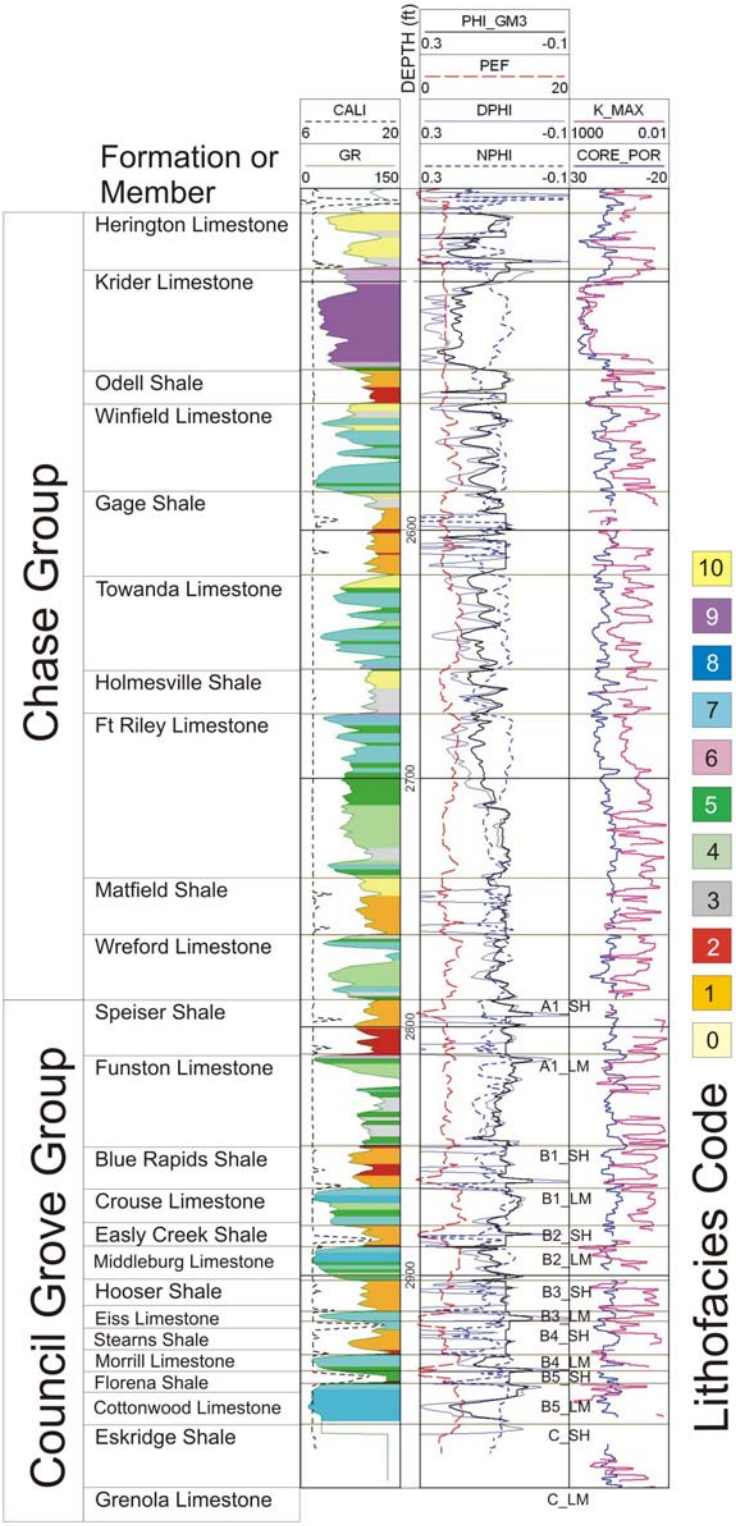

(See caption on next page.)

Figure B-3. Formation- and member-level stratigraphy correlated to wire-line well log in the Flower A-1 well, Stevens County, Kansas. Commonly used formation/member letter-number combinations are shown for the Council Grove. Twelve of the thirteen marine-continental (carbonate-siliciclastic) sedimentary cycles that are gas productive are shown (Grenola Limestone, C_LM is not logged). Stratigraphic names that include "Limestone" are marine half cycles when combined with an adjacent continental half-cycle, intervals with stratigraphic names that include "Shale," form a complete cycle. Color-coded lithofacies are derived from core. Three were deposited in a continental setting, L0- sandstone, L1- coarse siltstone, and L2- shaly siltstone, and eight in a marine environment, L3- siltstone, L4- carbonate mudstone, L5- wackestone, L6- very fine-crystalline dolomite, L7- packstone-grainstone, L8- phylloid algal bafflestone, L9- fine-medium crystalline moldic dolomite, and L10- sandstone. Wire-line log abbreviations are caliper (CALI), gamma ray (GR), corrected porosity (PHI_GM3), photoelectric effect (PEF), density porosity (DPHI), neutron porosity (NPHI), core permeability (K_MAX, and core porosity (CORE_POR). Logged interval is 520 ft (160 m).

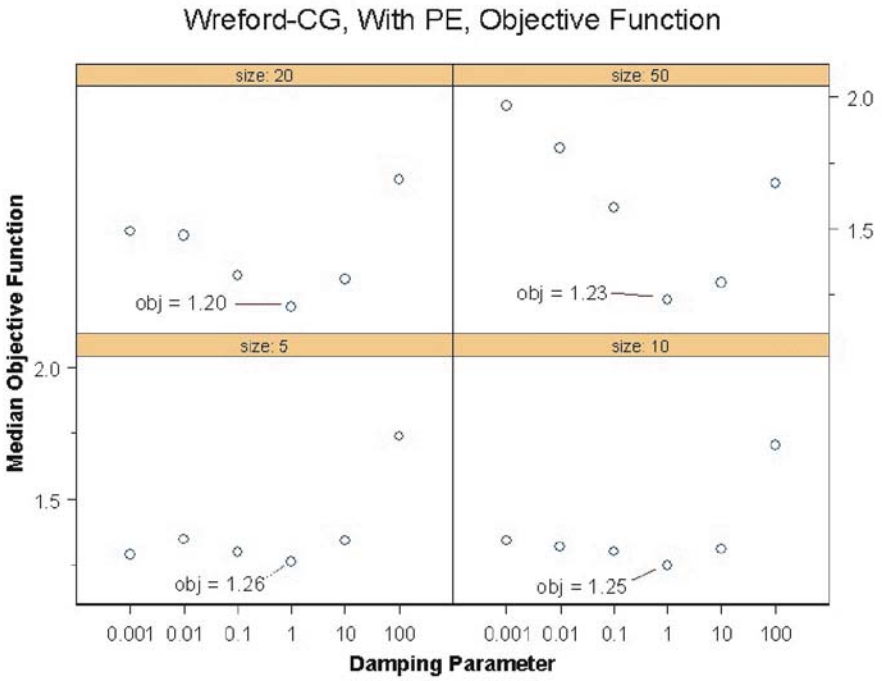

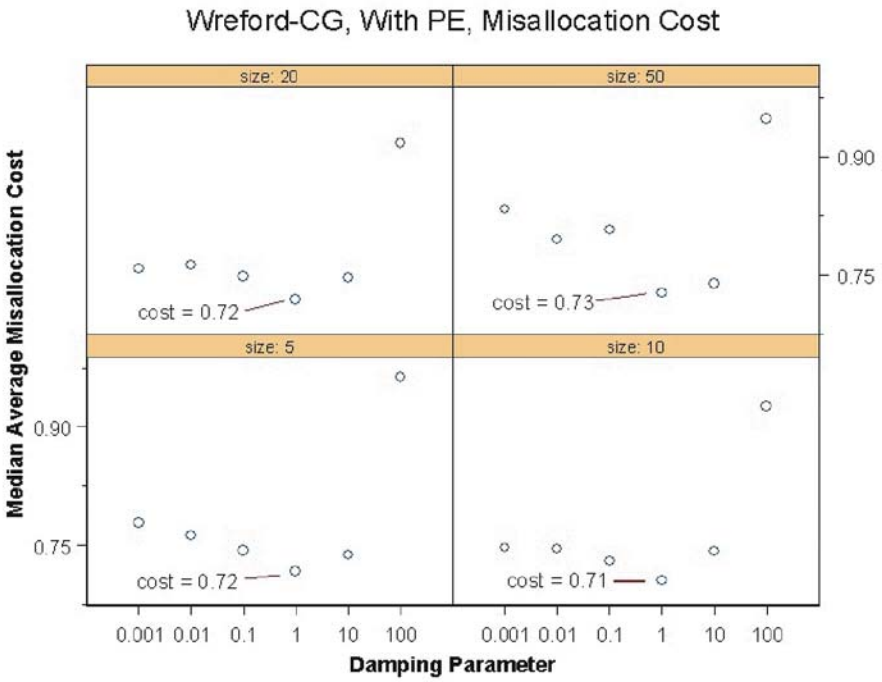

Figure B-4. Crossvalidation results for Wreford and Council Grove neural network with PE curve. Optimal parameters for network size and damping parameter is 20 nodes and 1 as determined by the objective function metric and 10 and 1 by the misallocation cost metric.

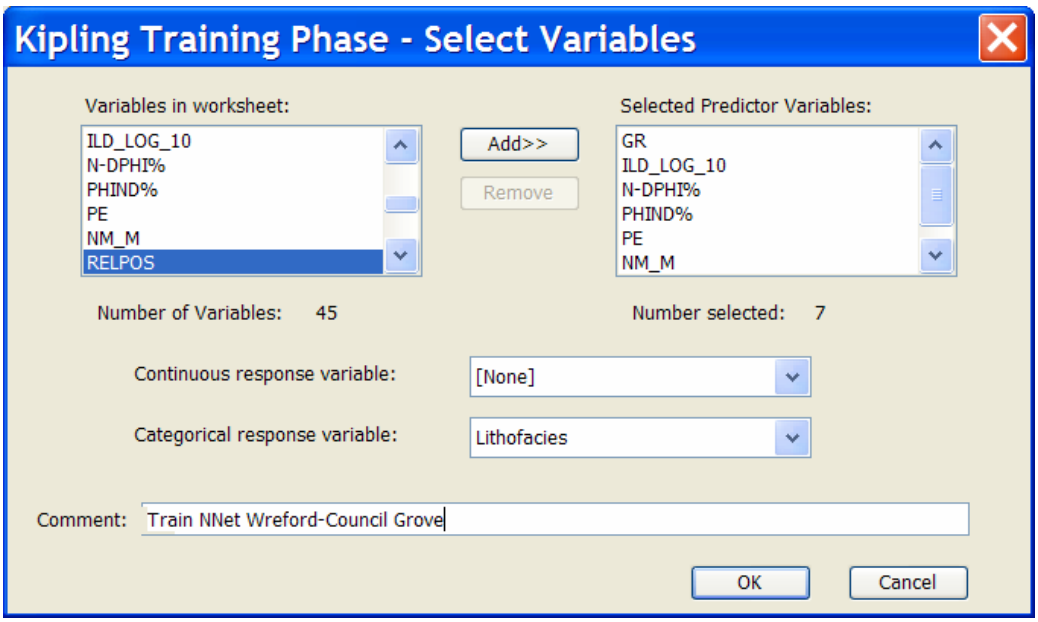

Figure B-5. First step in training a neural network is selection of the training data predictor variables

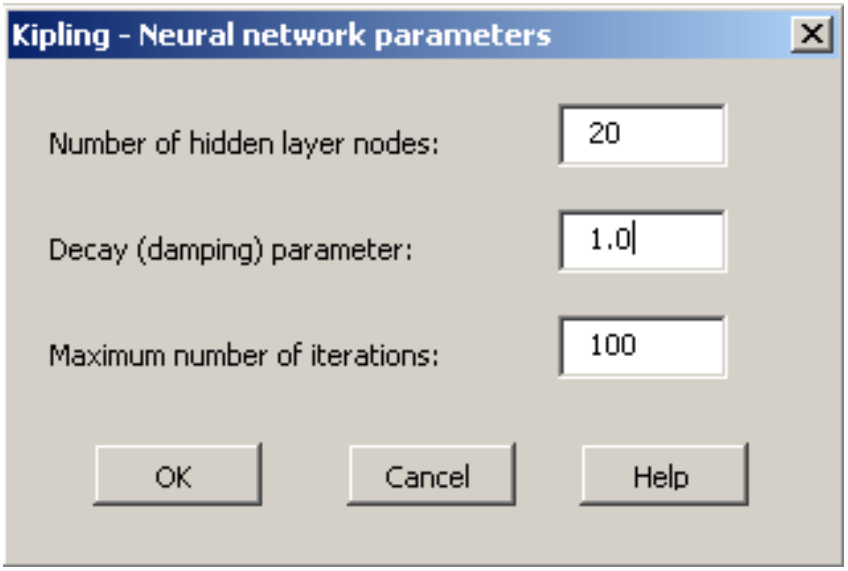

Figure B-6. Neural network parameters are set in the second step.

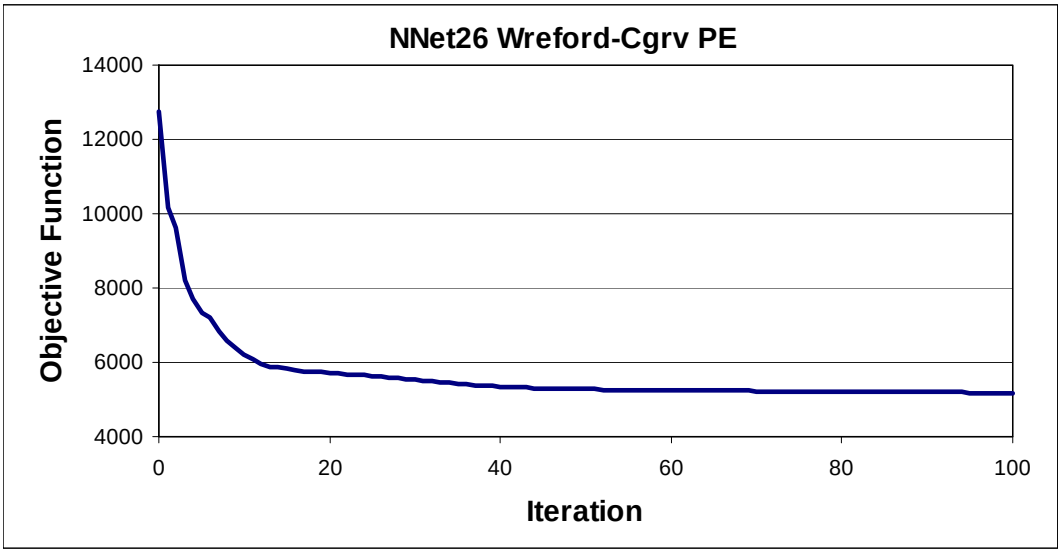

Figure B-7. Objective function versus iteration of a neural network training session. Objective function is a measure of mismatch between true and predicted facies.

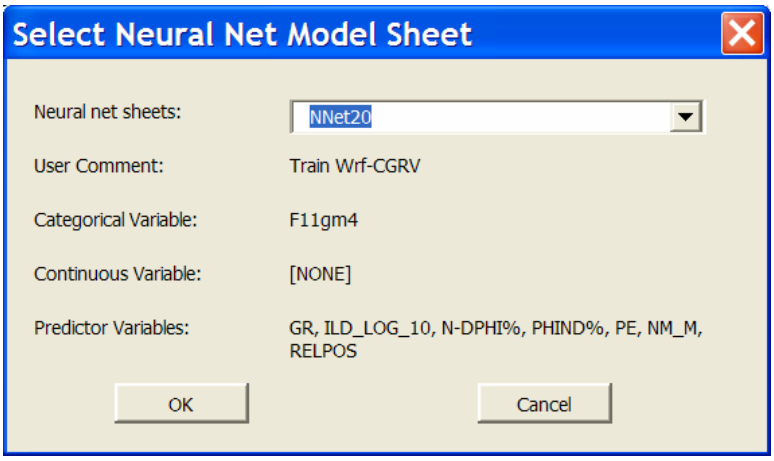

Figure B-8. Neural network selection for batch predicting lithofacies.

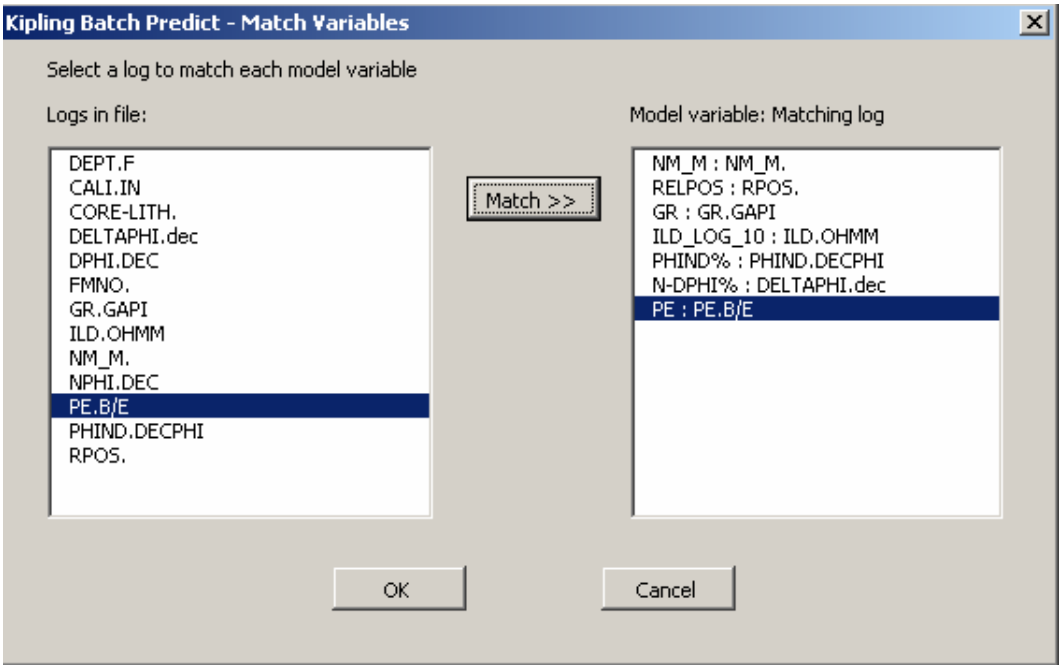

Figure B-9. Match predictor variables in LAS files to be processed with those in the trained neural network.

APPENDIX C

Comparison between Geomod3 and Geomod4

APPENDIX C – Comparison between Geomod3 and Geomod4

Introduction

In this appendix, the differences between Geomod3 and Geomod4 are discussed. Chapter 3 is based on version Geomod3, while Chapter 4 utilized Geomod4. Models for the Hugoton have evolved over the past several years as data have been added and lithofacies estimation techniques, free water level, and petrophysical property transform equations have been refined (Table C-1). The principal variables that have changed from Geomod3 to Geomod4 were and increase in data (core and node wells), slight modification in lithofacies classes, minor change in stratigraphic intervals for neural network training, lithofacies and porosity variograms, slight modification in the free-water level, and adjustments in porosity correction algorithms. Model dimensions, cell size, and layering are essentially the same, although a change in projections resulted in a slightly different orientation for the model and cell count. Differences between the models are summarized in Table C-2.

Model building, an iterative process

Building the Hugoton geomodel has been an iterative process where techniques and tools to manage large data volumes evolved. For details on Hugoton model building see Dubois et al., 2006a. Chapter 3 discussed a simple four-step workflow: 1) define lithofacies in core and correlate to electric log curves (training set), 2) train a neural network and predict lithofacies at non-cored wells, 3) populate a 3D cellular model with lithofacies using stochastic methods, and 4) populate model with lithofacies-specific petrophysical properties and fluid saturations, and also presented a more detailed workflow (Figure 3-1, Chapter 3). The workflows imply the process was linear. In practice, however, it involved feedback loops and multiple iterations at the subtask level. Experimentation, technique modification, testing, and validation occurred at several levels in the workflow as well as at the full model scale.

Data were added and improvements were made in each of the four model iterations (Table C-1). Geomod3 and Geomod4 are very similar and, although Geomod4 is viewed as an improvement over Geomod3, the improvements are not proportional to the amount of data added. Modeling the Hugoton is an ongoing project at the Kansas Geological Survey in collaboration with industry partners. Although the current geologic and petrophysical model (porosity and permeability) are considered satisfactory, refinements in the free-water level and water saturations, are currently being considered.

Data and model statistics

Core defined lithofacies (neural network training data) and lithofacies, predicted by neural networks in wells without core (node wells), are the basic data for building the Hugoton geomodel. Core training data were nearly doubled from Geomod3 to Geomod4 (Table C-1 and Figure C-1). Nine Council Grove cores and eight Chase cores were used in Geomod3 while the training set in Geomod4 included 15 Council Grove and 16 Chase core. Wells without core where lithofacies were predicted by neural networks numbered 1350 in Geomod3 and 1600 in Geomod4. Most of the additions to Geomod4 were in Texas County Oklahoma.

Lithofacies

Representation of lithofacies at varying scales is similar between the geomodels (Table C-3 and Figure C-2). Illustrated are the proportions of 11 lithofacies in the core training set, lithofacies at the node wells, upscaled lithofacies at node wells, and lithofacies in the cellular model. Node well lithofacies include core lithofacies and predicted lithofacies at wells without core. Most differences in lithofacies in core reflect the addition of core with more or less of a particular lithofacies. Four changes in lithofacies classes were made between modeling efforts:

1. Very-fined-grained sandstone (continental) was not modeled in the Chase in Geomod3 due to insufficient training data, but was modeled in Geomod4 after more core of this lithofacies was added in the Chase.
2. Very-fined-grained sandstone (marine) was not modeled in the Council Grove in Geomod3 due to insufficient training data, but was modeled in Geomod4 after more core of this lithofacies was added in the Council Grove.
3. Packstone and grainstone lithofacies were separate classes in Geomod3, but were combined in Geomod4 because trained neural networks were not effectively discriminating the two classes.
4. Phylloid algal bafflestone was added in Geomod4 after additional core training data were incorporated.

Lithofacies in the training set

Differences between core lithofacies (training) and predicted lithofacies at node wells *within* each model is not only a function of the distribution of the training data with respect to node well density, but also of neural network prediction accuracy (Appendix B). Variance in specific lithofacies at node wells *between* models is primarily due to differences in representation of the lithofacies in training data between models. For example, fine- to medium-crystalline moldic dolomite comprises only 1.4% of the node well volume in Geomod3, but 6.6% in Geomod4. The new core data for this lithofacies used in Geomod4 happens to be in the area where node well density is highest (Stevens County). Neural network models, improved by additional core training data for the lithofacies, more accurately predicted fine- to medium-crystalline moldic dolomite in Geomod4. An example where Geomod3 neural networks had higher accuracy a lithofacies is the mudstone lithofacies. The inter-model discrepancy for the mudstone lithofacies has not been resolved.

Lithofacies at node wells

There is little difference between node well lithofacies at the half-foot (0.15 m) scale and upscaled lithofacies at node wells (2-4 ft mean, 0.3-0.6 m scale) *within* each model except for the continental siliciclastic lithofacies. The decrease in proportions between scales is a function of layer thickness in the model and the upscaling process. Both models have 169 layers and have the same number of layers per stratigraphic interval. In marine, mostly carbonate intervals, layers are purposely thinner (mean 2 ft, 0.3 m) than in the continental siliciclastic strata (mean 4 ft, 0.6 m). Carbonate intervals are the main pay lithofacies. Due to computational constraints, layer numbers in the siliciclastic intervals were reduced (made thicker). Thus the cell counts are lower. It should be noted that the siliciclastic layers were doubled and remodeled in a later model version (Geomod4.4) for analysis of siliciclastic lithofacies discussed in Chapter 4).

Lithofacies proportions in the model

Lithofacies proportions vary little between upscaled lithofacies at node wells and the entire cellular model because the modeling process incorporates statistical lithofacies data from node wells. Sequential indicator simulation relies on data analysis of lithofacies in the node wells to guide it in the process of populating cells between node wells. However, node well upscaled lithofacies proportions may be skewed because of unequal well density in the node well set. No adjustments in upscaled lithofacies proportions were made in Geomd3 and node-well-upscaled lithofacies and model proportions are approximately equal. Upscaled lithofacies proportions in Geomd4 were adjusted downward for fine- to medium-crystalline moldic dolomite in certain stratigraphic intervals to take into account the effects of high node well densities in regions where the lithofacies dominates. This resulted in a reduction of the lithofacies occurrence and a more realistic distribution in the cellular model.

Neural networks

Neural network structure and input parameters are the same for both model iterations. They do vary, however, in the lithofacies being classified (discussed above) and a slight variation in the stratigraphic split between models. In both cases, neural network models were trained for three stratigraphic intervals, upper Chase, lower Chase, and the Council Grove. However, in Geomod4, the lowermost formation in the Chase, Wreford, was included in the Council Grove because it has lithofacies more similar to the Council Grove than to the rest of the Chase. Additional training data may have improved neural network prediction accuracy slightly (Table C-4). See Appendix B for details on neural network training.

Variograms

Variograms are important for stochastic simulation because they control, to a large degree, the distribution of the property being simulated. Variogram parameters used in both models are summarized in Table C-2. Geomod3 variograms were based on limited data analysis within Petrel™, the modeling application, and subjective observations of lateral and vertical lithofacies distribution in areas with close well control. Geomod4 variograms were based on extensive data analysis of data zone-by-zone, lithofacies-by-lithofacies (24 zones and 11 lithofacies) by Bohling. Variogram horizontal ranges do not vary significantly between the models. Data analysis confirmed observations that lithofacies bodies are laterally extensive and that long horizontal variogram ranges are justified. Vertical ranges are generally larger for Geomod4, on the basis of data analysis. In both models, the variogram ranges exceed node well spacing (less than variogram ranges) making the simulations more deterministic than stochastic in areas with close node well density. More detail on variograms for Geomod3 is provided in Chapter 3 and for Geomod4 in Dubois et al. (2006b).

Lithofacies in the models

Additional data, slight changes in lithofacies classes and stratigraphic intervals for trained neural networks resulted in only slight differences in the models overall (Table C-3). Differences are more apparent when comparing lithofacies by stratigraphic zone in the models. Figure C-3 is a series of 2-D views of 3-D connected volumes (CV), representing collections of touching cells in the cellular model having common properties. The figure shows examples of three important lithofacies in three stratigraphic intervals.

Figure C-3A illustrates the distribution of continental very-fine-grained sandstone in the Speiser Shale (A1_SH) having porosity > 12%. Regions where this sandstone is present is very similar between models, however, the continental very-fine-grained sandstone lithofacies is more continuous and covers a higher proportion of the region where it is present. The increase in continental very-fine-grained sandstone is consistent with data presented in Table C-3 where the cell count lithofacies in Geomod4 is 64% higher than it is in Geomod3. The model proportion is also closer to the proportion for upscaled lithofacies at the node wells and in the training data; however, it appears to be under represented in the model.

Packstone-grainstone (light blue) and very-fine-crystalline dolomite (pink) having porosity > 8% in the Crouse Limestone (B1_LM) is shown in Figure C-3B. Regions where these important lithofacies are present are similar, however packstone-grainstone is more widespread within the areas where it does occur. The differences in proportions are not reflected in Table C-3, possibly because the table is for the entire model and the packstone-grainstone lithofacies is the most common lithofacies in the model.

Two figures illustrate fine- to medium-crystalline moldic dolomite (purple) and packstone-grainstone (light blue) in the Krider Limestone (Figures C-3C and C-3D). Figure C-3C3 is for cells with having porosity> 16% in Geomod3 and > 17% in Geomod4. Figure C-3C4 is for cells with having porosity> 18% in Geomod3 and > 19% in Geomod4. The variation in porosity between models is due to porosity

correction algorithm changes between the models (Table C-5). Depicted are views of a known dolomitized ooid-bioclast shoal system, the most prolific reservoir in Stevens County. The main difference in the models is that there is more fine- to medium-crystalline moldic dolomite and less packstone-grainstone in Geomod4. This reflects the addition of core containing fine- to medium-crystalline moldic dolomite to the training data and better prediction of this lithofacies in the model. In Geomod3, neural networks predicted much of the dolomite lithofacies as packstone-grainstone.

Volumetric gas in place

Because water saturation and gas in place are functions of lithofacies and porosity (Chapter 3), volumetric gas in place is an effective metric for comparing models (Table C-6). However, comparisons cannot be made directly because multiple variables were changed between models: 1) lithofacies spectrum split differently, 2) slight, but important change in free-water level (FWL), and 3) modification of the porosity correction algorithm. Some of the differences in gas volume can be accounted for and it is useful to make comparisons, at least qualitatively. Raising the FWL in the eastern part of the model significantly reduced gas volume in continental siltstone (*_SH), particularly in the lower part of the gas column (Council Grove Group) but had almost no effect on other lithofacies higher in the gas column (Chase Group). Modification in the porosity correction algorithm increased pore volume (and gas volume) by approximately 3%. Geomod4 has increased dolomite that had been predicted as limestone in Geomod3. The difference may account for a 1-2% increase in pore volume. The 3-4% increase in the prediction in “pay” lithofacies that had been predicted as non-pay lithofacies (Table C-4) may account for another 1-2% increase in pore volume. As much as half the overall increase in gas volume (10.5% for the entire Wolfcampian) can be related to the net increase in pore volume discussed above.

Conclusions

Lithofacies in Geomod4 and Geomod3 are very similar overall, but do vary at smaller scales. The significant increase in core training data did improve the neural network prediction of certain lithofacies (e.g., continental very-fine-grained sandstone and fine- to medium-crystalline moldic dolomite). These improvements are reflected in their representation in the model. Water saturation is lower and gas in place is higher in Geomod4, due in part to higher pore volume because of changes in the porosity correction algorithm. Overall the models are very similar, but Geomod4 is considered a slightly improvement over Geomod3.

References

Bohling, G. C., 2006, Technology to manage large digital data sets: *chapter in*, M. K. Dubois, A. P. Byrnes, S. Bhattacharya, G. C. Bohling, J. H. Doveton, and R. E. Barba, Hugoton Asset Management Project (HAMP): Hugoton Geomodel Final Report, Kansas Geological Survey, Open-File Report 2007-6, chapter 5, 13 p. http://www.kgs.ku.edu/PRS/publication/2007/OFR07_06/index.html (Accessed March 22, 2007.)

Dubois, A. P. Byrnes, S. Bhattacharya, G. C. Bohling, J. H. Doveton, and R. E. Barba, 2006a, Hugoton Asset Management Project (HAMP): Hugoton Geomodel Final Report, Kansas Geological Survey, Open-File Report 2007-6, 682 p. http://www.kgs.ku.edu/PRS/publication/2007/OFR07_06/index.html (Accessed March 22, 2007.)

Dubois, M. K., G. C. Bohling, and A. P. Byrnes, 2006b, Static reservoir model: *chapter in*, M. K. Dubois, A. P. Byrnes, S. Bhattacharya, G. C. Bohling, J. H. Doveton, and R. E. Barba, Hugoton Asset Management Project (HAMP): Hugoton Geomodel Final Report, Kansas Geological Survey, Open-File Report 2007-6, chapter 5, 53 p. http://www.kgs.ku.edu/PRS/publication/2007/OFR07_06/index.html (Accessed March 22, 2007.)

	Geomod1	Geomod2	Geomod3	Geomod4
Council Grove core	8	9	9	15*
Chase core	0	2	8	16**
Combined core wells	8	9	14	27***
Wells without core	515	1250	1350	1574
Number of lithofacies	8	10	11	11
Model interval	Council Grove	Council Grove and Chase	Council Grove and Chase	Council Grove and Chase
Model area	Kansas	Kansas	Kansas and Oklahoma	Kansas and Oklahoma
Chapter	2	NA	3	4

***** 17 wells in study, 15 in Council Grove neural network training set
****** 17 wells in study, 16 in Chase neural network training set
******* 29 wells in study, 27 wells in neural network training set

Table C-1. Data volumes, model intervals, geographic coverage, and chapters where discussed for four Hugoton geomodel iterations.

		Geomod 3	Geomod 4
Dimensions	Cell count[1]	107,765,147	108,064,831
	Layers	169	169
	Cell size XY	660 ft (200 m)	660 ft (200 m)
Data			
Neural network training set	Chase wells	9	15
	Council Grove wells	8	16
	Combined wells	14	27
Node wells[2]	Chase wells	1060	1308
	Council Grove wells	1136	1250
	Combined wells	1364	1600
Structural framework	Well count	8850	8756
Model parameters			
Variograms - lithofacies	basis	limited data analysis and subjective observations	extensive data analysis by zone by lithofacies
	major axis (marine)	30,000 ft	18,000 - 30,000 ft
	minor axis (marine)	25,000 ft	15,000 - 25,000 ft
	azimuth (marine)	11 degrees[3]	11 degrees[3]
	major axis (continental)	30,000 ft	25,000 - 40,000 ft
	minor axis (continental)	30,000 ft	25,000 - 40,000 ft
	azimuth (continental)	NA	NA
	vertical range	mean layer h X 2	7-21
	nugget	0.1 - 0.22	0
	sill	1	1
Variograms - porosity	major axis (marine)	same as lithofacies	27,000 - 39,000 ft
	minor axis (marine)	same as lithofacies	23,000 - 33,000 ft
	azimuth (marine)	same as lithofacies	11 degrees[3]
	major axis (continental)	same as lithofacies	35,000 - 42,000 ft
	minor axis (continental)	same as lithofacies	35,000 - 42,000 ft
	azimuth (continental)	same as lithofacies	NA
	vertical range[4]	same as lithofacies	7-21
	nugget	same as lithofacies	0
	sill	same as lithofacies	1
Results			
Neural network accuracy[5]	correct (all facies)	63-66%	64-67%
	within 1 facies (all)	88-90%	90-91%
	correct (F6-10)	64-70%	68-74%
	within 1 facies (F6-10)	88-91%	89-90%
	predicted/actual (F6-10)	101-101%	106-103%
Model cell lithofacies	Continental lithofacies (F0-2)	24.5%	24.2%
	"Non-pay" marine (F3-5)	35.5%	36.0%
	"Pay" marine (F6-10)	40.1%	39.9%
Volumetric gas in place[6]	Chase	20,075	22,474
	Council Grove	1,699	1,582
	Combined	21,774	24,056

1 different projections caused slightly different cell count
2 includes core wells in count
3 approximate depositional strike
4 not constrained by layer h
5 entire Wolfcampian; first value is for NoPE case and second is for PE case; accuracy for train on all, predict on all basis (see Appendix B)
6 Grant and Stevens Counties, Kansas. Volume is in trillion cubic feet (TCF)

Table C-2. Summary statistics comparing Geomod3 and Geomod4.

Geomod 3

	Height	0.5 feet	0.5 feet	Variable*	Variable*
	Source	Actual	NNet Predicted	Upscaled	Modeled (SIS)
Code	**Lithofacies**	**Training**	**Node Wells**	**Node Wells**	**All cells**
0	Cont SS	5.6%	2.2%	1.0%	1.1%
1	Cont Crs Slt	23.3%	19.7%	17.0%	16.7%
2	Cont Fn Slt	12.9%	9.6%	7.1%	6.7%
3	Mar Slt	7.5%	9.6%	9.0%	9.1%
4	Mdst	5.4%	4.3%	3.6%	3.9%
5	Wkst	14.5%	20.1%	22.2%	22.5%
6	Vf-fxln Dol	2.8%	4.9%	3.9%	3.8%
7	Pkst	14.7%	24.7%	25.9%	25.2%
8	Grnst	2.3%	0.2%	0.2%	0.2%
9	F-mxln Dol	5.6%	1.4%	3.8%	3.8%
10	Mar SS	5.4%	3.4%	6.3%	7.1%
Count (N)		8,545	993,146	183,949	107,765,147

Geomod 4

	Height	0.5 feet	0.5 feet	Variable*	Variable*
	Source	Actual	NNet Predicted	Upscaled	Modeled (SIS)
Code	**Lithofacies**	**Training**	**Node Wells**	**Node Wells**	**All cells**
0	Cont SS	3.8%	2.4%	1.4%	1.8%
1	Cont Crs Slt	21.0%	18.6%	15.0%	14.6%
2	Cont Fn Slt	11.2%	8.9%	7.7%	7.8%
3	Mar Slt	7.6%	9.6%	9.7%	9.9%
4	Mdst	6.1%	1.6%	1.3%	1.6%
5	Wkst	13.4%	19.7%	22.2%	24.5%
6	Vf-fxln Dol	3.4%	3.5%	3.5%	3.6%
7	Pkst-Grnst	18.2%	22.1%	24.7%	23.9%
8	PA Baff	0.8%	0.6%	0.7%	0.7%
9	F-mxln Dol	7.3%	6.6%	6.9%	4.7%
10	Mar SS	7.0%	6.4%	6.9%	7.0%
Count (N)		13,512	1,383,653	211,720	108,064,831

* Model layer h: Average of mean h = 3.3 ft (1 m). Range of mean h = 1.9 to 5.2 ft 0.57-1.58 m). Lithofacies 0-2 tend to be in thicker layers.

Table C-3. Relative distribution of eleven lithofacies in core, node wells and cellular models. Core-defined lithofacies for 14 wells were used in neural network "Training" for lithofacies prediction in 1350 "Node Wells" in Geomod3, while cores defined lithofacies from 27 core wells and 1574 wells without core were used in Geomod4. Half-foot (0.15 m) lithofacies in node wells were upscaled to model layer thickness (Variable Upscaled). Sequential indicator simulation (SIS) was utilized to populate the cellular model (All Cells) between the node wells. Both models had the same number of layers (169) and cell width (660 ft, 200 m). Abbreviations include continental very-fine-grained sandstone (Cont SS), continental coarse-grained siltstone continental (Cont Crs Slt), continental fine-medium grained siltstone (Cont Fn Slt), marine siltstone (Mar Slt), carbonate mudstone (Mdst), wackestone (Wkst), very fine to fine crystalline dolomite (Vf-fxln Dol), packstone-grainstone (Pkst-Grnst), phylloid algal bafflestone (PA Baff), medium crystalline moldic dolomite (F-mxln Dol), and marine very-fine-grained sandstone (Mar SS).

Geomod 3

	Chase		Council Grove		Wolfcamp	
	NoPE	PE	NoPE	PE	NoPE	PE
All w/in 1F	89%	88%	92%	93%	90%	91%
All % correct	67%	70%	62%	64%	64%	67%
F6-10 w/in 1F	91%	88%	85%	89%	88%	91%
F6-10 %correct	71%	75%	51%	57%	64%	70%
F6-10 pred/actual	107%	106%	89%	88%	101%	101%

Geomod4

	Chase		Wreford &Council Grove		Wolfcamp	
	NoPE	PE	NoPE	PE	NoPE	PE
All w/in 1F	88%	89%	89%	91%	88%	90%
All % correct	67%	70%	58%	61%	63%	66%
F6-10 w/in 1F	90%	91%	86%	88%	89%	90%
F6-10 %correct	74%	79%	57%	60%	68%	74%
F6-10 pred/actual	109%	107%	98%	91%	106%	103%

Table C-4. Compiled summary statistics for neural-network-prediction accuracy. Data are for neural networks trained on all data by stratigraphic interval and lithofacies predicted for the same training data. Models were tested for the cases with PE and without PE curve (NoPE). Upper and lower Chase results are combined. Wreford from lower Chase is included in Council Grove in Geomod4. Results for the entire Wolfcampian (Wolfcamp all) are the sums of the results for the three stratigraphic intervals. See Appendix B for metrics and their discussions.

		For NDphi = 0.10		Difference	
	LithCode	Geomod4	Geomod3	Absolute	%
(F0)Continental ss	11 (0)	0.098	0.100	-0.002	-2.3%
crs silt	1	0.102	0.102	0.000	0.0%
fine silt	2	0.102	0.102	0.000	0.0%
marine silt	3	0.085	0.085	0.000	0.0%
mdst	4	0.085	0.085	0.000	0.0%
wkst	5	0.101	0.099	0.002	1.9%
fxln dol	6	0.131	0.125	0.007	5.4%
pkst	7	0.101	0.099	0.002	1.9%
grnst	8	0.101	0.099	0.002	1.9%
Cxln dol	9	0.131	0.125	0.007	5.4%
Marine ss	10	0.120	0.115	0.005	4.3%

Table C-5. Impact of the change in porosity correction algorithms used in Geomod3 and Geomod4 for 10% porosity. Algorithm modification resulted in an approximately 3% increase in pore volume in Geomod4.

Zone	Geomod3	Gmod4	%Change
HRNGTN	1227	1411	15.0%
KRIDER	2795	3368	20.5%
ODELL	295	294	-0.3%
WINF	3215	3500	8.9%
GAGE	807	970	20.2%
TWND	4686	5270	12.5%
HLMVL	663	821	23.8%
FTRLY	5212	5351	2.7%
MATFIELD	127	110	-13.4%
WREFORD	1048	1379	31.6%
A1_SH	331	136	-58.9%
A1_LM	656	772	17.7%
B1_SH	76	53	-30.3%
B1_LM	143	175	22.4%
B2_SH	9	10	11.1%
B2_LM	167	192	15.0%
B3_SH	56	6	-89.3%
B3_LM	34	39	14.7%
B4_SH	67	10	-85.1%
B4_LM	22	30	36.4%
B5_SH	3	1	-66.7%
B5_LM	113	138	22.1%
C_SH	2	1	-50.0%
C_LM	20	19	-5.0%
Chase	**20075**	**22474**	**12.0%**
Cgrv	**1699**	**1582**	**-6.9%**
Wolfcamp	**21774**	**24056**	**10.5%**

Table C-6. Volumetric gas in place by zone for Grant and Stevens counties, Kansas, for Gomod 3 and Geomod4. Gas volumes are in billion cubic feet.

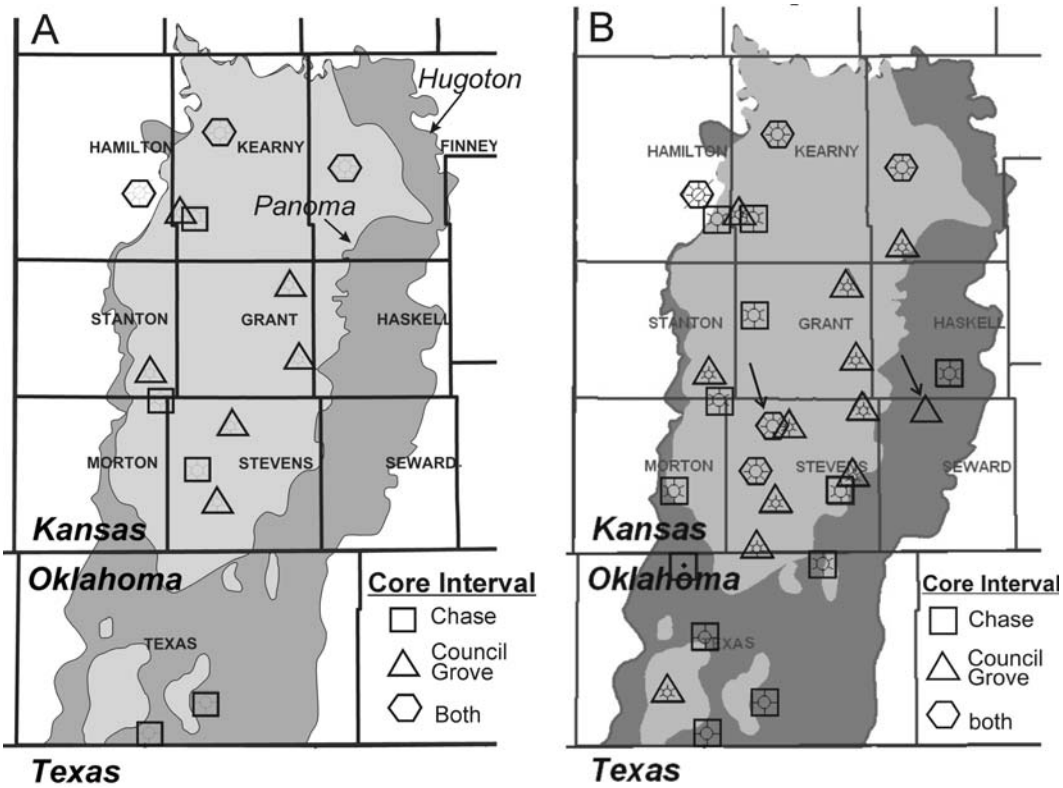

Figure C-1. (A) Core lithofacies for neural network training for Geomod3 includes data from 14 wells, three with both Chase and Council Grove core, five with only Chase core, and six with only Council Grove Core. **(B)** Core lithofacies training set for Geomod4 includes data from 27 wells, four with both Chase and Council Grove core, twelve with Chase only, and eleven with Council Grove only. Two wells with arrows were not part of the training set. Wireline logs for the one in Stevens County were not satisfactory and the well in Seward County was added late.

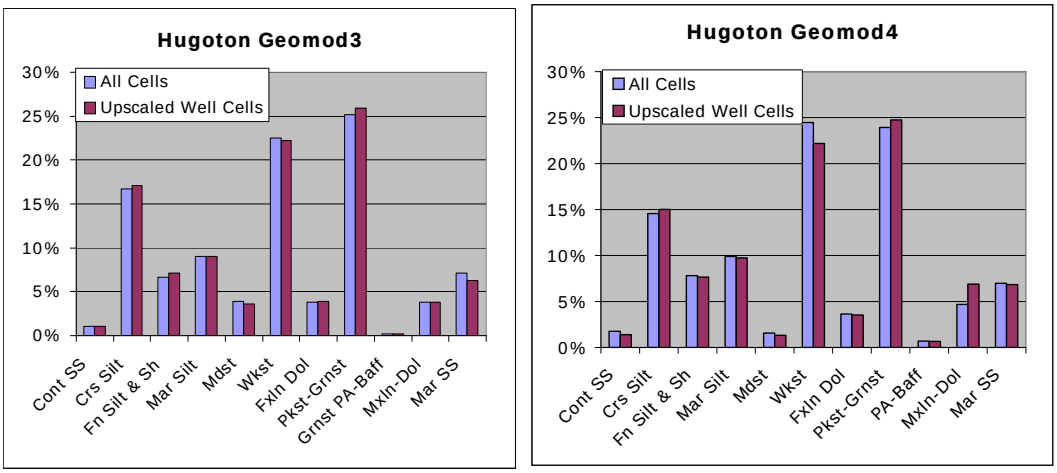

Figure C-2. Graphical representation of lithofacies in upscaled cells at node wells and all cells in the two geomodels.

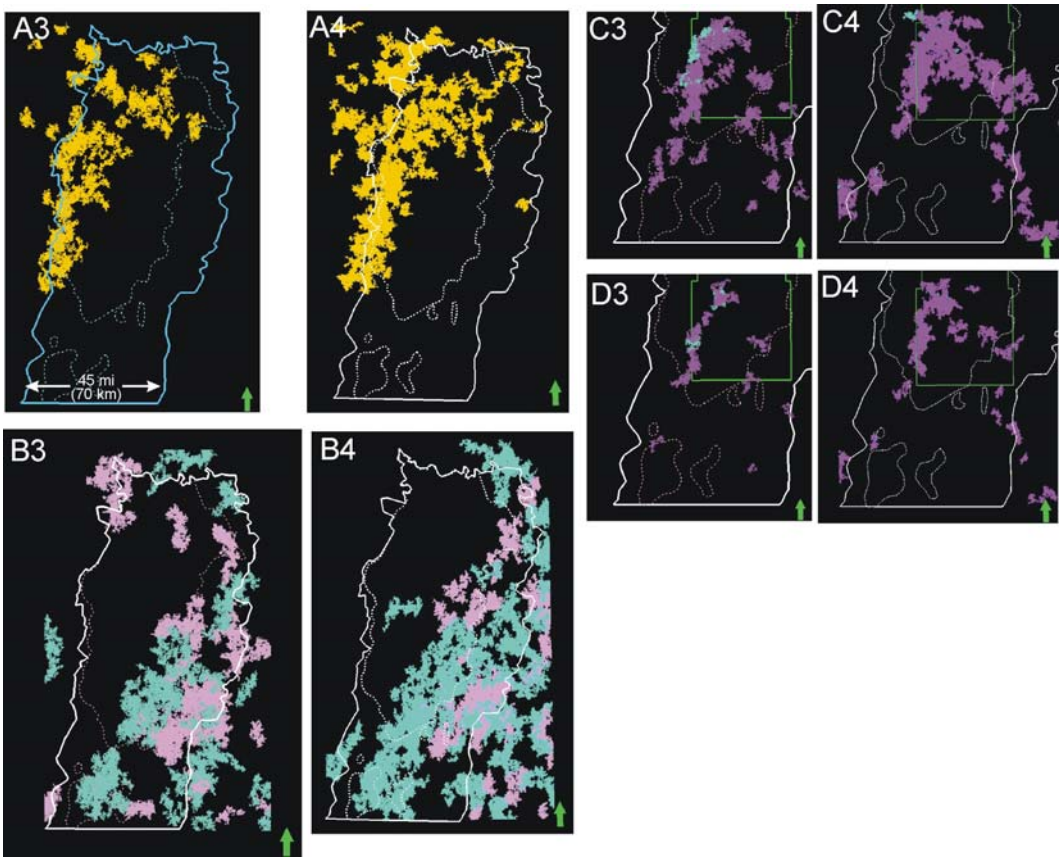

Figure C-3. Comparison of important lithofacies in Geomod3 and Geomod4. Illustrated are 2-D views of 3-D connected volumes (CV), collections of touching cells in the cellular model having common properties. Numbers 3 and 4 in the figure labels corresponds with the model version. **(A3, A4)** Fifteen CV of continental very-fine-grained sandstone in the Speiser Shale (A1_SH) having porosity > 12%. Geomod3 is on the left and Geomod4 on the right. **(B3, B4)** Thirty largest CV of packstone-grainstone (light blue) and very-fine-crystalline dolomite (pink) having porosity > 8% in the Crouse Limestone (B1_LM). **(C3, C4)** Twenty largest CV of fine- to medium-crystalline moldic dolomite (purple) and packstone-grainstone (light blue) in the Krider Limestone having porosity > 16% in Geomod3 and > 17% in Geomod4. Stevens County, Kansas is outlined in green. **(D3, D4)** Same as in C3 and C4 except for porosity > 18% in Geomod3 and > 19% in Geomod4.

APPENDIX D
Paleoslope and water depth estimate, lower Wolfcampian, Hugoton embayment of the Anadarko basin

APPENDIX D - Paleoslope and water depth estimate, lower Wolfcampian, Hugoton embayment of the Anadarko basin

Published as an open-file report. Dubois, M. K., 2006, Paleoslope and water depth estimate, lower Wolfcampian, Hugoton embayment of the Anadarko basin: Kansas Geological Survey, Open-File Report 2006-30, 21 p.
http://www.kgs.ku.edu/PRS/publication/2006/OFR06_30/index.html (Accessed March 21, 2007.)

ABSTRACT

Three criteria are used in combination to estimate paleoslope and maximum water depth during deposition of seven lower Wolfcampian (Council Grove Group) sedimentary cycles on a low relief shelf in Kansas and Oklahoma. Landward extent of paleo-shoreline establishes zero water depth at maximum flooding, and the updip extent of depth-specific fauna (fusulinids) establishes approximate water depth along a sub parallel linear trace. Slope is the depth divided by the distance between the two traces. Rate of change in thickness of a large interval of strata (most of Wolfcamp) serves as another estimate of slope for comparison. Maximum water depth on the basinward edge of the shelf is estimated by adding the depth along a trace established by fauna to additional depth determined by applying approximated slope to the distance between the faunal trace and the shelf margin. Paleoslope on the Kansas portion of the shelf is estimated to be 1 ft/mi (0.2 m/km). Beyond the shelf margin the slope increased by a factor of ten. Maximum water depths vary by cycle from a minimum of <50 ft (15 m) to a maximum of 110 ft (34 m).

Introduction

Shelf geometry (paleoslope) and water depth are important variables for understanding sedimentation patterns in the lower Wolfcampian Council Grove group (Figure D-1) in southwest Kansas (Figure D-2), and their determination is the object of this study. Rocks of the upper seven marine-continental, carbonate-siliciclastic sedimentary cycles of the Council Grove (Figure D-3) were deposited in a shallow

shelf setting in the Hugoton embayment of the Anadarko basin (Dubois et al., 2006). Marine carbonates thin landward and continental siliciclastic strata thin basinward in nearly reciprocal fashion (Figure D-4). Paleoslope, a function of subsidence and sedimentation, and glacial eustacy controlled water depth (or elevation above sea level) on the shallow shelf and the rate of shoreline movement during sea level rise and fall. Paleoslope and water depth estimates are based on three criteria: 1) accommodation space indicated by isopachs of relatively large intervals, 2) paleo-shoreline location (updip extent of marine carbonates), and 3) updip extent of depth-specific fauna (fusulinids).

Shelf geometry

Present-day structure of Wolfcampian-age rocks was strongly influenced by a Laramide-age eastward tilt (Figure D-5), whereas the Wolfcampian isopach (Figure D-6) better reflects the shelf geometry at the time of deposition. From the west field margin, Wolfcampian strata thicken basinward (eastward) at a rate of approximately 0.24 m/km (1.3 ft/mi) to a position on the shelf where the rate of thickening increases by a factor of 10 to 24 m/km (13 ft/mi). The axis of thickening is coincident with an area of present-day steep dip and may mark a shelf margin or axis of a steepened slope. It is also nearly coincident with the edge of a Virgilian-age starved basin and transition from marine carbonate to marine shale (Rascoe, 1968; Rascoe and Adler, 1983). The minimum paleoslope estimated for the older Lansing-Kansas City (Pennsylvanian, Missourian) on the Kansas shelf was 0.1-0.2 m/km (0.5-1.1 ft/mi) (Watney et al., 1995), however, relief across the Kansas portion of the shelf in the Hugoton embayment during Council Grove deposition has not been estimated.

Subsidence history and sedimentation record

The Anadarko basin experienced maximum subsidence in early Pennsylvanian and by Permian subsidence had waned to the point that the entire basin had nearly filled (Kluth and Coney, 1981; Rascoe and Adler, 1983; Kluth, 1986; Perry, 1989).

The isopach encompassing most of the Wolfcampian (upper thirteen cycles, from the top of the Chase Group to the base of the Grenola Limestone formation in the lower Council Grove Group) thickens only 80 ft (24 m), 480-560 ft (146-170m) in 60 mi (100 km) across the shelf, a rate of 1.3 ft/mi (0.24 m/km) (Figure D-6). Individual cycles show considerably less thickening, but the rate of thickening within a single cycle cannot be considered a proxy for slope because the depositional systems were not efficient at filling accommodation space that varied rapidly in response to glacial eustacy. Two marine carbonate half-cycles in the middle of the Council Grove (B2_LM and B3_LM) pinch out at or near the west updip margin of the Hugoton field (Figures D-4 and D-7) pinning the water depth as zero along a linear trace, and marking the maximum extent of marine flooding on the shelf for those cycles. Other Council Grove cycles thin substantially, especially the B1_LM and B4_LM.

Fusulinid occurrence on the shelf

The use of fusulinids as paleo-water depth indicators in the Pennsylvanian and Permian has been debated extensively (e.g., Imbrie et al., 1964; Elias, 1964; Laporte, 1962; Laporte and Imbrie, 1964; McCrone, 1964). Fusulinids may live in a wide range of water depths and can transported into an even wider range of depths. Mazzulo et al. (1995) provides an overview of the debate and the writer agrees with their assessment that a typical minimum depth for Early Permian fusulinids is approximately 50-60 ft (15-18 m). All Council Grove cycles studied except the Eiss (B3_LM) and Morrill (B4_LM) have thin, distinctive fusulinid-rich intervals that are adjacent to or mark the maximum flooding of their respective marine half-cycles (Figure D-8). Occurrences in cores studied are usually characterized by an abrupt appearance and disappearance (vertically) of very abundant, large (cm-size) fusulinids, in contrast with occasional scattered individuals, sometimes present in adjacent strata. Boardman and Nestell (1993) and Boardman et al. (1995) place the occurrence of fusulinid biofacies in the transgressive limestone and at the base of the regressive limestone, which are separated by the deeper-water core shale interval of

the idealized Pennsylvanian-Permian cyclothem (Heckel, 1977). This places the biofacies in the approximate middle of the relative depth scale for outcropping cycles in eastern Kansas and northeastern Oklahoma. Recognized in this study is the notable absence on the Hugoton shelf of the dark, fissile “core shale” common to Wolfcampian cycles in outcrop (Mazzullo et al., 1995; Boardman and Nestell, 2000), suggesting that water depths on the Hugoton shelf were less than those at the present day outcrop 300 miles (480 km) to the east. The closest equivalent to the typical deep water lithofacies in Council Grove core in the Hugoton are dark marine siltstones found near the base of the marine carbonate intervals in two of the seven cycles studied, the Grenola (C_LM) and Funston (A1_LM).

The maximum updip extent of the fusulinid biofacies (Figure D-7) by cycle form sub-parallel traces in a sequential pattern that may be related to systematic variability in sea level amplitude. Of the seven Council Grove cycles studied the fusulinid facies the furthest updip extent occurs in the two outermost cycles (A1_LM and C_LM), while the updip limit of fusulinids in the next cycles inward (B1_LM and B5_LM) are downdip slightly. Maximum updip position for the biofacies in the B2_LM is further downdip, and neither the B3_LM nor B4_LM have the fusulinid biofacies present in cores studied. If fusulinids occurred at similar depths from cycle to cycle water depths would have been at a maximum during A1_LM and C_LM deposition, and at a minimum during B2 through B4_LM deposition. Relative depths for B1_LM and B5_LM deposition would have been intermediate to the two extremes.

Furthermore, the lack of fusulinids in the cores studied for the B3_LM and B4_LM suggests the water never exceeded 50-60 ft (15-18 m) in the study area where core data are available (most of the Hugoton in Kansas and Oklahoma), if the fusulinid biofacies is assumed to be present in all cycles where water depths exceeded 50-60 ft (15-18 m).

Maximum updip position of shoreline and paleoslope estimate

Based on examination of approximately 200 examples of the transition from marine carbonate to continental siliciclastic strata in core from 29 wells, thinning and pinchouts of the Wolfcampian (both Chase and Council Grove) marine carbonates at the updip margin of the Hugoton are not a result of erosion. The maximum shoreline extent is defined for two of the Council Grove marine carbonates, B2_LM and B3_LM, by their updip limit (Figures D-4 and D-7). In the Middleburg (B2_LM) marine carbonate, the maximum extent of the fusulinid facies is approximately 50 miles (80km) from its pinchout (Figure D-7), suggesting a slope of 1 ft/mi (0.2 m/km), assuming that the minimum water depth for the fusulinid facies is 50ft (15m). The estimated slope is very close to the rate of thickening in the Wolfcamp (1.3 ft/mi, 0.24 m/km). Noteworthy is the shoreline position for the B3_LM, which is basinward of that for the B2_LM, and that no fusulinids were observed in the B3_LM. This suggests that the water depth was shallower during the deposition of the B3_LM carbonate than for the B2_LM. Marine carbonate in the other four cycles (A1, B4, B5 and C) does not pinch out in core in the study area, but thins in a westerly direction (Figure D-4). Based upon the spatial relationship between the updip limit fusulinid occurrence and paleo-shorelines, and overall rates of change in the Wolfcamp isopach, the paleoslope shelf is estimated to have been 1 ft/mi (0.2 m/km) during the deposition of Council Grove Group. Beyond the shelf break the slope may have increased by a factor of 10 to 10 ft/mi (2 m/km).

Maximum water depth

Based on criterion established above (paleoslope, updip extent of fusulinids and paleo-shorelines), the maximum water depth for the Council Grove marine intervals in the study area can be estimated. Points along a trace where the updip limit of fusulinids are established are assumed to have had a maximum water depth of 50 ft (15 m). The additional depth from the biofacies trace to the northwest portion of Seward County (proximal to the shelf margin) can be estimated as the product of

paleoslope and distance that is added to the depth at the biofacies trace for maximum depth on the shelf (maximum depth = 50 ft + [1 ft/mi X distance]). Immediately northwest of the shelf margin in northwest Seward County I estimate water reached a maximum depth of approximately 110 ft (34m) during deposition of the A1_LM and C_LM, the outer two of the seven cycles studied. For the B1_LM and B5_LM, one cycle in from the end cycles, a maximum depth is estimated at 80ft (24m). Water depths for the middle three cycles are estimated to have reached 50 ft (15m) for the B2_LM and slightly less than 50 ft (<15m) for the B3_LM and B4_LM.

Inter-cycle variability in sea level and higher order cyclicity

As noted earlier, there appear to be systematic shifts in shoreline position of marine carbonate (Figures D-4 and D-7), updip extent of the fusulinid biofacies (Figure D-7), and the estimated maximum water depth, all of which are synchronized. Within the seven cycles studied, maximums of the three variables occur at the outermost cycles (A1 and C), minimums occur at the inner cycles (B2, B3 and B4), and the cycles between are intermediate (B1 and B5). The ordered shift in sea level may reflect a higher order of glacial cyclicity (than for the individual cycles).

Conclusions

Paleoslope and water depths for the Hugoton embayment of the Anadarko basin can be estimated for the Council Grove by considering three criterion: 1) Wolfcamp isopach, 2) shoreline position indicated by the landward extent of marine carbonate, and 3) the updip extent of fusulinids. Paleoslope on the Kansas portion of the shelf is estimated to be 1 ft/mi (0.2 m/km). Beyond the shelf margin the slope increased by a factor of ten (10 ft/mi, 2 m/km). Maximum water depth on the shelf ranges from approximately 50 ft (15 m) in the innermost cycles to 110 ft (34 m) in the outer most cycles (top and bottom) of the seven cycles studied. Systematic inter-cycle variability in water depth may indicate higher order glacial-eustatic cyclicity.

References

Boardman, D. R., II, and M. K. Nestell, 1993, Glacial-eustatic sea-level curve for Carboniferous-Permian boundary strata based on outcrops in North American midcontinent and north-central Texas: *in* R. E. Crick, ed., Transactions and Abstracts, American Association of Petroleum Geologists Southwest Section Geological Convention, p.15-25.

Boardman, D. R., II, M. K. Nestell, and L. W. Knox, 1995, Depth-related microfaunal biofacies model for the Late Carboniferous and Early Permian cyclothemic sedimentary sequences in mid-continent North America, *in* N.J. Hyne, ed., Sequence stratigraphy of the mid-continent: Tulsa Geological Society, Special Publication no. 4, p. 93-118.

Boardman, D. R. II, and M. K. Nestell, 2000, Outcrop-based sequence stratigraphy of the Council Grove Group of the Midcontinent: *in* K. S. Johnson ed., Platform Carbonates in the Southern Midcontinent, 1996 Symposium. Circular 101, Oklahoma Geological Survey, Norman, p. 275-306.

Dubois, M.K., A.P. Byrnes, T.R. Carr, G.C. Bohling, and J.H. Doveton, 2006, Multiscale geologic and petrophysical modeling of the giant Hugoton gas field (Permian), Kansas and Oklahoma: *in* P. M. Harris and L. J. Weber, eds., Giant reservoirs of the world: From rocks to reservoir characterization and modeling: American Association of Petroleum Geologists Memoir 88, 307-353.

Elias, M. K., 1964, Depth of Late Paleozoic sea in Kansas and its megacyclic Sedimentation: *in* D. F. Merriam, ed., Symposium on cyclic sedimentation: Kansas Geological Survey Bulletin 169, p. 87-106.

Heckel, P. H., 1977, Origin of phosphatic black shale facies in Pennsylvanian cyclothems of mid-continent North America: American Association of Petroleum Geologists, Bulletin, v. 61, p. 1045-1068.

Imbrie, J., L. F. Laporte, and D. F. Merriam, 1964, Beattie Limestone facies (Lower Permian) of the Northern Mid-Continent: *in* D. F. Merriam, ed., Symposium on cyclic sedimentation: Kansas Geological Survey Bulletin, v.169, p. 219-238.

Kluth, C. F., and P. J. Coney, 1981, Plate Tectonics of the Ancestral Rocky Mountains: Geology, v. 9, no. 1, p 10-15.

Kluth, C. F, 1986, Plate Tectonics of the Ancestral Rocky Mountains: *in* J. A. Peterson, ed., Paleotectonics and Sedimentation in the Rocky Mountains, United States: American Association of Petroleum Geologists Memoir 41, p. 353-369.

Laporte, L. F., 1962, Paleoecology of the Cottonwood Limestone (Permian), Northern Mid-Continent: Geological Society of America Bulletin, v. 73, p. 521-544.

Laporte, L. F. and J. Imbrie, 1964, Phases and facies in the interpretation of cyclic deposits, *in* D. F. Merriam, ed., Symposium on cyclic sedimentation: Kansas Geological
Survey Bulletin 169, p. 275-281.

McCrone, A. W., 1964, Water depth and Midcontinent cyclothems, *in* D. F. Merriam, ed., Symposium on cyclic sedimentation: Kansas Geological Survey Bulletin 169, p. 275-281.

Mazzullo, S. J., C. S. Teal, and C. A. Burtnett, 1995, Facies and stratigraphic analysis of cyclothemic strata in the Chase Group (Permian Wolfcampian, south-central Kansas, *in* N.J. Hyne, ed., Sequence stratigraphy of the mid-continent: Tulsa Geological Society Special Publication no. 4, 1995, p. 217-248.

Perry, W. J., 1989, Tectonic evolution of the Anadarko basin region, Oklahoma: U.S. Geological Survey Bulletin 1866-A, p. A1-16.

Peterson, J. A., 1980, Permian Paleogeography and sedimentary provinces, west central United States: *in* T. D. Fouch and E. R. Magathan, eds., Paleozoic Paleogeography of the West-Central United States, Rocky Mountain Paleogeography Symposium 1, Rocky Mountain Section of Society of Economic Paleontologists and Mineralogists, Denver, CO, p. 271-292.

Rascoe, B., Jr., 1968, Permian System in Western Midcontinent: Mountain Geologist, v. 5, p. 127-138.

Rascoe, B., Jr., and F. J. Adler, 1983, Permo-Carboniferous Hydrocarbon Accumulations, Midcontinent, USA: American Association of Petroleum Geologists Bulletin, v. 67, p. 979-1001.

Sawin, R. S., R. R. West, E. K. Franseen, W. L. Watney, and J. R. McCauley, 2006, Carboniferous-Permian boundary in Kansas, mid-continent U.S.A, in Current Research in Earth Sciences: Kansas Geological Survey, Bulletin 252, part 2, http://www.kgs.ku.edu/Current/2006/sawin/ (accessed August 23, 2006).

Scotese, C. R., 2004, A continental drift flipbook: The Journal of Geology, v. 112, p. 729-741.

Sorenson, R. P., 2005, A dynamic model for the Permian Panhandle and Hugoton fields, western Anadarko basin: American Association of Petroleum Geologists Bulletin, vol. 89, no. 7, p. 921-938.

Watney, W. L., J. A. French, J. H. Doveton, J. C. Youle, and W. J. Guy, 1995, Cycle hierarchy and genetic stratigraphy of middle and upper Pennsylvanian strata the upper mid-continent, *in* N. J. Hyne, ed., Sequence Stratigraphy of the Mid-Continent: Tulsa Geological Society, Special Publication, no. 4, p. 141-192.

Zeller, D. E., ed., 1968, The stratigraphic succession in Kansas: Kansas Geological Survey, Bulletin 189, 81 p.

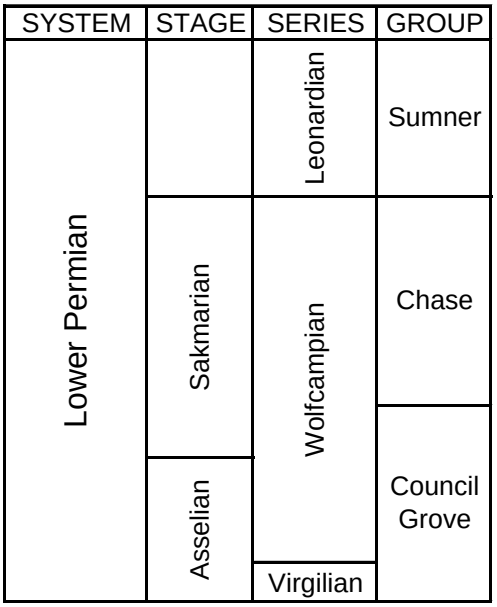

Figure D-1. Lower Permian stratigraphy, Hugoton embayment of the Anadarko basin (compiled from Zeller, 1968; Sawin et al., 2006). Approximate position of Asselian-Sakmarian boundary is from Boardman and Nestell (2000). Readers are referred to Peterson (1980) for correlations to stratigraphic nomenclature in Ancestral Rocky Mountain basins. Hugoton field produces gas from the Chase while Panoma gas production is from the Council Grove. The two fields are likely one common reservoir system (Dubois et al., 2006) and are referred to collectively as the Hugoton in this study.

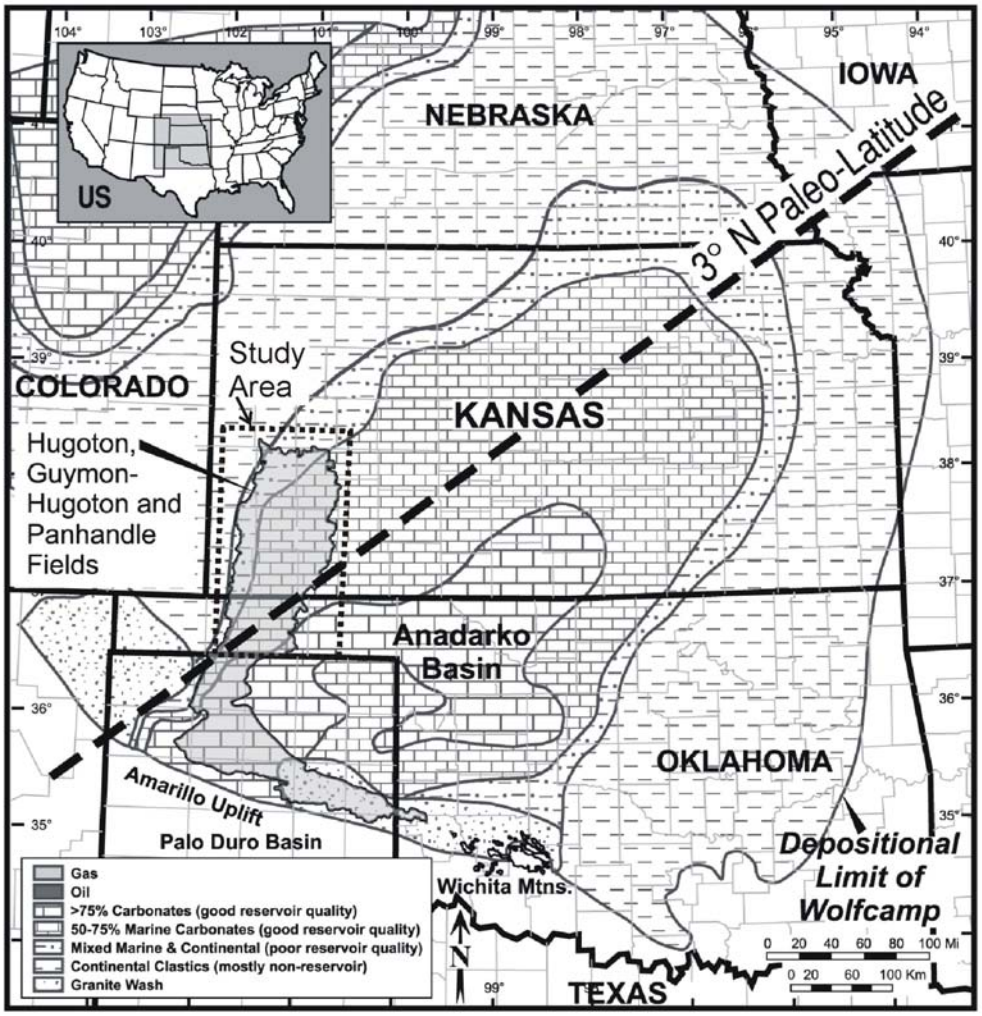

Figure D-2. Distribution of major lithofacies in the midcontinent during the late Wolfcampian (modified after Rascoe, 1968; Rascoe and Adler, 1983; Sorenson, 2005). Approximate paleo-latitude was 3 degrees north (Scotese, 2004).

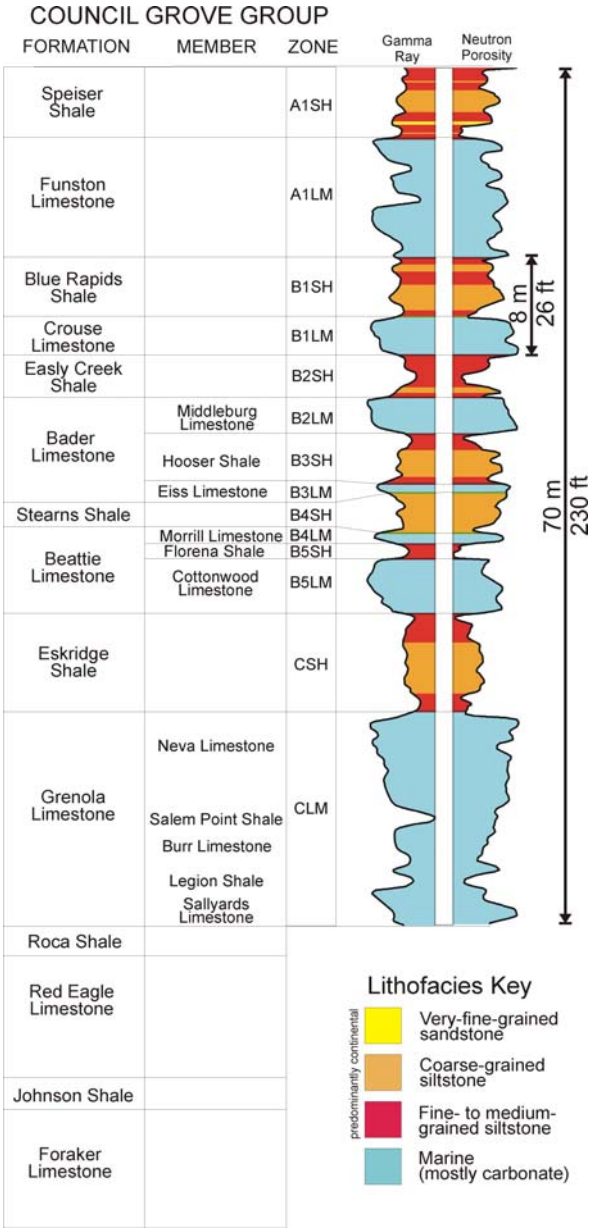

Figure D-3. Formation and member level stratigraphy for the Council Grove, Hugoton embayment, in the Alexander D well. The upper seven of nine marine-continental cycles (color-filled wire-line log traces) are the subject of this study. Stratigraphic names that include "Limestone" are marine half cycles that when combined with an adjacent continental half cycle, intervals with stratigraphic names that include "Shale," form a complete cycle. Informal alphanumeric zone designations commonly used in the field provide stratigraphic orientation and are used throughout the paper.

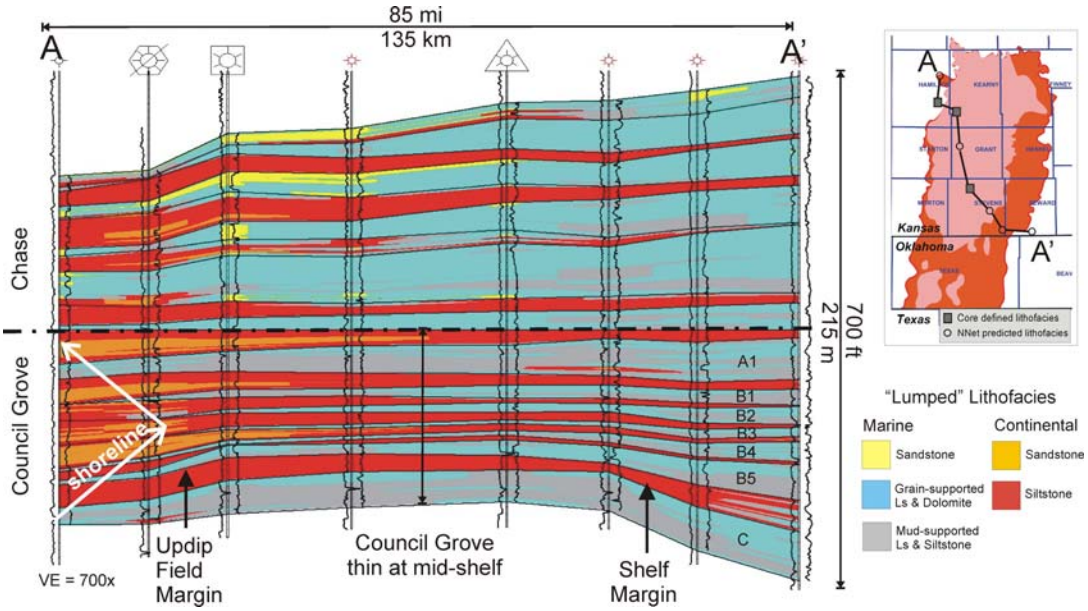

Figure D-4. Regional stratigraphic cross-section of the Wolfcampian (Chase and Council Grove Groups) with the top of the Council Grove as the datum. At the wells, "lumped" lithofacies are from core (large symbols) or those predicted by neural network models (small well symbols) or and are interpolated in Geoplus Petra™ between wells. The Upper seven cycles of the Council Grove are the subject of the study and are thinnest at a mid-field position. Log curves are gamma ray (left) and corrected porosity (right). (Modified after Dubois et al., 2006)

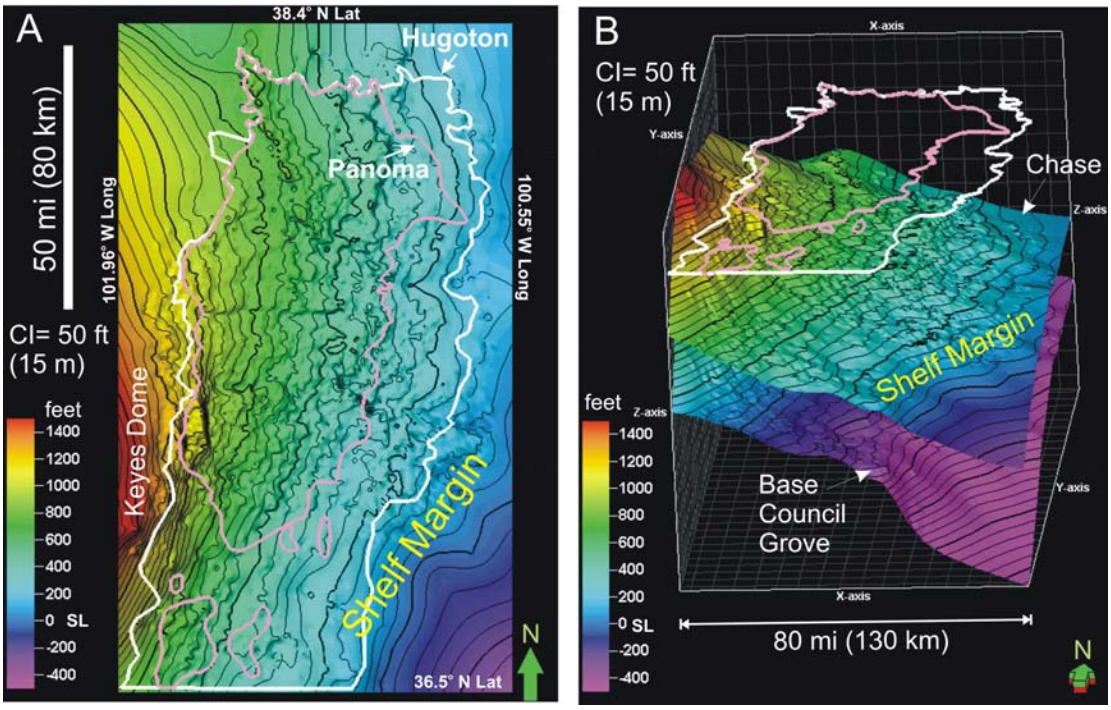

Figure D-5. A) Present day structure on the top of the Wolfcampian (top of Chase Group) is mostly a function of eastward tilt during the Laramide orogeny. Note the "shelf margin" or area of steepened slope at the southeast boundary of the Hugoton fields. The Council Grove surface parallels the top of the Chase. **B)** 3-D view of the same area. Present day structure on the top of the Chase and a surface near the base of the Council Grove. (After Dubois et al., 2006)

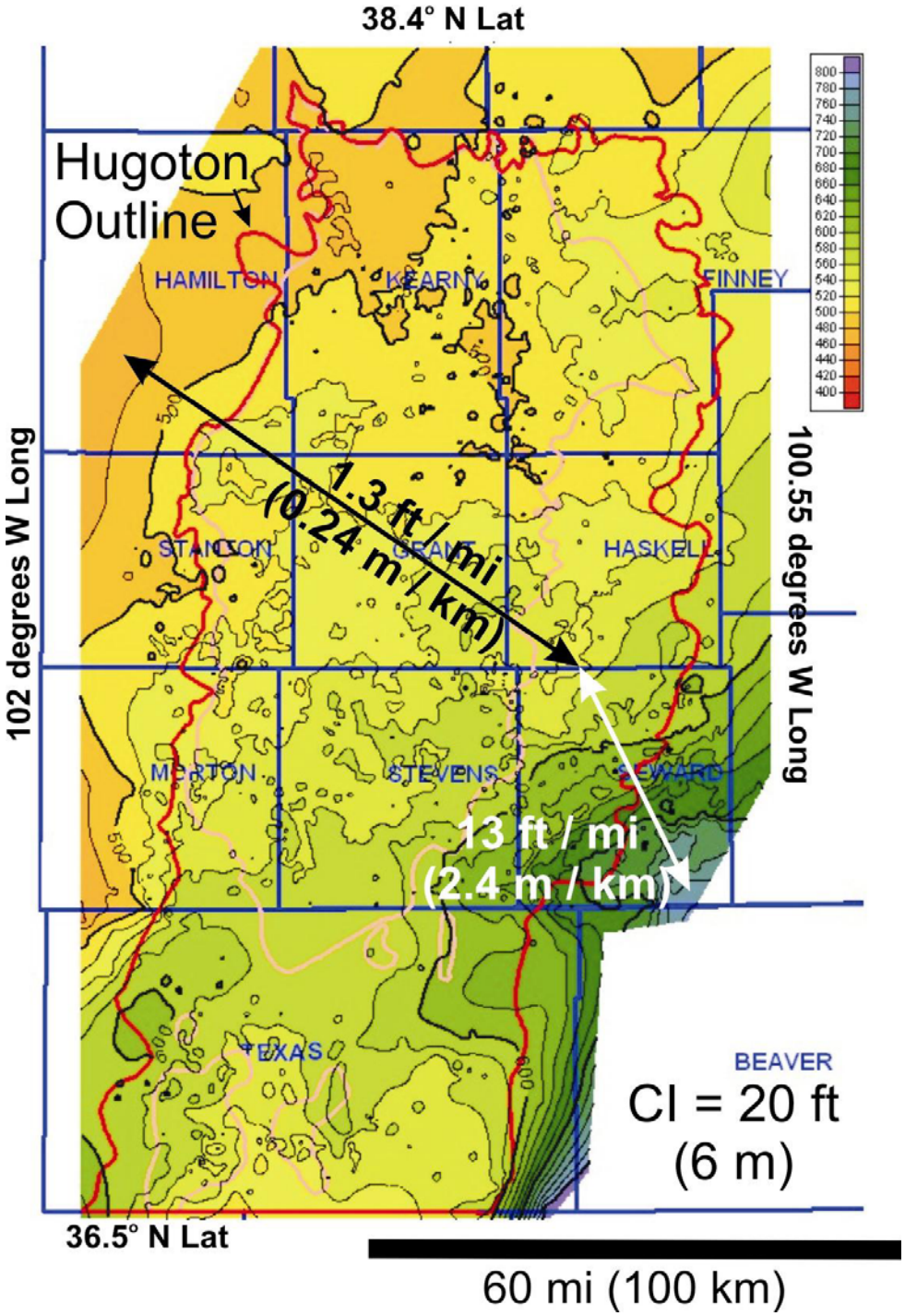

Figure D-6. Isopach of the Wolfcampian reservoir (top of Chase Group to base of Grenola Limestone, Council Grove Group). Wolfcampian rate of thickening increases by a factor of ten at the "shelf margin." (After Dubois et al., 2006)

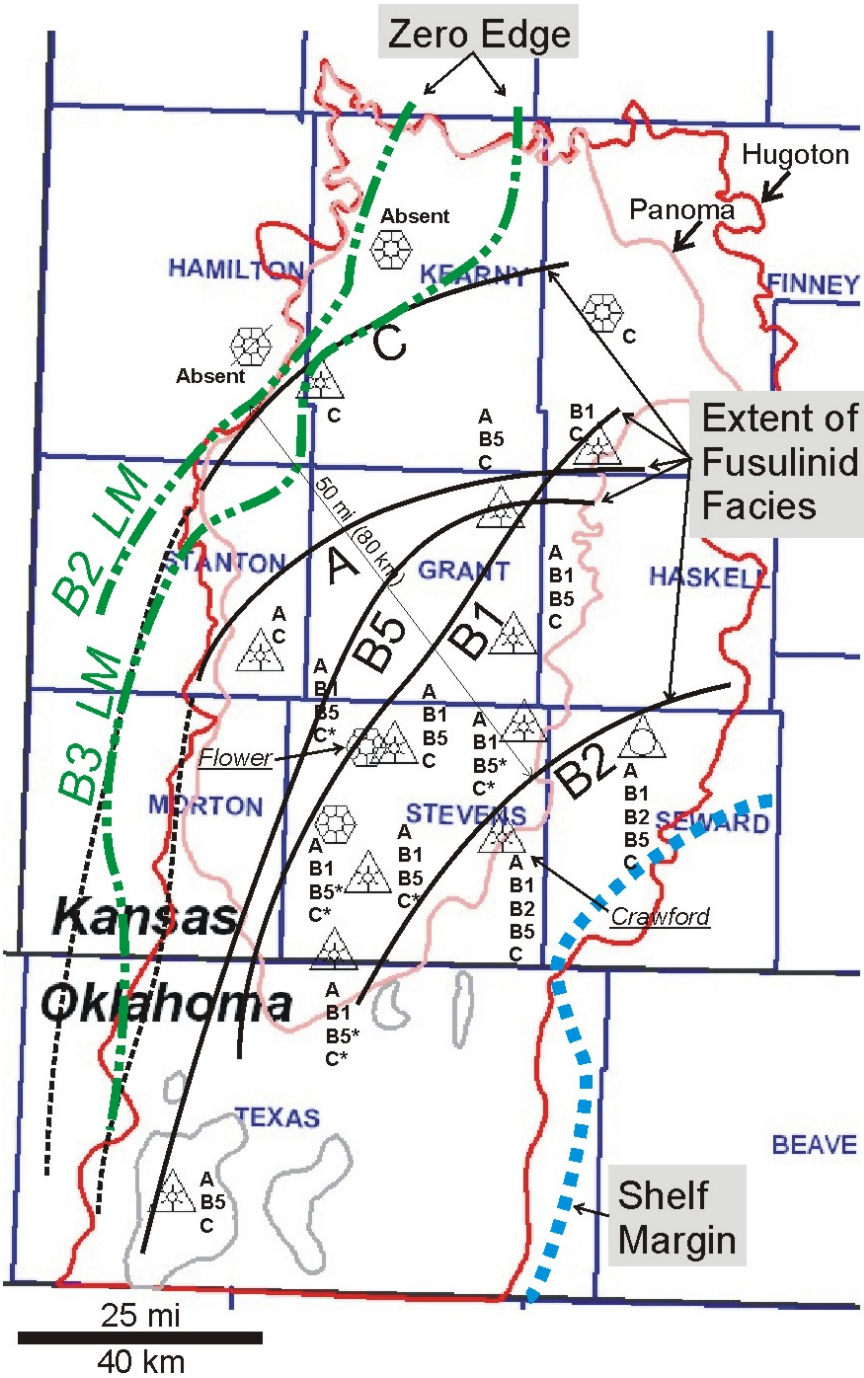

Figure D-7. Study area showing updip limit of B2_LM and B3_LM (zero edge) and updip extent of fusulinid biofacies in five of seven Council Grove cycles (not present in B3_LM and B4_LM). Occurrence of fusulinid biofacies in core is indicated by Council Grove cycle letter code adjacent to 17 wells in study. Asterisk (*) means interval was not cored but fusulinid biofacies is assumed to be present. No core was available below the shelf margin.

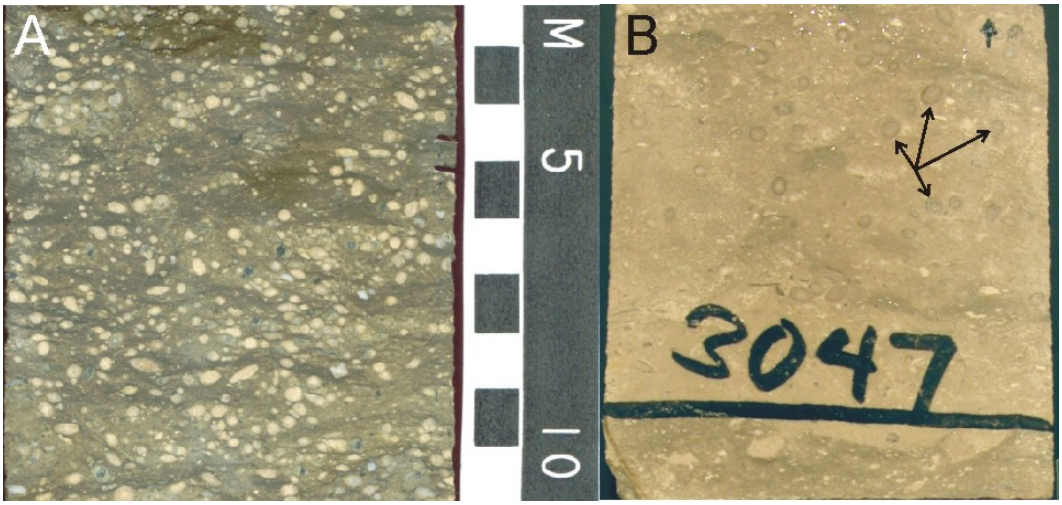

Figure D-8. Fusulinid biofacies in core slabs. **A)** Abundant in fusulinid (white) dominated silty wackestone (upper part of transgressive limestone, subjacent to maximum flooding, in Funston, A1_LM, Flower A1 well). **B)** Scattered in fusulinid (arrows) -mixed skeletal wackestone (maximum flooding in Crouse, B2_LM, Crawford 2 well). Depth shown is in feet. Well locations are shown in Figure D-7.